MINIMUM-FUEL ATTITUDE CONTROL AND STABILIZATION OF AN INERTIALLY-ORIENTEDSPACE
FEARNSIDES, JOHN JOSEPH
ProQuest Dissertations and Theses; 1971; ProQuest Dissertations & Theses Global

72-12,750

FEARNSIDES, John Joseph, 1934-

MINIMUM-FUEL ATTITUDE CONTROL AND STABILIZATION OF AN INERTIALLY-ORIENTED SPACE STATION.

University of Maryland, Ph.D., 1971
Aerospace Studies

University Microfilms, A XEROX Company, Ann Arbor, Michigan

THIS DISSERTATION HAS BEEN MICROFILMED EXACTLY AS RECEIVED

Reproduced with permission of the copyright owner. Further reproduction prohibited without permission.

MINIMUM-FUEL ATTITUDE CONTROL AND STABILIZATION OF AN INERTIALLY-ORIENTED SPACE STATION

by
John Joseph Fearnsides

Dissertation submitted to the Faculty of the Graduate School
of the University of Maryland in partial fulfillment
of the requirements for the degree of
Doctor of Philosophy
1971

Reproduced with permission of the copyright owner. Further reproduction prohibited without permission.

APPROVAL SHEET

Title of Thesis: Minimum-Fuel Attitude Control and Stabilization of an Inertially-Oriented Space Station

Name of Candidate: John Joseph Fearnsides
Doctor of Philosophy, 1971

Thesis and Abstract Approved: William S. Levine
William S. Levine
Assistant Professor
Electrical Engineering

Date Approved: August 20, 1971

Reproduced with permission of the copyright owner. Further reproduction prohibited without permission.

PLEASE NOTE:

Some pages have indistinct print. Filmed as received.

UNIVERSITY MICROFILMS.

Reproduced with permission of the copyright owner. Further reproduction prohibited without permission.

ABSTRACT

Title of Thesis: Minimum-Fuel Attitude Control and Stabilization of an Inertially-Oriented Space Station

John Joseph Fearnsides, Doctor of Philosophy, 1971

Thesis directed by: Assistant Professor William S. Levine

Using Newtonian Mechanics, a mathematical model is derived to represent small motions relative to an inertial reference coordinate system of a large, unsymmetrical, rigid spacecraft in low, circular Earth-orbit. The resulting system equation is a set of coupled, linear differential equations with periodic coefficients and periodic forcing functions whose state-space representation is given by $\dot{\underline{x}} = A(t)\underline{x} + \underline{z}(t)$ where $\underline{x} \in R^n$ is the state vector, $\underline{A}(t) = A(t+T)$ is an $n \times n$ matrix, $\underline{z}(t) = \underline{z}(t+T) \in R^n$, and $n = 6$. The periodicity of the elements of $\underline{A}(t)$ and two of the elements of $\underline{z}(t)$ are due to the effects of the Earth's gravitational field on the unsymmetrical spacecraft. The periodicity of the remaining elements of $\underline{z}(t)$ are caused by the aerodynamic torque, which becomes significant because of the size of the vehicle and the density of the Earth's atmosphere in low orbits. The attitude of the spacecraft is kept close to the inertial reference by a set of

Reproduced with permission of the copyright owner. Further reproduction prohibited without permission.

reaction-jet thrusters that are physically constrained to produce on-off or bang-bang controls. A minimum-fuel control law $\underline{u}(\underline{x}, t)$ is sought.

The first main result of this research is the development of the zero-fuel mode; a three-axis oscillatory motion corresponding to the unique, forced periodic solution of the system equation. This motion is then used in lieu of the point $\underline{x} = \underline{0}$ as a target set for the development of a control law. It is called the zero-fuel mode because, (assuming an ideal, deterministic system) once the state of the system is properly initialized by the thrusters no further control action is required. When the parameters of an early model of NASA's Skylab vehicle are substituted into the system equation, the amplitudes of the oscillations are relatively small and cause no significant reduction in the performance of the spacecraft's mission. In physical terms the trajectory of the zero-fuel mode is similar to the usual controlled trajectory produced by the thrusters and is viewed as a "natural" limit cycle that is produced in part by the aerodynamic torque. In abstract terms this result is shown to be the generalization to multi-dimensional, coupled periodic systems of a series of recent results on the minimum-fuel control of constant, single-input single-output systems with a constant forcing function.

The next phase of the study is concerned with the development of a control law to keep the actual motion of the

Reproduced with permission of the copyright owner. Further reproduction prohibited without permission.

system close to the trajectory of the zero-fuel mode. This is especially important for the Skylab model for which motions away from the target set are shown to be unstable. The chosen control law $\underline{u}(\underline{y})$, where $\underline{u}$ is a piecewise constant function of $\underline{y}$ and $\underline{y}$ a linear function of $\underline{x}$, is selected for its ease of implementation and because it produces a feedback system with excellent closed-loop stability properties.

A demonstration of the stability of the controlled system is provided by the second main result contained herein: an application of some recent generalizations of Lyapunov Stability Theory by Yoshizawa and LaSalle. In particular, because the selected control law includes a deadband and the open-loop system is unstable, the origin is not a limit set of the controlled motion. In addition, the combination of a bounded controller and open-loop instability dictate a finite domain of attraction. However, the above mentioned theory can be used to determine a compact set E^* that includes the positive limit set of solutions of the closed-loop system equation as well as an estimate of the domain of attraction. It is also shown that this theory can be used to provide information on a type of bounded-input, bounded-output stability for many systems.

Reproduced with permission of the copyright owner. Further reproduction prohibited without permission.

ACKNOWLEDGEMENTS

Various members of the Electrical Engineering Department of the University of Maryland were helpful to me during the course of this research. Professors Newcomb, Emad, Rao, and Robinson read the dissertation and provided helpful criticisms. Professor Steven Tretter was also very helpful in guiding the early phases of this research. In particular, I would like to express my gratitude to Professor William Levine, who directed the major part of this research and who extended friendship and encouragement as well as constructive criticism.

Among those at Bellcomm to whom I am grateful are: Drs. Jack Kranton and John Strand who have cheerfully tolerated the inconveniences imposed on them by a graduate student; Drs. Sherwood Chu and Bryant Elrod with whom I have shared valuable discussions; and Patricia Dowling, Nancy Kirkendall, and Ronald Grutzner who provided programming help at various times over the past three years.

The most important contributions, however, have been made by my wife. She seemed always to know when to be helpful, when encouraging, and when sympathetic.

Reproduced with permission of the copyright owner. Further reproduction prohibited without permission.

TABLE OF CONTENTS

Chapter		Page
I.	INTRODUCTION	1
II.	THE MATHEMATICAL MODEL	10
III.	A ZERO-FUEL MODE	35
IV.	THE TRACKING PROBLEM	54
V.	STABILITY OF THE CONTROLLED SYSTEM	76
VI.	CONCLUSIONS AND SUGGESTIONS FOR FUTURE RESEARCH	107
APPENDIX A.	ILLUSTRATIONS	111
APPENDIX B.	THE DISTURBANCE TORQUES ON A SATELLITE IN LOW, CIRCULAR EARTH ORBIT	140
APPENDIX C.	DERIVATION OF SYSTEM EQUATIONS FOR THE TRACKING PROBLEM	149
SELECTED BIBLIOGRAPHY		154

Reproduced with permission of the copyright owner. Further reproduction prohibited without permission.

LIST OF TABLES

Table		Page
1	MAXIMUM VALUES OF PERIODIC SYSTEM VARIABLES .	49
2	COMPARISON OF THE PERFORMANCE OF THREE CONTROL LAWS	74

Reproduced with permission of the copyright owner. Further reproduction prohibited without permission.

LIST OF NOTATIONAL CONVENTIONS

Symbol	Definition
$\underline{b}$	A vector expressed explicitly in terms of a set of three-dimensional basis vectors; e.g., $\underline{b} = b_1\underline{e}_1 + b_2\underline{e}_2 + b_3\underline{e}_3$.
$\underline{b}$	An n-dimensional vector expressed as an n × 1 column matrix.
$\underline{B}$	An n × n matrix.
$\underline{B}'$	The transpose of $\underline{B}$.
$\tilde{\underline{a}}$	A 3 × 3 skew symmetric matrix that is isomorphic to the vector cross-product operator; e.g., $\tilde{\underline{a}}\,\underline{b}$ is isomorphic to $\underline{a} \times \underline{b}$.
$\|\|\underline{b}\|\|$	The Euclidean norm of $\underline{b}$.
b	A scalar quantity.
$\|b\|$	The absolute value of b.

Reproduced with permission of the copyright owner. Further reproduction prohibited without permission.

CHAPTER I

INTRODUCTION

The problem studied herein is the attitude control and stabilization of a large vehicle (e.g., a space station) in a low, circular Earth orbit. In particular, we will be concerned with a satellite that has a symmetrically cylindrical primary structure to which is attached a pair of rectangular solar panels of significant extent (Figure 1).* These solar panels are used to convert incident solar radiation into electrical energy for powering various on-board systems and their presence causes an important a priori attitude constraint to be imposed on the spacecraft. That is, the vector that is normal to the plane of the panels must be pointed toward the Sun. The maintenance of this attitude will be shown to require a substantial amount of fuel (propellant) from the reaction-jet thrusters (also called the reaction control system or RCS) that act as the controller for this system.

The significant external perturbations of the attitude of a satellite in a low Earth orbit are gravitational, atmospheric and magnetic. However, the spacecraft under

---

*All referenced illustrative figures are aggregated in Appendix A.

Reproduced with permission of the copyright owner. Further reproduction prohibited without permission.

consideration is designed to have a trivially small magnetic moment. Therefore, a "nominal" spacecraft attitude will be chosen which is consistent with the solar pointing constraint and for which the effects of the gravitational and atmospheric torques are relatively small. However, as will be shown in the sequel, even this attitude requires a substantial outlay of propellant. This is because the necessity for solar pointing constrains the desired attitude of the spacecraft to be fixed with respect to an inertial reference coordinate system and, therefore, to be in a non-equilibrium attitude relative to the gravitational torque. We now explore the details of the desired nominal attitude more fully.

As mentioned above, the requirement of pointing the solar panels towards the Sun precludes a gravity stabilized attitude and, in fact, will introduce a forcing term about the axis which is normal to the orbital plane. If the spacecraft's z-axis is aligned along this normal as in Figure 11, the forcing term will be proportional to the difference $(I_y - I_x)$ where I_y and I_x are respectively the principal moments of inertia about the spacecraft's y and x axes. This torque can be minimized by selecting the axis of minimum moment of inertia (the axis of symmetry of the cylinder) to be normal to the orbital plane. Notice that, if the solar panels were not attached to the cylinder $I_y = I_x$ and the forcing term about the spacecraft z axis would vanish. The desired attitude thus described is illustrated in Figure 1 where there are two points worthy of note:

Reproduced with permission of the copyright owner. Further reproduction prohibited without permission.

1. In order to accommodate both the minimum torque and the solar pointing constraints, the solar panels must be allowed a single degree of freedom rotation;
2. When the spacecraft is perfectly aligned with the desired attitude, its motion about an axis along the flight path is in an unstable equilibrium with respect to the gravitational field; and, as mentioned above, motion about the z axis is not in equilibrium at all.

The presence of the solar panels influences the motion of the spacecraft in another important way. The center of mass (CM) of the composite vehicle now lies between the centers of mass as well as the centers of geometry (or pressure) of the cylinder and the rectangular panels (e.g., Figure 5). Thus, an imbalance in the effects of the atmosphere exists about the composite CM. This effect is called the aerodynamic torque; and, when the vehicle is aligned with the desired attitude, it acts about the local vertical axis (i.e., the axis parallel to the radius vector from geocenter to the spacecraft's mass center).

In summary, then, the external torques acting on this satellite are: a gravitational torque about the axis normal to the orbital plane, a gravitational torque acting about the flight path velocity vector when the spacecraft deviates from the desired attitudes, and the aerodynamic torque acting about the local vertical vector. Note that these three vectors are mutually orthogonal and would be the natural selection for a

Reproduced with permission of the copyright owner. Further reproduction prohibited without permission.

desired or reference attitude for an Earth-pointing satellite. However, these axes are rotating at a constant rate relative to the inertial reference frame that has been selected according to the previously mentioned criteria. Thus, relative to a set of spacecraft axes aligned with an inertial reference, the aerodynamic torque acts as a periodic forcing function about the axes lying in the orbital plane. In addition, the tendency of the spacecraft to rotate into the gravity field about the axis parallel to the flight path velocity vector is also periodic because the inertially-fixed spacecraft axes are in motion relative to an Earth-pointing reference system. This will show up as a set of periodic coefficients for the attitude variables that measure the effect of rotations about spacecraft axes that are nominally parallel to the orbital plane. The differential equation that describes this physical situation will, then, have periodic coefficients and periodic forcing functions in the equations for the motion about each axis. Also, the equations will, in general, be coupled.

The purpose of this research was to develop an efficient strategy for controlling and stabilizing the above-mentioned physical event with a set of reaction-jet thrusters. The minimum-fuel control law that results is, as expected, a function of the vehicle dynamics and of the characteristics of the environment and the controller. It is shown that the greatest reductions in propellant consumption (relative to a linear control law) derives from the establishment of an

Reproduced with permission of the copyright owner. Further reproduction prohibited without permission.

oscillatory or limit-cycle motion as a desired attitude rather than the inertial reference specified above and illustrated in Figure 1. The motion about the axis that is perpendicular to the orbital plane is shown, for reasonably small angular excursions, to be independent of the motion about the other, orthogonal spacecraft axes. This axis is defined to be the roll axis, whose motion is controlled in such a way as to have the gravitational torque act as a restoring force rather than a perturbing force. The oscillatory motion about the pitch and yaw axes is produced in an original way. First, the thrusters initialize the motion such that the response to the aerodynamic torque is a two-axis oscillation, or more precisely, a precession of the axis of symmetry about the normal to the orbital plane. This rotational motion counteracts the effects of the aerodynamic torque while maintaining an equilibrium position vis-à-vis the gravity torque. This periodic solution of the equations that serve as a mathematical model for this problem is seen to be a generalization of the results announced by numerous other workers [3.3 - 3.6] in the investigation of minimum-fuel control laws for spacecraft in the presence of non-conservative external torques. Whereas the previous results applied to single axis control of linear, time-invariant systems in the presence of constant forcing functions, these apply to a class of multi-axis, non-autonomous systems in the presence of constant or periodic forcing terms. In review, the first important result is physical; the existence of

Reproduced with permission of the copyright owner. Further reproduction prohibited without permission.

three-axis oscillatory motion as a result of the interaction of the gravitational and aerodynamic torques acting on the spacecraft; and the second is abstract: the generalization of a control law concept from constant dynamical systems to periodic systems.

It should be noted that the three-axis oscillation discussed above is very similar to the usual type of steady-state control law for the thrusters of a satellite. That is, the motion is usually a set of controlled single-axis limit cycles where the thrusters provide at least one turning point. The three-axis oscillation, then, can be thought of as a set of "natural" limit cycles in which the environment (ideally) produces all of the turning points. It also incorporates the coupling that exists between axes rather than ignoring it.

Of course, no mathematical model can perfectly describe a system and, even if it could, the errors that exist in the sensors and controller cause the spacecraft to deviate from the desired motion. Further, it is shown that the three-axis oscillation is an unstable solution of the equations of motion. Therefore, a control law must be developed to keep the actual state of the system close to the desired state. At first, a minimum-fuel control law is investigated by applying optimal control techniques to the dynamical system that represents small motions of the spacecraft away from the limit-cycle motion described above,

Reproduced with permission of the copyright owner. Further reproduction prohibited without permission.

which is taken to be the target set for the analytical control problem. For purposes of distinguishing the phases of control mentioned so far, the establishment of the three-axis oscillation (or, abstractly, the periodic solution to the vector differential equation that describes the dynamical system) is called the solution to the steady-state control problem or the zero-fuel mode. The control law that keeps the motion of the spacecraft close to the desired state will be considered a solution of the tracking problem.

As mentioned above, a minimum-fuel solution to the tracking problem is sought. Since the roll axis motion is uncoupled from the pitch and yaw motions, the equation describing it can be considered a separate dynamical system. A linearization of the equation representing small excursions of the actual state of the roll axis motion from the desired state results in a special form of the Mathieu equation. The solution of this uncontrolled, homogeneous equation, given a set of initial conditions, is shown to be stable in the sense that the motion is bounded. When the Pontryagin Maximum Principle is applied to establish the minimum-fuel of the tracking problem, the results are seen to bear a physically satisfying resemblance to the well known results [4.5] for constant systems with periodic solutions. However, these results are shown to be computationally difficult and to possess undesireable stability properties. These facts, along with the prohibitive computational aspects attendant to optimal solutions of the coupled pitch-yaw equations, lead to the

Reproduced with permission of the copyright owner. Further reproduction prohibited without permission.

selection of a three-axis linear deadband control law relative to the minimum-fuel mode as an alternative solution to the tracking problem. A comparative study of this control law with deadband control laws not using the zero-fuel mode as a target set was made using a digital computer simulation of the full non-linear equations of motion. The results of this study are that a 65% reduction in control system activity (propellant consumption and number of thruster firings) is achieved. Moreover, as shown by the last phase of the research, the control law has excellent closed-loop stability properties.

The linearized equations of motion of the spacecraft relative to the zero-fuel mode trajectory are representable as a nonstationary, linear, vector differential equation. The deadband control law is modelled as a nonlinear piecewise-continuous function of the output vector. More precisely, the closed-loop system equations are given by

$$\begin{aligned} \dot{\underline{x}} &= \underline{A}(t)\underline{x} - \underline{B}\ \underline{u}(\underline{y}) \\ \underline{y} &= \underline{C}\underline{x} \end{aligned} \qquad (1\text{-}1)$$

where, if R^p is taken to be a p-dimensional vector space over the field of real numbers, then $\underline{x} \in R^n$, $\underline{u} \in R^r$, and $\underline{y} \in R^m$. Further, $\underline{A}(t) = \underline{A}(t + T)$ is an unstable periodic matrix and $\underline{B}$ and $\underline{C}$ are constant matrices. The closed-loop stability analysis of (1.1) by standard Lyapunov methods is complicated

Reproduced with permission of the copyright owner. Further reproduction prohibited without permission.

by its (already calculated) instability when $\underline{u}(\underline{y}) = \underline{0}$, and by the boundedness of the control. That is, if (1-1) is to be stable, the region of stability or domain of attraction is a subset of R^n that is disjoint both from the set specified by the deadband and an unbounded set containing the state points that lie beyond the limited stabilizing effects of $\underline{u}(\underline{y})$. However, some relatively recent results of Yoshizawa [5.4] and LaSalle [5.5, 5.6] are used to establish a framework for describing the stability properties of such systems.

The development of the mathematical model for the system under study is contained in Chapter II. Chapter III is concerned with the development of the zero-fuel mode and Chapter IV, with the tracking problem. The stability of the closed-loop system is considered in Chapter V. Finally, in Chapter VI, the main conclusions are summarized; and some suggestions for future research are made.

Reproduced with permission of the copyright owner. Further reproduction prohibited without permission.

CHAPTER II

THE MATHEMATICAL MODEL

It has often been noted that the dynamical system, from whose definition the fundamentals of modern control theory are developed, is an abstraction. It is a mathematical model whose structure permits deductive generalization by the system theorist. However, the application of control theory to a physical event requires a rigorous justification of the mathematical model (or dynamical system) that is chosen to represent such an event. The purpose of this chapter is to provide this justification by using Newtonian mechanics to develop a dynamical system model of a rigid satellite acted upon by torques due to the gravitational field and the atmospheric density of the Earth.

2.1 Rigid Body Dynamics

The equations of motion of a rigid body are usually developed by considering the body to be a system of n particles subject to the constraint that the distance between any two particles is fixed. For the problem of an Earth-pointing spacecraft, this system of particles is in motion relative to a set of coordinates that are fixed in

Reproduced with permission of the copyright owner. Further reproduction prohibited without permission.

inertial space and whose origin, 0, is at the center of the Earth (the geocenter). The total angular momentum of the spacecraft relative to 0 is given by [2.1]*†

$$\underline{L}_0 = \sum_{i=1}^{n} \underline{R}_i \times m_i \dot{\underline{R}}_i \qquad (2.1\text{-}1)$$

where $\underline{R}_i$ (see Fig. 2) is the vector distance from the geocenter to the i^{th} particle and $\dot{\underline{R}}_i$ is the velocity of that particle relative to inertial coordinates. The time rate of change of angular momentum, $\dot{\underline{L}}_0$, is then

$$\dot{\underline{L}}_0 = \sum_{i=1}^{n} \underline{R}_i \times m_i \ddot{\underline{R}}_i \qquad (2.1\text{-}2)$$

since $\dot{\underline{R}}_i \times \dot{\underline{R}}_i = 0$. Further, from Newton's Second Law,

$$\dot{\underline{L}}_0 = \sum_{i=1}^{n} \underline{R}_i \times \underline{F}_i \triangleq \sum_{i=1}^{n} \underline{N}_i = \underline{N}_0 \qquad (2.1\text{-}3)$$

where $\underline{F}_i$ is the total force acting on the i^{th} particle and $\underline{N}_0$ is defined to be the total torque acting on the rigid body. Since internal forces and torques can be neglected for a rigid

---

*References to the Bibliography are denoted by brackets.

†Notational conventions are explained on p. v.

Reproduced with permission of the copyright owner. Further reproduction prohibited without permission.

body, $\underline{F}_i$ and $\underline{N}_i$ represent respectively the total external force and torque acting on the i^{th} particle. The principle of conservation of angular momentum follows directly from (2.1-3) with $\underline{N}_0 = \underline{0}$.

Consider now another set of coordinates that are parallel to the inertial coordinates but whose origin, 0', is at the center of mass (CM) of the rigid body. As in Fig. 2, the distance 00' will be designated by the vector $\underline{R}_0$ and the position vector to the i^{th} particle from the CM by $\underline{r}_i$. Thus

$$\underline{R}_i = \underline{R}_0 + \underline{r}_i \quad . \tag{2.1-4}$$

The substitution of (2.1-4) into (2.1-2) leads to

$$\dot{\underline{L}}_0 = \sum_{i=1}^{n} (\underline{R} + \underline{r}_i) \times m_i (\ddot{\underline{R}}_0 + \ddot{\underline{r}}_i) \quad . \tag{2.1-5}$$

Using the definition of the CM, $\sum_{i=1}^{n} m_i \underline{r}_i = \underline{0}$, which implies that $\sum_{i=1}^{n} m_i \ddot{\underline{r}}_i = \underline{0}$, and the independence of $\underline{R}_0$ and $\ddot{\underline{R}}_0$ with respect to the summation yields

$$\dot{\underline{L}}_0 = \underline{R}_0 \times M\ddot{\underline{R}}_0 + \sum_{i=1}^{n} \underline{r}_i \times m_i \ddot{\underline{r}}_i \tag{2.1-6}$$

where $M = \sum_{i=1}^{n} m_i$ is the total mass of the system. Thus, the rate of change of angular momentum relative to the geocenter can be considered as a linear combination of the angular

Reproduced with permission of the copyright owner. Further reproduction prohibited without permission.

momentum of the CM relative to the origin plus the angular momentum of the rigid body relative to its CM. It would be convenient if (2.1-6) could be further decomposed into

$$\dot{\underline{L}}_1 = \underline{R}_0 \times \underline{F}_0 = \underline{N}_1 \quad , \tag{2.1-7}$$

and

$$\dot{\underline{L}}_2 = \sum_{i=1}^{n} \underline{r}_i \times \underline{F}_i = \underline{N}_2 \tag{2.1-8}$$

where $\dot{\underline{L}}_0 = \dot{\underline{L}}_1 + \dot{\underline{L}}_2$ and $\underline{N}_1$ and $\underline{N}_2$ represent, respectively, the total external torques acting on the CM relative to the geocenter and on the rigid body relative to its CM. In fact, this is the assumption that is made in most analyses of spacecraft attitude control systems: the motion of a spacecraft can be separated into the motion of the CM about the geocenter and the motion of the spacecraft about its CM. From a practical viewpoint, this assumption is usually perfectly acceptable. Strictly speaking, however, this separation cannot be made and a demonstration of this fact leads to an intuitive introduction to the gravity-gradient torque.

The effect of gravity on a satellite is that of a central force field. That is, the gravitational force acting on the i^{th} particle is parallel to $\underline{R}_i$. Thus, in the absence of all other external forces and from (2.1-3), $\dot{\underline{L}}_0 = \underline{0}$ which, with (2.1-6), implies

Reproduced with permission of the copyright owner. Further reproduction prohibited without permission.

$$\underline{0} = \underline{R} \times M\ddot{\underline{R}}_0 + \sum_{i=1}^{n} \underline{r}_i \times m_i \ddot{\underline{r}}_i \ . \qquad (2.1\text{-}9)$$

Consider the dumbbell in Fig. 3. Since $|\underline{f}_1| > |\underline{f}_2|$ a torque exists about 0', the CM of the rigid body. This implies that the second term on the right hand side of (2.1-8) is non-zero and defines the gravity-gradient torque. Note, however, that this implies that $\underline{R}_0$ and $M\ddot{\underline{R}}_0 = \underline{F}_0$ are not collinear and that a non-central force acts on the CM. Thus, the CM experiences a tangential acceleration as well as a centrifugal [2.2] acceleration. Fortunately, this is very small [2.3] and the approximation (2.1-8) will be assumed throughout this study. In summary, we will be concerned with the control of the rotational motion (or attitude) of a rigid satellite of non-zero extent about its CM.

2.2 Coordinate Systems, Transformations, and Euler Angles

In order to give precise definition to the concept of an attitude, three sets of coordinates must be defined as well as the transformations that relate them. The first of these, illustrated in Figure 4, is the local vertical coordinate system represented by the unit basis vectors $\underline{u}_i$; i = 1,2,3, where:

$\underline{u}_1$ lies along the line joining the center of the Earth (or the geocenter) and the center of mass (CM) of the spacecraft,

Reproduced with permission of the copyright owner. Further reproduction prohibited without permission.

$\underline{u}_3$ is perpendicular to the orbital plane, and

$\underline{u}_2 = \underline{u}_3 \times \underline{u}_1$ completes the orthogonal right triad.

The positive directions of these unit vectors are shown in Figure 4. A three element column vector expressed in this coordinate system will be denoted by $\underline{x}_V$ when the basis vectors are not written explicitly.

The inertial coordinate system and its relationship with the local vertical system is also shown in Figure 4. The unit basis vectors for the inertial system are denoted by $\underline{e}_i$; i = 1,2,3, where:

$\underline{e}_1$ is parallel to the intersection of the noon meridian plane with the orbit plane (That is, if the orbit plane were coplanar with the ecliptic plane, $\underline{e}_1$ would be parallel to the line joining the geocenter with the center of the Sun.),

$\underline{e}_3$ is perpendicular to the orbital plane, and

$\underline{e}_2 = \underline{e}_3 \times \underline{e}_1$ completes the orthogonal right triad.

The positive directions of these vectors are also shown in Figure 4. A three element column vector expressed in the inertial coordinate system will be denoted by $\underline{x}_I$.

Finally, a coordinate system which is fixed relative to the spacecraft is defined. The unit basis vectors, denoted by $\underline{a}_i$; i = 1,2,3, are taken to be coincident with the principal axes of the spacecraft. For a symmetrical vehicle such as that shown in Figure 5, these axes correspond

Reproduced with permission of the copyright owner. Further reproduction prohibited without permission.

with the axes that are controlled by the reaction-jet thrusters. In an unsymmetrical vehicle the application of a control torque about one axis may perturb another. A three element column vector expressed in this coordinate system will be denoted by $\underline{x}_S$.

The origin of each of these coordinate systems is taken to be the spacecraft CM. This is because the motion to be studied (and controlled) is the rotational motion of the spacecraft about its CM.

In order to express the relationships between these coordinate systems, a transformation symbol will be defined. $\underline{\underline{T}}_{\nu}^{y}$ will represent a positive* rotation about the y axis through an angle ν. For example, Figure 4 indicates that a vector whose components in the local vertical system are known can be expressed in the inertial coordinate system by the equation (2.2-1)

$$\underline{x}_I = \underline{\underline{T}}_{-\eta}^{\underline{e}_3} \underline{x}_v = \underline{\underline{T}}_{-\eta}^{\underline{u}_3} \underline{x}_v \ , \qquad (2.2\text{-}1)$$

where if t is the time variable and ω_0 is the constant magnitude of the orbital angular velocity, then $\eta = \omega_0 t$. Further, since the vectors are expressed as 3 x 1 matrices, the transformation is given by a 3 x 3 matrix which is orthogonal.

---

*A positive rotation about a given axis is defined by the familiar right hand rule.

Reproduced with permission of the copyright owner. Further reproduction prohibited without permission.

Due to this fact, the transformations will be referred to as x, y, or z transformations where:

$$\underline{T}^{x}_{\nu} = \begin{bmatrix} 1 & 0 & 0 \\ 0 & \cos\nu & \sin\nu \\ 0 & -\sin\nu & \cos\nu \end{bmatrix} ,$$

$$\underline{T}^{y}_{\nu} = \begin{bmatrix} \cos\nu & 0 & -\sin\nu \\ 0 & 1 & 0 \\ \sin\nu & 0 & \cos\nu \end{bmatrix} ,$$

and

$$\underline{T}^{z}_{\nu} = \begin{bmatrix} \cos\nu & \sin\nu & 0 \\ -\sin\nu & \cos\nu & 0 \\ 0 & 0 & 1 \end{bmatrix} .$$

The letters x, y, and z will correspond respectively to basis vectors with the subscripts 1, 2, and 3. Thus, (2.2-1) can be rewritten as

$$\underline{x}_{I} = \underline{T}^{z}_{-\eta}\, \underline{x}_{v} \quad . \tag{2.2-2}$$

Figure 6 illustrates the relationship of the spacecraft coordinate system relative to the inertial system. This is what is meant by attitude; the rotational displacement of the spacecraft axes from some set of reference coordinates. There are many parameters [2.4] that may be used to specify attitude. The parameters selected for this study are the

Reproduced with permission of the copyright owner. Further reproduction prohibited without permission.

Euler angles [2.1]. These were chosen because they have low dimensionality and, since we will always be dealing with small angles, they are not adversely affected by the "gimbal lock" problem [2.4]. One particularly convenient sequence of these angles is given by

$$\underline{x}_S = \underline{T}_\phi^x \, \underline{T}_\theta^y \, \underline{T}_\psi^z \, \underline{x}_I \qquad (2.2\text{-}3)$$

where the order of operation

$$\underline{x}_S = (\underline{T}_\phi^x(\underline{T}_\theta^y(\underline{T}_\psi^z \underline{x}_I)))$$

is implied. Finally, it is noted that (2.2-2) and (2.2-3) imply

$$\underline{x}_S = \underline{T}_\phi^x \underline{T}_\theta^y \underline{T}_\psi^z \underline{T}^z{}_{-\eta} \, \underline{x}_V \triangleq \underline{T} \, \underline{x}_V \qquad (2.2\text{-}4)$$

and that ψ, θ, and ϕ are defined respectively as the roll, pitch, and yaw angles.

2.3 The Equations of Motion

The equations of rotational motion relative to spacecraft coordinates may now be derived. The Euler equation for such a rigid body motion is given [2.1] by:

$$\underline{I} \, \dot{\underline{\omega}} + \tilde{\underline{\omega}} \, \underline{I} \, \underline{\omega} = \underline{N} \qquad (2.3\text{-}1)$$

where:

$\underline{\omega}$ is a 3 x 1 vector representing the velocity of the spacecraft relative to inertial coordinates,

Reproduced with permission of the copyright owner. Further reproduction prohibited without permission.

$\dot{\underline{\omega}} = d\underline{\omega}/dt$,

$\underline{I}$ is the 3 x 3 inertial matrix,*

$\underline{N}$ is the column vector representation of the sum of all the external torques acting on the spacecraft, and

$\tilde{\underline{\omega}}$ is the 3 x 3 matrix which is isomorphic to the vector cross product and is defined by

$$\tilde{\underline{\omega}} = \begin{bmatrix} 0 & -\omega_3 & \omega_2 \\ \omega_3 & 0 & -\omega_1 \\ -\omega_2 & \omega_1 & 0 \end{bmatrix}$$

where ω_i; i = 1, 2, 3 are the components of $\underline{\omega}$.

All quantities will be expressed in spacecraft coordinates.

Since it is desired to express the spacecraft motion in terms of the Euler angles and their time derivatives, a transformation between $\underline{\omega}$ and the Euler angle rates is required. This transformation illustrated in Figure 6, reflects the unsymmetrical nature of the Euler angles and is developed as follows:

$$\dot{\underline{\phi}}_s = \underline{T}_\phi^x \, \dot{\underline{\phi}} = \dot{\underline{\phi}}$$

$$\dot{\underline{\theta}}_s = \underline{T}_\phi^x \, \underline{T}_\theta^y \, \dot{\theta} = \underline{T}_\phi^x \, \dot{\underline{\theta}}$$

$$\dot{\underline{\psi}}_s = \underline{T}_\phi^x \, \underline{T}_\theta^y \, \underline{T}_\psi^z \, \dot{\underline{\psi}} = \underline{T}_\phi^x \, \underline{T}_\theta^y \, \dot{\underline{\psi}}$$

$$\omega_i = \dot{\phi}_{si} + \dot{\theta}_{si} + \dot{\psi}_{si} \; ; \; i = 1,2,3. \qquad (2.3\text{-}2)$$

---

*This matrix is defined in (B-6) of Appendix B.

Reproduced with permission of the copyright owner. Further reproduction prohibited without permission.

(2.3-2) implies the vector relationship

$$\underline{\omega} = \begin{bmatrix} \omega_1 \\ \omega_2 \\ \omega_3 \end{bmatrix} = \underline{D}\,\dot{\underline{a}} = \underline{D} \begin{bmatrix} \dot{\phi} \\ \dot{\theta} \\ \dot{\psi} \end{bmatrix} . \qquad (2.3\text{-}3)$$

where

$$\underline{D} = \begin{bmatrix} 1 & 0 & -\sin\theta \\ 0 & \cos\phi & \sin\phi\cos\theta \\ 0 & -\sin\phi & \cos\phi\cos\theta \end{bmatrix} .$$

The matrix $\underline{D}$ and the $\tilde{\underline{\omega}}\,\underline{I}\,\underline{\omega}$ term in (2.3-1) assure, in general, a highly nonlinear system even before the determination of the disturbance torques $\underline{N} = \underline{N}(\phi,\theta,\psi,t)$. However, since the control system will be used to keep the spacecraft coordinate very close to the inertial coordinates, some approximations seem possible. These approximations, however, must be verified *a posteriori* by the results of this analysis.

1. The Small Angle Approximation -- If ν is a small Euler angle (ϕ,θ, or ψ), then $\sin\nu \approx \nu$ and $\cos\nu \approx 1$.
2. The Linearization Approximation -- Terms in (2.3-1) that are of order greater than or equal to two are neglected. It will be seen that this approximation is not entirely justified for the example problem considered here and must be replaced by a more accurate approximation. When both of these approximations are applied to (2.3-1) one obtains $\underline{\omega} \approx \dot{\underline{a}}$ and $\tilde{\underline{\omega}}\,\underline{I}\,\underline{\omega} \approx \underline{0}$. Finally, since the spacecraft axes

Reproduced with permission of the copyright owner. Further reproduction prohibited without permission.

coincide with the principal axes of this symmetrical body, $\underline{I}$ is diagonal and

$$\begin{aligned} I_1\ddot{\phi} &= N_1(\phi,\theta,\psi,t) \\ I_2\ddot{\theta} &= N_2(\phi,\theta,\psi,t) \\ I_3\ddot{\psi} &= N_3(\phi,\theta,\psi,t) \end{aligned} \qquad (2.3\text{-}4)$$

where:

I_i; i = 1,2,3 are the moments of inertia about the corresponding principal axis, and N_i; i = 1,2,3 are the components of the external torque along the spacecraft's axes.

The next three sections of this chapter deal with the mathematical models of the gravity-gradient torque, the aerodynamic torque and the control torque.

2.4 The Gravity-Gradient Torque [2.5, 2.6, 2.7]

In §2.1 it was shown that, in general, a torque exists about the CM of a satellite of non-zero extent due to the imbalance of the gravitational force exerted at various points on the body. As might be expected, this torque is a function of the attitude and of the inertial properties of the spacecraft. As shown in Appendix A, the assumptions of an inverse-square law force and a circular orbit lead to the following expression for this effect:

Reproduced with permission of the copyright owner. Further reproduction prohibited without permission.

$$\underline{N}_{gg} = 3\omega_0^2 \, \tilde{\underline{e}}_{ns} \, \underline{I} \, \underline{e}_{ns} \qquad (2.4\text{-}1)$$

where:

ω_0 = the scalar magnitude of the orbital rate; that is the rate at which the CM rotates about the geocentric origin of an inertial coordinate system, and

$\underline{e}_{ns} \triangleq$ the local vertical vector and is a 3 1 column matrix that represents the unit vector $\underline{u}$, in spacecraft coordinates.

The matrix $\underline{I}$ and the tilde operator have been previously defined.

In spacecraft coordinates $\underline{e}_{ns}$ is given by

$$\underline{e}_{ns} = \underline{T} \, \underline{e}_{nv} = \underline{T} \begin{bmatrix} 1 \\ 0 \\ 0 \end{bmatrix} \qquad (2.4\text{-}2)$$

using (2.2-4). Another application of the approximations discussed in §2.3 leads to

$$\underline{e}_{ns} = \begin{bmatrix} \cos(\omega_0 t - \psi) \\ \sin(\omega_0 t - \psi) \\ \theta \cos(\omega_0 t - \psi) - \phi \sin(\omega_0 t - \psi) \end{bmatrix} \qquad (2.4\text{-}3)$$

where it will be recalled that ω_0 represents the magnitude of the orbital angular velocity vector. Note that these expressions have not been expanded to obtain a linear form for ψ. This is explained in the sequel.

Reproduced with permission of the copyright owner. Further reproduction prohibited without permission.

Using (2.4-3) for $\underline{e}_{ns}$ and for the elements of the operator $\tilde{\underline{e}}_{ns}$ results in the following form for the gravity-gradient torque.

$$\underline{N}_{gg}(t) = \begin{bmatrix} K_1\{\phi[1-\cos 2(\omega_0 t-\psi)] - \theta \sin 2(\omega_0 t-\psi)\} \\ K_2\{-\phi \sin 2(\omega_0 t-\psi) + \theta[1+\cos 2(\omega_0 t-\psi)]\} \\ K_3 \sin 2(\omega_0 t-\psi) \end{bmatrix} \qquad (2.4\text{-}4)$$

where:

$$K_1 = \frac{3\omega_0^2}{2}(I_2 - I_3)$$

$$K_2 = \frac{3\omega_0^2}{2}(I_1 - I_3)$$

$$K_3 = \frac{3\omega_0^2}{2}(I_2 - I_1) \quad .$$

Note from (2.4-4) that $\underline{N}_{gg}(t)$ has the following properties:

(i) The torque about a spacecraft principal axis is proportional to the numerical difference between the moments of inertia about the other two principal axes.

(ii) The x and y components of $\underline{N}_{gg}(t)$ are proportional to x and y attitude displacements and enter the differential equation (2.3-4) as time-varying coefficients of the dependent variables θ and ϕ. On the other hand, the z component of $\underline{N}_{gg}(t)$ is

Reproduced with permission of the copyright owner. Further reproduction prohibited without permission.

easily expanded into a periodic forcing term plus a term that acts as a time varying coefficient of ψ.

(iii) If $\psi(t)$ were periodic of period $T/N = \pi/N\omega_0$, $N = 1,2,\ldots$, then all the time-varying coefficients become periodic with period T. For example,

$$\cos 2[\omega_0(t+T) - \psi(t+T)] = \cos 2[\omega_0(t+T) - \psi(t)]$$

$$= \cos 2\omega_0(t+T)\cos 2\psi(t) +$$

$$+ \sin 2\omega_0(t+T)\sin 2\psi(t)$$

$$= \cos 2\omega_0 t \cos 2\psi(t) +$$

$$+ \sin 2\omega_0 t \sin 2\psi(t)$$

$$= \cos 2[\omega_0 t - \psi(t)].$$

2.5 The Aerodynamic Torque

After the rediscovery of the effects of the gravitational torque acting on an Earth satellite, some research was directed towards the analysis of the effect of the Earth's atmosphere. This effect is called the aerodynamic torque and is a function of the geometry of the spacecraft and of the density of the atmosphere. The work done in this area in [2.8] through [2.12] was concerned with Earth-pointing rather

Reproduced with permission of the copyright owner. Further reproduction prohibited without permission.

than inertially stabilized satellites and all but [2.11] assumed a constant atmospheric density. An analysis of the aerodynamic torque acting on spacecraft with rectangular solar panels was given by Yu [2.13]. Elrod [2.14] later showed that [2.13] was in agreement with the results obtained by Meirovitch and Wallace [2.10]. A derivation of the mathematical model for the aerodynamic torque that is based on the above results is given in Appendix A. If this model is combined with an accurate mathematical model for the atmospheric density, then results are obtained that are in close agreement with those obtained with the detailed model used by Nurre [2.11]. An explanation of the atmospheric density model used in this analysis is now given.

The atmosphere of the Earth has been studied for many years [2.15]. One of the results of this work is that the density of the atmosphere varies not only with altitude but also with solar activity [2.16]. The latter causes some interesting cyclic variations in the atmospheric density at a given altitude. They are:

1. An eleven-year cycle over which the atmospheric density varies because of the cyclic nature of solar activity. A plot of this variation vs. time (in years) is given in Figure 7.
2. An effect that varies as the orbital frequency. This is due to the fact that, to first order, the atmosphere may be considered to be rotating in

Reproduced with permission of the copyright owner. Further reproduction prohibited without permission.

inertial space with the Earth at one revolution per day. As the atmosphere becomes more or less heated by the Sun, it becomes more or less dense at a given altitude. This effect is known as the diurnal bulge and is considered in the sequel.

3. Various other seasonal effects that are much less significant and, therefore, will be neglected in this analysis.

The atmospheric density variation with the 11-year solar cycle can be neglected for periods of several days. If necessary, for long missions, measurements could be taken to allow occasional updates of this information to be commanded by the ground crew. On the other hand, the effects are included in general by considering the atmospheric density to be modelled by a Fourier Series. But, since a too complicated model obscures the effects illustrated in later chapters, the atmospheric density, ρ, will be considered constant. It should be remembered, however, that the results given in Chapter 3 are valid for, and would be implemented using, the Fourier Series model of the density.

The expression for the aerodynamic torque derived in Appendix A is repeated in (2.5-1).

Reproduced with permission of the copyright owner. Further reproduction prohibited without permission.

$$\underline{N}_a(t) = \begin{bmatrix} [2.08\ N_{MC} + 2\sigma_r(2-\sigma')N_{MP}|\sin(\omega_0 t-\psi)|]\cos(\omega_0 t-\psi) \\ [2.08\ N_{MC} + 2(2-\sigma')N_{MP}|\sin(\omega_0 t-\psi)|]\sin(\omega_0 t-\psi) \\ 0 \end{bmatrix} \quad (2.5\text{-}1)$$

The quantities in (2.5-1) are defined in Appendix B. In particular N_{MC} and N_{MP} are proportional to ρ.

Since ρ and $|\sin(\omega_0 t-\psi)|$ can both be represented by Fourier series whose fundamental radian frequency is ω_0, $\underline{N}_a(t)$ appears as a periodic torque that is phase-modulated by the variation of $\psi(t)$. It will be recalled that $\psi(t)$ may be solved for independently of ϕ and θ. The most important result of the periodicity of $N_a(t)$ is that it can be used to develop the zero-fuel oscillatory attitude of the spacecraft that was discussed in Chapter 1.

2.6 The Control Torque and Typical RCS Control Laws

The control torque for this problem is supplied by two triads of reaction-jet thrusters (or rockets) affixed 180 degrees apart on the lower end of the spacecraft as shown in Figure 5. These thrusters impart a constant torque on the spacecraft by expelling part of their mass;* the variability of control effort being achieved by changing the firing time (also called ignition time or just "on-time"). Control systems with thrusters acting as the controller are usually called reaction control systems (RCS).

---

*This mass is very much less than the mass of the space-station considered in the sequel which is taken to be constant.

Reproduced with permission of the copyright owner. Further reproduction prohibited without permission.

The basic thruster equation is [3.3]

$$F = \dot{m} v_e = \frac{\dot{w} v_e}{g} = \dot{w} I_{sp} \qquad (2.6\text{-}1)$$

where:

F = the force (in lbs.) imparted to the spacecraft by the thruster,

$\dot{m}$ = the time rate of mass (or propellant) expulsion in slugs/sec,

v_e = exhaust velocity in ft/sec,

g = gravitational constant = 32.2 ft/sec^2,

$\dot{w}$ = propellant flow rate in lbs/sec,

$I_{sp} = v_e/g$ = specific impulse in sec.

For attitude control applications the firing time is very much shorter than any of the time constants associated with the system dynamics. In addition, the magnitude of the control torque is considerably larger than the maximum of the sum of the disturbance torques. These two factors lead to certain approximations* in the calculation of the response of the spacecraft to thruster ignitions.

We begin with a modification of (2.3-1).

$$\underline{I}\,\dot{\underline{\omega}} + \tilde{\underline{\omega}}\,\underline{I}\,\underline{\omega} = \underline{N} = \underline{N}_D + \tilde{\underline{r}}_T\,\underline{F} \qquad (2.6\text{-}2)$$

---

*These approximations, considered only generally in this section, are specifically evaluated for this application in Chapter III.

Reproduced with permission of the copyright owner. Further reproduction prohibited without permission.

where:

$\underline{N}_D$ = the vector sum of all external disturbance torques acting on the spacecraft, and

$\underline{r}_T$ = the moment arm of the thruster relative to the CM of the spacecraft.

All of the other quantities are defined in (2.3-1) or (2.6-1). If (2.6-2) is integrated over the firing interval, Δt, of a thruster, we get

$$\underline{I}\ \underline{\Delta\omega} + \int_{t_0}^{t_0+\Delta t} \tilde{\underline{\omega}}\ \underline{I}\ \underline{\omega}\ dt = \int_{t_0}^{t_0+\Delta t} \underline{N}_D(t)dt + \tilde{\underline{r}}_T\underline{F}\ \Delta t \qquad (2.6\text{-}3)$$

where $\underline{\Delta\omega}$ is the change in angular rate over the interval. Now if as mentioned above, $\tilde{\underline{r}}_T\underline{F} >> \max||\underline{N}_D(t)||$ and Δt is such that

$$||\underline{I}\ \underline{\Delta\omega}|| >> ||\int_{t_0}^{t_0+\Delta t} \tilde{\underline{\omega}}\ \underline{I}\ \underline{\omega}\ dt||$$

then

$$\underline{\Delta H} = \underline{I}\ \underline{\Delta\omega} \simeq \tilde{\underline{r}}_T\underline{I}_t \qquad (2.6\text{-}4)$$

where:

$\underline{\Delta H}$ = the total change in spacecraft angular momentum during the firing interval, and

Reproduced with permission of the copyright owner. Further reproduction prohibited without permission.

$\underline{I}_t = \underline{F}\Delta t \triangleq$ the total impulse imparted to the spacecraft by the thruster.

It is also possible to calculate the amount of propellant (or fuel) that is expended per firing. From (2.6-1) and (2.6-4) it follows that

$$w = \dot{w}\Delta t = \frac{F\Delta t}{I_{sp}} = \frac{I_t}{I_{sp}} \quad . \tag{2.6-5}$$

The basic properties of thrusters explained above are necessary for the following discussion of typical RCS control laws. Consider Figure 8, which is a plot of specific impulse, I_{sp}, vs. thruster on-time, Δt. Because of the time constants associated with the relays, valves, and propellant ignitions in a thruster system, the exhaust velocity and, therefore, (from 2.6-1) the I_{sp} requires a certain interval to build up to a steady-state value. Further, it is seen from (2.6-5) that the amount of propellant required to produce a given I_t is inversely proportional to I_{sp}. This means that I_t's requiring a $\Delta t < t_1$ (Fig. 8) represent an inefficient use of propellant. For this reason, RCS control laws usually specify a minimum allowable firing time, Δt_m. Another quantity, $I_{tm} = F\Delta t_m$ is then defined as the minimum impulse bit or MIB.

Reproduced with permission of the copyright owner. Further reproduction prohibited without permission.

The MIB requirement precludes the possibility of a linear feedback RCS control law. This can be shown by considering the uncoupled, scalar, second-order system with scalar control given by (2.6-6).

$$\ddot{x} = f(x, \dot{x}, t) + \mu(x, \dot{x})$$
$$\mu(x, \dot{x}) = -c_1 x - c_2 \dot{x} \qquad (2.6\text{-}6)$$

where x and $\dot{x}$ are the system state variables and μ is the control. A graphical representation of this problem is shown in Figure 9a in which Γ_- is the region of negative torque application, Γ_+ is the region of positive torque application and Γ is the switching line. Note that the small control effort required by (2.6-6) for state points close to Γ cannot be realized by a control system with a MIB requirement, without causing a chattering system response. To avoid this problem, a deadband or region of no control as shown in Figure 9b is usually incorporated into RCS control laws.

In summary, the logical sequence of this section has been as follows:

i- in order to use propellant in an efficient manner, a minimum firing time, which results in a MIB, is always specified for an RCS,

Reproduced with permission of the copyright owner. Further reproduction prohibited without permission.

ii- the MIB in turn leads to the incorporation of a deadband in RCS control laws.

These properties will be referred to extensively in the sequel.

2.7 Summary

Combining the results of sections 2.3 to 2.6 leads to the mathematical model for an inertially-oriented satellite with RCS control. It is convenient to divide equations (2.3-4), (2.4-4) and (2.5-1) by the appropriate moments of inertia to yield

$$\ddot{\phi} = \{\alpha_1^2[\phi(1-\cos 2(\omega_0 t-\psi) - \theta \sin 2(\omega_0 t-\psi)] + \\ + [\lambda_{1c} + \lambda_{1p}|\sin(\omega_0 t-\psi)|] \cos(\omega_0 t-\psi) + \lambda_{c1}\}$$

$$\ddot{\theta} = \{\alpha_2^2[-\phi \sin 2(\omega_0 t-\psi) + \theta(1+\cos 2(\omega_0 t-\psi))] + \\ + [\lambda_{2c} + \lambda_{2p}|\sin(\omega_0 t-\psi)|] \sin(\omega_0 t-\psi) + \lambda_{cs}\} \qquad (2.7\text{-}1)$$

$$\ddot{\psi} = -\alpha_3^2 \sin 2(\omega_0 t-\psi) + \lambda_{c3} \simeq 2\alpha_3^2 \psi \cos 2\omega_0 t - \alpha_3^2 \sin 2\omega_0 t + \lambda_{c3} .$$

where:

$\alpha_i^2 = K_i|I_i$; $i = 1,2,3$, are the coefficients of that component of spacecraft angular acceleration $\dot{\underline{\omega}}$ produced by the gravity-gradient torque,

$\lambda_{jc} = 2.08\ N_{MC}|I_j$; $j = 1,2$, are the coefficients of $\dot{\underline{\omega}}$ produced by the aerodynamic torque on the cylindrical portion of the spacecraft,

Reproduced with permission of the copyright owner. Further reproduction prohibited without permission.

$\lambda_{1p} = 2\sigma_r(2-\sigma')N_{MP}|I_1$ is the x-axis coefficient of $\dot{\underline{\omega}}$ produced by the aerodynamic torque on the solar panels,

$\lambda_{2p} = 2(2-\sigma')N_{MP}|I_2$ is the y-axis coefficient of $\dot{\underline{\omega}}$ produced by the aerodynamic torque on the solar panels, and

λ_{ck}; k = 1,2,3 are the coefficients of $\dot{\underline{\omega}}$ produced by the control torque.

There are several aspects of (2.7-1) which are worthy of note. First, as previously mentioned, the equation for ψ is uncoupled and may be solved independently of the other equations. Next, note the reason for not using the small angle approximation to expand sines and cosines of the argument $(\omega_0 t-\psi)$; it is more accurate and, because $\psi(t)$ will be known, does not make the system non-linear. In addition, it illustrates the way the roll axis motion, ψ, modulates the sinusoidal functions in the pitch, θ, and the yaw, ϕ, axis equations. Finally, note that, using standard techniques, e.g.[4.2], equations (2.7-1) can be expressed as a single, linear, vector differential equation of the form

$$\dot{\underline{x}} = \underline{A}(t)\underline{x} + \underline{z}(t) + \underline{Gu}(t) \qquad (2.7\text{-}2)$$

where:

$\underline{x}$ is a 6 x 1 column vector defining the state of the system, i.e., the transpose of $\underline{x}$ is

$\underline{x}' = [\phi\ \dot{\phi}\ \theta\ \dot{\theta}\ \psi\ \dot{\psi}]$,

Reproduced with permission of the copyright owner. Further reproduction prohibited without permission.

$\underline{z}(t) = \underline{z}(t+T)$ is a 6 x 1 vector of disturbance torques divided by appropriate moments of inertia,

$\underline{G}$ is a 6 x 3 constant matrix,

$\underline{u}(t)$ is a 3 x 1 vector of control torques divided by appropriate moments of inertia, and

$\underline{A}(t)$ is given by

$$\begin{bmatrix} 0 & 1 & 0 & 0 & 0 & 0 \\ \alpha_1^2[1-\cos 2(\omega_0 t-\psi)] & 0 & -\alpha_1^2 \sin 2(\omega_0 t-\psi) & 0 & 0 & 0 \\ 0 & 0 & 0 & 1 & 0 & 0 \\ -\alpha_2^2 \sin 2(\omega_0 t-\psi) & 0 & \alpha_2^2[1+\cos 2(\omega_0 t-\psi)] & 0 & 0 & 0 \\ 0 & 0 & 0 & 0 & 0 & 1 \\ 0 & 0 & 0 & 0 & -\alpha_3^2 \sin(\omega_0 t-\psi) & 0 \end{bmatrix}. \quad (2.7\text{-}3)$$

In Chapter III, extensive reference will be made to the uncontrolled system

$$\dot{\underline{x}} = \underline{A}(t)\underline{x} + \underline{z}(t) \quad (2.7\text{-}4)$$

where $\underline{A}(t)$ is given by (2.7-3) and $\underline{z}(t)$ by

$$\underline{z}(t) = \begin{bmatrix} 0 \\ [\lambda_{1c} + \lambda_{1p}|\sin(\omega_0 t-\psi)|]\cos(\omega_0 t-\psi) \\ 0 \\ [\lambda_{2c} + \lambda_{2p}|\sin(\omega_0 t-\psi)|]\sin(\omega_0 t-\psi) \\ 0 \\ 0 \end{bmatrix}.$$

Reproduced with permission of the copyright owner. Further reproduction prohibited without permission.

CHAPTER III

A ZERO-FUEL MODE

3.1 Introduction

As discussed in Chapters I and II, the gravity-gradient and aerodynamic torques act as persistent external torques on an inertially stabilized Earth-satellite. This means, in general, that the reaction control system (RCS) must act continuously to offset the effects of these disturbances. Therefore, a control law designed without considering a minimum-fuel strategy could result in considerable expenditure of propellant and a large number of thruster firings.* The latter effect is noteworthy because the reliability of the RCS is inversely dependent on the number of operations. A practical example of these statements is furnished by an early model of the Orbital Workshop (OWS) of NASA's Skylab Program. The OWS was planned to be manned for successive missions of 28 and 56 days while being controlled by an RCS with a linear deadband control law. The estimated total propellant consumption for holding an inertial attitude was in excess of 60% of the total propellant capability and the

*Details of thruster operation were discussed in §2.6.

Reproduced with permission of the copyright owner. Further reproduction prohibited without permission.

estimated total number of thruster ignitions exceeded the number of times for which these engines had ever been tested [3.1], [3.2].

Optimal control of a process acted on by external disturbances is a problem that has not received much attention in the literature; the machinery of Pontryagin's Maximum Principle and the calculus of variations being more suited to the analysis of systems driven only by controlled inputs. However, some work has been done ([3.3] - [3.6]) regarding the minimum-fuel solution for the case of a system described by (3.1-1)

$$\dot{\underline{x}} = \underline{A}_0\underline{x} + \underline{z}_0 + \underline{u}(\underline{x}) \qquad (3.1\text{-}1)$$

where $\underline{A}_0$ is a constant 2 x 2 matrix, $\underline{z}_0' = [0 \quad z_0]$* a constant vector, and $\underline{u}' = [0 \quad u(x)]$ a control vector with $\underline{u}(\underline{x})$ including a deadband. The generalization of the results of [3.3] to [3.6] to n-dimensional periodic systems with periodic forcing functions provides the main result of this Chapter. Further, it is shown that the basic motivation leading to this result arises from purely physical considerations. These ideas are presented in detail in §3.2.

---

*The prime indicates the transpose of a matrix.

Reproduced with permission of the copyright owner. Further reproduction prohibited without permission.

3.2 Some Physical Considerations

The essence of the results in [3.3] - [3.6] can be explained using Figure 10. In this figure a typical state-space trajectory is given that corresponds to the zero-state solution of the scalar differential equation

$$\ddot{x} = \lambda_0 + \lambda_c(x) \qquad (3.2\text{-}1)$$

where λ_0 is a constant disturbance and $\lambda_c(x)$ is the deadband control law* defined by the switching lines Γ_1 and Γ_2. The state-space trajectory that corresponds to the zero state solution of (3.2-1) when $|x| < x_d$ is denoted by γ_1 in Figure 10. When $x = x_d$, a thruster firing occurs† that can produce one of three possible trajectories.

γ_2 represents the case when the system is given so much negative velocity that the resulting trajectory is caused to contact the opposite deadband at $x = -x_d$. This results in another firing that reverses the velocity (produces a turning point) of the trajectory before it can be reversed (produced) by λ_0. On the contrary, trajectories γ_3 and γ_4 of Figure 10 do allow the turning point to be produced by λ_0 and are shown

---

*See §2.6 and Figs. 20 and 21.

†Usually $\lambda_c(x_d) >> \lambda_0$.

Reproduced with permission of the copyright owner. Further reproduction prohibited without permission.

by Regetz and Nelson [3.3] to be minimum-fuel solutions.* However, as observed in [3.3], trajectory γ_4 is preferable to γ_3 because it corresponds to a longer coasting time, thereby requiring fewer thruster ignitions. Mendel [3.6] extended this analysis to systems described by the scalar equation.

$$\ddot{x} \pm ax = \lambda_0 + \lambda_c(x)$$

where a is constant and all other variables are as defined in (3.2-1).

The previous analyses contain two unstated basic principles that can be used to extend the above results to obtain a minimum-fuel RCS control strategy for systems with non-constant disturbances. In particular, we wish to investigate systems with periodic disturbances. These principles are:

(P1) control action should be taken only when its effects oppose the effects of the disturbances, and

(P2) the control action should act so as to maximize the coasting time between firings.

For a system with periodic forcing functions, the application of these two principles leads to the concept of firing the thrusters in such a way as to allow the periodic

---

*This result, which assumes ideal thruster characteristics, implies that the amount of propellant consumed with the minimum-fuel strategy is proportional to the integral over time of λ_0.

Reproduced with permission of the copyright owner. Further reproduction prohibited without permission.

disturbance torque to produce as many consecutive turning points as possible. In fact, given the initial value problem corresponding to (2.7-4) with $\underline{x}(t_0) = \underline{x}_0$, i.e.,

$$\dot{\underline{x}}(t) = \underline{A}(t)\underline{x}(t) + \underline{z}(t);\ \underline{x}(t_0) = \underline{x}_0$$
$$\underline{A}(t) = \underline{A}(t+T),\ \underline{z}(t) = \underline{z}(t+T)\ , \tag{3.2-1}$$

the following question could be asked. Does there exist an $\underline{x}_0$ such that the solution $\underline{x}(t;\ \underline{x}_0,\ t_0)$ of (3.2-1) is periodic? If the answer is in the affirmative, if $\underline{x}_0$ can be established by the RCS, and if the amplitude of $\underline{x}(t;\ \underline{x}_0,\ t_0)$ is small enough to be compatible with program objectives, then a three-axis limit cycle motion that is produced entirely by the disturbances exists. This means, under ideal circumstances, that once the state point is properly initialized, no further control action is necessary. The oscillatory solution, $\underline{x}_p(t;\ \underline{x}_0,\ t_0)$ of (3.2-1) is then a trajectory which requires no fuel expenditure beyond initialization. It will be called the zero-fuel mode.

It must now be demonstrated to what extent the three hypotheses of the above paragraph can be met by a system that is controlled by an RCS. In the next section a proof for the existence of a periodic solution of (3.2-1) that also provides an algorithm for achieving the zero-fuel mode with a practical control system is given. The results of §3.3 are applied in §3.4 to the system under study. In addition, the second and third hypotheses of the previous paragraph are discussed.

Reproduced with permission of the copyright owner. Further reproduction prohibited without permission.

In §3.5 an attempt is made to verify a posteriori the approximations made in §2.3. A failure to achieve this verification leads to an improved linearized model for the system (2.7-4).

3.3 Conditions for Periodicity and an Algorithm

The original approach for the determination of a unique $\underline{x}_0$ for the periodic solution of (3.2-1) was reported in [3.2]. This approach demonstrated the existence of such a solution by the method of successive approximations. Subsequent to [3.2] an alternative proof was developed by S. C. Chu [3.7] that also provided an algorithm for the computation of the desired $\underline{x}_0$ by a digital computer. A similar existence proof is given by Brockett in [3.8]. The material in this section is due to Chu.

THEOREM 3.1

Let $\underline{\Phi}(t, t_0)$ be the state transition matrix of the homogeneous system corresponding to (3.2-1), i.e.,

$$\dot{\underline{x}} = \underline{A}(t)\underline{x} \quad . \tag{3.3-1}$$

Assume also that $\det[\underline{\Phi}(T+t_0, t_0) - \underline{I}] \neq 0$ or, equivalently, that $\underline{\Phi}(T+t_0, t_0)$ does not have one as an eigenvalue. Then,

(a) there exists a unique solution to system (2.7-4) that is periodic with period T for $\underline{z}(t) = \underline{z}(t+T)$, and

(b) system (3.3-1) possesses no periodic solutions of period T.

PROOF: Part (b) is proved first. Any solution of (3.2-1) can be written as

Reproduced with permission of the copyright owner. Further reproduction prohibited without permission.

$$\underline{x} = \underline{\Phi}(t, t_0)\underline{x}_0 + \int_{t_0}^{t} \underline{\Phi}(t,\tau)\underline{z}(\tau)d\tau \quad . \qquad (3.3\text{-}2)$$

Suppose that $\underline{x}$ is a solution of (3.3-2) with $\underline{z}(t) = \underline{0}$ and is periodic with period T. Then,

$$\underline{x}(T+t_0) = \underline{x}_0 = \underline{\Phi}(T+t_0, t_0)\underline{x}_0 \quad , \qquad (3.3\text{-}3)$$

which contradicts the hypothesis that 1 is not an eigenvalue of $\Phi(T+t_0, t_0)$.

Next, the uniqueness part of (a) is proved. Suppose that $\underline{x}(t)$ is a periodic solution of (3.2-1) with period T. Then, from (3.3-2)

$$\underline{x}(T+t_0) = \underline{x}_0 = \underline{\Phi}(T+t_0, t_0)\underline{x}_0 + \int_{t_0}^{T+t_0} \underline{\Phi}(T+t_0,\tau)\underline{z}(\tau)d\tau \quad . \qquad (3.3\text{-}4)$$

Multiplying (3.3-4) by $\underline{\Phi}(t_0, T+t_0) = \underline{\Phi}^{-1}(T+t_0, t_0)$ and subtracting $\underline{x}_0$ yields

$$[\underline{\Phi}(t_0, T+t_0)-\underline{I}]\underline{x}_0 = \int_{t_0}^{T+t_0} \underline{\Phi}(t_0,\tau)\underline{z}(\tau)d\tau \quad . \qquad (3.3\text{-}5)$$

Since the eigenvalues of an inverse matrix, $\underline{M}^{-1}$, are reciprocals of the eigenvalues of $\underline{M}$

$$\det[\underline{\Phi}(t_0, t_0+T)-\underline{I}] \neq 0$$

Reproduced with permission of the copyright owner. Further reproduction prohibited without permission.

Thus, $\underline{x}_0$ is uniquely determined from (3.3-5) and yields in turn the unique solution, $\underline{x}(t)$, of (3.3-2).

Finally, the existence of the periodic solution is proved. Since $[\underline{\Phi}(t_0, t_0+T)-\underline{I})]$ is nonsingular, define $\underline{x}_0$ by (3.3-4). For this $\underline{x}_0$ define $\underline{x}_p(t)$ to be the solution of the initial value problem (3.2-1) with $\underline{x}_0$ defined by (3.3-5). We wish to show that $\underline{x}_p(t+t_0) = \underline{x}_p(t+T+t_0)$. By (3.3-2)

$$\underline{x}_p(t+T+t_0) = \underline{\Phi}(t+T+t_0,t_0)\underline{x}_0 + \int_{t_0}^{t+T+t_0} \underline{\Phi}(t+T+t_0,\tau)\underline{z}(\tau)d\tau \quad . \quad (3.3\text{-}6)$$

In addition to the well-known properties of the state transition matrix, the following property that holds when $\underline{A}(t) = \underline{A}(t+T)$ will be useful [3.7]:

$$\underline{\Phi}(t+T+t_0, t_0) = \underline{\Phi}(t+t_0, t_0)\underline{\Phi}(T+t_0, t_0) \quad .$$

Use of these properties leads to the rewriting of (3.3-6) as

$$\underline{x}_p(t+T+t_0) = \left\{ \underline{\Phi}(t+t_0,t_0)\left[\underline{\Phi}(T+t_0,t_0)\underline{x}_0 + \int_{t_0}^{T+t_0} \underline{\Phi}(T+t_0,\tau)\underline{z}(\tau)d\tau \right] + \int_{T+t_0}^{t+T+t_0} \underline{\Phi}(t+T+t_0, \tau)\underline{z}(\tau)d\tau \right\} . \quad (3.3\text{-}7)$$

Reproduced with permission of the copyright owner. Further reproduction prohibited without permission.

But the quantity within the square brackets has been defined to be $\underline{x}_0$. Thus,

$$\underline{x}_p(t+T+t_0) = \underline{\Phi}(t+t_0,t_0)\underline{x}_0 + \int_{T+t_0}^{t+T+t_0} \underline{\Phi}(t+T+t_0,\tau)\underline{z}(\tau)d\tau \quad . \quad (3.3\text{-}8)$$

Now let the variable $\mu \triangleq \tau - T$ in (3.3-8) and note by the periodicity of $\underline{A}(t)$ that $\underline{\Phi}(t+t_0+T,\ \tau+T) = \underline{\Phi}(t_0+t,\tau)$. Then

$$\underline{x}_p(t+T+t_0) = \underline{\Phi}(t+t_0,t_0)\underline{x}_0 + \int_{t_0}^{t_0+t} \underline{\Phi}(t_0+t,u)\underline{z}(u)du = \underline{x}_p(t+t_0)$$

which was to be proved.

As previously mentioned, this proof leads to an algorithm for determining the periodic solution of system (2.7-4), i.e.,

$$\begin{aligned} &\dot{\underline{x}}(t) = \underline{A}(t)\underline{x}(t) + \underline{z}(t) \quad , \\ &\underline{A}(t) = \underline{A}(t+T),\ \underline{z}(t) = \underline{z}(t+T) \quad . \end{aligned} \qquad (2.7\text{-}4)$$

The procedure is as follows:

(a) Obtain $\underline{\Phi}(t_0+T,\ t_0)$ by numerically integrating

$$\dot{\underline{\Phi}}(t,t_0) = \underline{A}(t)\Phi(t,t_0)$$

from t_0 to $T+t_0$.

Reproduced with permission of the copyright owner. Further reproduction prohibited without permission.

(b) If $[\underline{\Phi}(t_0+T, t_0)-\underline{I})$ is nonsingular, then by (3.3-5)

$$\underline{x}_0 = [\underline{\Phi}(t_0+T, t_0)-\underline{I}]^{-1} \int_{t_0}^{T+t_0} \underline{\Phi}(t_0, \tau)\underline{z}(\tau)d\tau \quad . \qquad (3.3\text{-}9)$$

(c) Solve the initial value problem (3.2-1) with x_o defined by (3.3-9).

3.4 Applications and Insights

If the maximum value of the solution, $\underline{x}_p(t)$ of (3.2-1) is within bounds that are compatible with mission constraints, then $\underline{x}_p(t)$ is the desired trajectory for the system. However, no real system is capable of establishing exactly the desired state at any instant although the continuity of solutions of (3.2-1) with initial conditions assures that small errors in the establishment of, say $\underline{x}_o$ will result in a solution that closely approximates $\underline{x}_p(t)$ (at least for some period). If $\underline{A}(t)$ were a stable matrix, then the above-mentioned continuity would guarantee that, barring changes in $\underline{z}(t)$, any initialization close to $\underline{x}_o$ would result in a solution that remains close to $\underline{x}_p(t)$. However, if $\underline{A}(t)$ is unstable (as it is shown to be in Chapter V for the system under study), then the RCS must be used to keep the actual trajectory close to the desired trajectory. A control law for accomplishing this is developed in Chapter IV.

Reproduced with permission of the copyright owner. Further reproduction prohibited without permission.

The proof in §3.3 also provides some physical insight into the nature of the periodic motion $\underline{x}_p(t)$, which will henceforth be called the zero-fuel mode. First, since $[\underline{\Phi}(T+t_0, t_0) - I]$ is non-singular, the unique periodic solution of (2.7-4) is forced. That is, the homogeneous system (3.3-1) cannot possess a periodic solution of period T. Now, for the system under study, an examination of (2.7-4) reveals that the ψ equation is uncoupled and unaffected by the aerodynamic torque. Thus, the periodic ψ motion (of period T/2) is produced by the gravity-gradient torque. This torque is caused by the fact that the solar panels, being held in an inertial attitude, are almost never in equilibrium with the Earth's gravitational field (see Figure 11). On the other hand, the only forcing terms in the coupled equations for ϕ and θ are aerodynamic torque terms. Thus, the oscillatory ϕ and θ solutions are produced by aerodynamic rather than by gravity-gradient effects. A physical explanation of these statements is given by the following example.

EXAMPLE

Consider the special case of (2.7-4) when $I_1 = I_2$, that is when the spacecraft is a perfect cylinder without solar panels. This assumption implies the following relationships:

Reproduced with permission of the copyright owner. Further reproduction prohibited without permission.

$$\alpha_1^2 = \alpha_2^2 = \alpha^2 \quad , \quad \alpha_3^2 = 0 \quad ,$$

$$\lambda_1^c = \lambda_2^c = \lambda \quad , \quad \lambda_1^p = \lambda_2^p = 0 \quad ,$$

and (2.7-4) takes the form

$$\ddot{\psi} = 0$$

$$\begin{aligned} \ddot{\phi} &= \alpha^2[\phi(1-\cos 2\omega_0 t) - \theta \sin 2\omega_0 t] + \lambda \cos(\omega_0 t - \psi) \\ \ddot{\theta} &= \alpha^2[-\phi \sin 2\omega_0 t + \theta(1+\cos 2\omega_0 t)] + \lambda \sin(\omega_0 t - \psi) \end{aligned} \qquad (3.4\text{-}1)$$

where, it will be recalled, the bracketed terms are due to the gravity-gradient torque $\underline{N}_{gg}(t)$ and the forcing terms to the aerodynamic torque, $\underline{N}_a(t)$. Suppose further that the solution to $\ddot{\psi} = 0$ is $\psi = \dot{\psi} = 0$. Now, if the forcing function is to provide the turning points of the motion as discussed in §3.2, then we expect the motions ϕ and θ to be in opposition to the disturbances. Therefore, we test the solution

$$\begin{aligned} \phi_p &= -\lambda \cos \omega_0 t / \omega_0^2 \\ \theta_p &= -\lambda \cos \omega_0 t / \omega_0^2 \end{aligned} \qquad (3.4\text{-}2)$$

for the nontrivial equations of (3.4-1). When ϕ_p and θ_p are inserted into (3.4-1), it is found that not only does (3.4-2) qualify as a solution but it causes an exact cancellation of

Reproduced with permission of the copyright owner. Further reproduction prohibited without permission.

the bracketed terms in (3.4-1). That is, the x and y axis acceleration caused by $\underline{N}_{gg}(t)$ is identically zero. The physical interpretation of this result is that the spacecraft is driven by the aerodynamic torque in such a way that it is always in equilibrium with the gravitational field.

When $I_1 \neq I_2$, the algorithm of §3.3 is applied first to the uncoupled equation for ψ. Once ψ is a known function of time, the ϕ and θ equations are linear and may be subjected to a second application of the algorithm. When the parameters of the system under study are used with appropriate models of the disturbances, the oscillations obtained are as shown in Figure 12. This motion* results in a reduction of approximately 1% of the average electrical power from the solar panels.

Two final remarks can be made regarding the periodic solution of (2.7-4). First, it adheres to the two principles stated in §3.2. That is, a proper initialization causes the motion to act in opposition to the disturbance and the resulting coasting time is maximized (ideally it is infinite). Secondly, since the determination of $\underline{x}_o$ by the algorithm depends only on the nonsingularity of $[\underline{\Phi}(T+t_0, t_0) - \underline{I}]$, which in turn depends only on $\underline{A}(t)$, the result holds for any forcing function with period T. Thus, as mentioned in Chapter II, any Fourier series model of the aerodynamic torque can be used.

3.5 Refinement of Mathematical Model

The mathematical model for the physical event under consideration was presented in detail in Chapter II. In the

---

*The maximum values shown in Figure 12 are $\max|\phi(t) \simeq 3°$, $\max|\theta(t) \simeq 4°$ and $\max|\dot{\psi}(t)| \simeq 9.8°$.

Reproduced with permission of the copyright owner. Further reproduction prohibited without permission.

course of the development of this model certain linearizing assumptions were made. In this section it is seen that these approximations are not entirely justified but that a more refined set of linear equations can be developed to produce excellent results.

As mentioned in Chapter II, an a posteriori test for the validity of the linearization procedure was planned. The nature of this test is as follows:

1. Apply the algorithm of §3.3 with the linearized equation (2.7-4) to determine the $\underline{x}_0$ that results in a periodic solution of (2.7-4);
2. Use this $\underline{x}_0$ as an initial condition for the non-linear equations of motion given by (2.3-1), i.e., solve

$$\underline{I}\,\dot{\underline{\omega}} + \tilde{\underline{\omega}}\,\underline{I}\,\underline{\omega} = \underline{N} \quad , \qquad (2.3\text{-}1)$$

with $\underline{\omega}_0$ defined by $\underline{x}_0$ through (2.3-3) and (2.7-2).

The results, as shown in Figure 13, are that the solution to the non-linear initial-value problem is not periodic and grows without bound as $t \to \infty$.

In an effort to refine the model, the magnitudes of the state variables of the periodic solution to the linearized equations (Figure 12) were determined. The equations of motion beginning with (2.3-1) were rederived and terms were kept or dropped depending on their contribution to the total motion rather than on the basis of linearity. A short description of this process is given for illustrative purposes.

Reproduced with permission of the copyright owner. Further reproduction prohibited without permission.

We begin with the z-axis equation because of its simplicity. The z component of equation (2.3-1) after division by I_3 is given by

$$\dot{\omega}_3 + K_3\omega_1\omega_2 = N_3/I_3 \quad .$$

As mentioned in §2.3, the principal contributing non-linearities enter the system equation through:

(1) the relationship between $\underline{\omega}$ and the Euler rates $\dot{\underline{a}}$ given by (2.3-3), and

(2) the $\tilde{\underline{\omega}}\ \underline{I}\ \underline{\omega}$ term.

Using the small angle approximation (§2.3), which is valid to 0.5%, it can be shown that

$$\begin{aligned} \dot{\omega}_3 &= \ddot{\psi} - \phi\ddot{\theta} - \dot{\phi}\dot{\theta} \quad , \text{ and} \\ \omega_1\omega_2 &= \dot{\phi}\dot{\theta} - \theta\dot{\theta}\dot{\psi} + \phi\dot{\phi}\dot{\psi} - \phi\theta\dot{\psi}^2 \end{aligned} \qquad (3.5\text{-}1)$$

An investigation of the maximum values of ϕ, θ, ψ, and their first and second derivatives leads to the results in Table 1.

It is seen that the

$(\cdot)$ \ $f(\cdot)$	$\max\lvert(\cdot)\rvert$	$\max\lvert(\dot{\cdot})\rvert$, $(\text{sec})^{-1}$	$\max\lvert(\ddot{\cdot})\rvert$, $(\text{sec})^{-2}$
ϕ	.051	9.6×10^{-5}	7.5×10^{-8}
θ	.073	7.0×10^{-5}	12.3×10^{-8}
ψ	.166	34.4×10^{-5}	78.0×10^{-8}

MAXIMUM VALUES OF PERIODIC SYSTEM VARIABLES

TABLE 1

Reproduced with permission of the copyright owner. Further reproduction prohibited without permission.

only linear term in (3.5-1) is $\ddot{\psi}$, whose maximum value is 78.0×10^{-8} radians/sec^2. If the maximum values of all other variables in (3.5-1) are appropriately multiplied and compared with max $|\ddot{\psi}|$, it is seen that the largest of these is less than 1% of max $|\ddot{\psi}|$. Based on these results, the linearization approximation of §2.3 is considered to be justified and the ψ equation, rewritten as (3.5-2), is still uncoupled.

$$\ddot{\psi} = \alpha_3^2[2\psi \cos 2\omega_0 t - \sin 2\omega_0 t] \qquad (3.5\text{-}2)$$

The y-axis component of (2.3-1) after division by I_2 is given by

$$\dot{\omega}_2 + K_2 \omega_1 \omega_3 = N_2/I_2$$

where, from (2.3-5)

$$\dot{\omega}_2 = \ddot{\theta} + \phi\ddot{\psi} + \dot{\phi}\dot{\psi} \ , \quad \text{and}$$

$$\omega_1\omega_3 = \dot{\phi}\dot{\psi} - \theta\dot{\psi}^2 - \phi\dot{\phi}\dot{\theta} + \phi\theta\dot{\theta}\dot{\psi} \ . \qquad (3.5\text{-}3)$$

Now, the linear term in (3.5-3) is $\ddot{\theta}$, where maximum value is 12.3×10^{-8} radians/sec^2. Compared to max $|\ddot{\theta}|$, and letting the maximum of the absolute value of a variable be represented by a subscripted m, i.e.,

$$\max |\ddot{\theta}| = \ddot{\theta}_m$$

Reproduced with permission of the copyright owner. Further reproduction prohibited without permission.

we find:

$$\frac{\phi_m \ddot{\psi}_m}{\ddot{\theta}_m} = .32 \ ,$$

$$\frac{\dot{\phi}_m \dot{\psi}_m}{\ddot{\theta}_m} = .27 \ ,$$

$$\frac{K_2 \dot{\phi}_m \dot{\psi}_m}{\ddot{\theta}_m} = .26 \ , \qquad (3.5\text{-}4)$$

$$\frac{K_2 \theta_m \dot{\psi}_m^2}{\ddot{\theta}_m} = .07 \ .$$

The remaining two terms, which are less or equal to 0.2% of $\ddot{\theta}_m$ are dropped, but equations (3.5-4) must be included in the mathematical model of the y-axis motion. Two aspects of equations (3.5-4) are worthy of note.

(1) their large size is due to the large variation of ψ relative to the variations of ϕ and θ;

(2) the fact that the z-axis equation is still uncoupled implies that the y-axis equation is still linear in ϕ and θ once $\dot{\psi}$ is known.

The x-axis equation after division by I_1, is given by

$$\dot{\omega}_1 + K_1 \omega_2 \omega_3 = N_1/I_1$$

where, from (2.3-3)

Reproduced with permission of the copyright owner. Further reproduction prohibited without permission.

$$\dot{\omega}_1 = \ddot{\phi} - \theta\ddot{\psi} - \dot{\theta}\dot{\psi}$$

$$\omega_2\omega_3 = \dot{\theta}\dot{\psi} + \phi\dot{\psi}^2 - \phi\dot{\theta}^2 - \phi^2\dot{\psi}\dot{\theta} \quad . \qquad (3.5\text{-}5)$$

The linear term in (3.5-4) is $\ddot{\phi}$ whose absolute value $|\ddot{\phi}_m| = 7.5 \times 10^{-8}$ sec^{-1}. Compared to this term

$$\frac{\theta_m\ddot{\psi}_m}{\ddot{\phi}_m} = .76$$

$$\frac{\dot{\theta}_m\dot{\psi}_m}{\ddot{\phi}_m} = .32 \qquad (3.5\text{-}6)$$

$$\frac{|K_1|\dot{\theta}_m\dot{\psi}_m}{\ddot{\phi}_m} = .28$$

$$\frac{|K_1|\phi_m\dot{\psi}_m^2}{\ddot{\phi}_m} = .07 \quad .$$

The remaining terms are less than 0.2% of $\ddot{\phi}_m$ and are dropped but equations (3.5-6) must be included in the x-axis equation. Also, as with the y-axis equation, the unusual size of the terms in (3.5-6) is due to the relatively large size of the ψ motion relative to the variation of the ϕ and θ motions.

Reproduced with permission of the copyright owner. Further reproduction prohibited without permission.

When the expressions for the mathematical models of the gravity-gradient and aerodynamic torques are rederived using the linearization procedure of this section, the results justify the standard linearization procedures of Chapter II to within 0.4%. These expressions will remain unchanged in the new mathematical model of the system and the environment, which is given by equation (3.5-7).

$$\ddot{\psi} = \alpha_3^2[2\,\psi \cos 2\omega_0 t - \sin 2\omega_0 t] \qquad \text{(a)}$$

$$\ddot{\theta} = \{-\phi[\alpha_2^2-\alpha_3^2]\sin 2(\omega_0 t-\psi) + \theta[K_2\dot{\psi}^2 + \alpha_2^2(1 + \cos 2(\omega_0 t-\psi))] \qquad \text{(b)}$$

$$- (1+K_2)\dot{\phi}\dot{\psi} + (\lambda_2^c + \lambda_2^p|\sin(\omega_0 t-\psi)|)\sin(\omega_0 t-\psi)\} \qquad (3.5\text{-}7)$$

$$\ddot{\phi} = \{\phi[|K_1|\dot{\psi}^2 + \alpha_1^2(1 - \cos 2(\omega_0 t-\psi))] - \theta(\alpha_1^2+\alpha_3^2)\sin 2(\omega_0 t-\psi) \qquad \text{(c)}$$

$$+ (1+|K_1|)\dot{\psi}\dot{\theta} + (\lambda_1^c + \lambda_1^p|\sin(\omega_0 t-\psi)|)\cos(\omega_0 t-\psi)\} .$$

The most noteworthy aspects of (3.5-7) are that the ψ equation is still uncoupled and once ψ, $\dot{\psi}$, and $\ddot{\psi}$ are known functions of time, equations (b) and (c) of (3.5-7) are linear. Thus, the algorithm of §3.3 can still be used to determine the initialization vector and the desired trajectories for variables ϕ, θ, and ψ. When the new value of $\underline{x}_o$ is used as an initial condition, the results are as shown in Figure 14. In the light of errors in the exact specification of an $\underline{x}_o$ by a real system, these results are considered acceptable for any practical application.

Reproduced with permission of the copyright owner. Further reproduction prohibited without permission.

CHAPTER IV

THE TRACKING PROBLEM

As previously mentioned, the zero-fuel mode developed in Chapter III can be implemented with a reaction-control system (RCS) by specifying the oscillatory motion as a desired trajectory and devising a control policy that keeps the actual state near the desired state. The nature of the control policy will depend on the stability of the oscillatory motion. If this motion is asymptotically stable, i.e., if every motion close to the desired trajectory approaches that trajectory with increasing time, then the function of the control system is merely one of initialization. If, however, the zero-fuel mode is an unstable motion (as it will be shown to be for the system under study, then the control system must act continuously to keep the actual state close to the desired state. In either case, the control system causes the state of the system to "track" the desired state.

In §4.2 the question of the stability of the zero-fuel motion for the system under study in considered. First, since the z-axis motion is uncoupled, it can be considered separately. It is found that this motion is stable (but not

Reproduced with permission of the copyright owner. Further reproduction prohibited without permission.

asymptotically stable). Next, necessary and sufficient conditions are demonstrated for the instability of the x and y axis motion. Both of these results are obtained from an application of Floquet theory.

§4.3 is concerned with optimal control laws for the z-axis tracking problem. The Maximum Principle of Pontryagin is applied and leads to a sub-optimal policy, which is, in turn, rejected for physical reasons. However, this study yields considerable insight into the nature of the z-axis motion and proves useful in explaining the results obtained with a more easily implemented control strategy.

A modified form of the aforementioned linear deadband control law is chosen to control the required x, y, and z axis tracking. No optimal control law for the x and y axis problem is considered because of the complicated form of the appropriate dynamical equations. Once again, however, some physical insight is gained from the results of §4.2 and used to determine control parameters. A digital computer simulation of the plant and its environment is employed to demonstrate the superiority of the overall approach (zero-fuel mode plus tracking) taken in this paper compared with conventionally designed systems.

4.2 Stability of the Uncontrolled Minimum-Fuel Mode Motion

We begin this section with some basic definitions [4.1]. Consider the forced dynamical system described by the vector differential equation

Reproduced with permission of the copyright owner. Further reproduction prohibited without permission.

$$\dot{\underline{x}} = f(\underline{x}, t, \underline{z}(t)) \qquad (4.2\text{-}1)$$

Where as usual $\underline{x}\varepsilon R^n$ is the state vector, $t\varepsilon R$ the independent time variable and $\underline{z}\varepsilon R^n$ a vector of forcing functions. Solutions to (4.2-1) will be denoted by $\underline{\phi}_z(t; \underline{x}_0, t_0)$ where $\underline{x}_0$ and t_0 respectively represent the initial state and the initial time. Solutions of (4.2-1) are also called motions or trajectories and can be represented as curves in the state space.

Definition 4.1 The motion $\underline{\phi}_z(t; \underline{x}_0, t_0)$ is stable if for all t_0 and positive ε there is a $\delta(\varepsilon, t_0)$ such that

$$||\underline{\phi}_z(t; \underline{x}_0, t_0) - \underline{\phi}_z(t; x_1, t_0)|| < \varepsilon$$

for all $t \geq t_0$ if $||\underline{x}_0 - \underline{x}_1|| < \delta$. If the motion is stable and also converges, i.e., if for any t_0 there is a $\delta_1(t_0) > 0$ such that $||\underline{x}_0 - \underline{x}_1|| < \delta_1$ implies

$$\lim_{t\to\infty} ||\underline{\phi}_z(t; \underline{x}_0, t_0) - \underline{\phi}_z(t; \underline{x}_1, t_0)|| = 0 \qquad (4.2\text{-}2)$$

then the motion is defined to be asymptotically stable.

The problem of the stability of a desired motion can always be reduced to the problem of the stability of an equilibrium point by considering perturbations away from the desired trajectory. This technique is considered in detail in Appendix C and forms the basis for the analysis that follows. However, since the zero-fuel mode trajectory is a

Reproduced with permission of the copyright owner. Further reproduction prohibited without permission.

bounded periodic motion, it might be interesting to discuss the concept of orbital stability [4.1] and reasons why we have not applied it to the system under study.

Definition 4.2 A periodic solution, $\underline{\phi}_z(t; \underline{x}_0, t_0)$ of (4.2-1) generating a closed trajectory C in the state space is orbitally stable if, for any positive ε and for any $\underline{x}_0$ and t_0 that yield the solution traversing C, there exists a $\delta > 0$ such that

$$||\underline{x}_1 - \underline{x}_0|| < \delta$$

implies

$$d[\underline{\phi}_z(t; \underline{x}_1, t_0), C] \triangleq d[\underline{\phi}_{z1}, C] < \varepsilon$$

for $t \geq t_0$. The distance $d[\underline{\phi}_{z1}, C]$ of the state point from the curve C is defined as

$$d[\underline{\phi}_{z1}, C] = \inf(||\underline{x} - \underline{y}||), \ \underline{y} \in C \quad . \quad (4.2\text{-}3)$$

Note that orbital stability requires only that the actual motion be close to the totality of points on C or, alternatively, to any point in the set C at any time. This concept is useful for stationary systems. For non-stationary systems, such as the one studied in this research, stability must be considered as in Definition 4.1. That is, the actual

Reproduced with permission of the copyright owner. Further reproduction prohibited without permission.

phase* of a stable system must remain close to the desired phase. This definition is stronger than orbital stability.

It is shown in Appendix C that if the variable ε measures perturbations from the periodic solution of (3.5-7) then

$$\underline{\dot{\varepsilon}} = \hat{\underline{A}}(t)\underline{\varepsilon} + 0(\varepsilon^2) \qquad (4.2\text{-}4)$$

where the elements $\hat{a}_{ij}$ of $\hat{A}(t)$ are given by (C-10) and the variables ψ_p, θ_p and ϕ_p are defined by the periodic solution of (3.5-7). Thus, the entire matrix $\hat{\underline{A}}(t)$ is periodic of period $T = 2\pi/\omega_0$. The local stability of the null solution of (4.2-4) can be determined by analyzing the stability of the null solution of linear system

$$\dot{\underline{\varepsilon}} = \hat{\underline{A}}(t)\underline{\varepsilon} \quad . \qquad (4.2\text{-}5)$$

Theorems to this effect are given in [4.1] and [4.2]. The stability properties of (4.2-5) are well known and are usually attributed to Floquet and/or Lyapunov. The basic result is presented as

---

*A phase space is a state space which has been augmented by the addition of the time axis. A phase point is an element of the phase space. The expression "the phase of the system $(\underline{x}_0, t_0)$" is preferable to "the state of the system $\underline{x}_0$ at time t_0". More precisely, if the state of the system is described by points in an n-dimensional Euclidean space R^n and if R is the set of all real numbers, elements of the phase space are points in the space defined by the Cartesian product $R^n \times R$.

Reproduced with permission of the copyright owner. Further reproduction prohibited without permission.

THEOREM 4.1

The transition matrix, $\underline{\hat{\Phi}}(t, t_0)$ of the periodic system (4.2-5) can always be written as

$$\underline{\hat{\Phi}}(t, t_0) = \underline{P}(t)\underline{e}^{\underline{J}(t-t_0)}\underline{P}(t_0)^{-1}$$

where $\underline{P}(t)$ is a nonsingular periodic matrix with the same period as $\underline{A}(t)$ and $\underline{J}$ is a constant matrix.

The proof of this theorem is straightforward and can be found in either of the previously cited references. The stability of (4.2-5) is determined by the eigenvalues of $\underline{\hat{\Phi}}(T, 0) = \underline{e}^{\underline{J}T}$. The main results are presented as theorems after the following definition.

Definition 4.2. The eigenvalues of $\underline{\hat{\Phi}}(T, 0) = \underline{e}^{\underline{J}T}$ are called the characteristic multipliers of the matrix.

THEOREM 4.2

The null solution of (4.2-5) is uniformly stable if and only if the matrix $\underline{\hat{A}}(t)$ has no characteristic multipliers of magnitude greater than one.* If all characteristic multipliers have magnitudes that are strictly less than one, then the null solution of (4.2-5) is uniformly asymptotically stable.

---

*Theorems 4.2 and 4.2 hold only when $\underline{\hat{\Phi}}(T, 0)$ has distinct eigenvalues. Extensions of these theorems to the multiple eigenvalue case is discussed in [4.1].

Reproduced with permission of the copyright owner. Further reproduction prohibited without permission.

THEOREM 4.3

The null solution of (4.2-5) is unstable if and only if one or more of the characteristic multipliers is greater in magnitude than one. The proofs of Theorems 4.2 and 4.3 can be found in Gantmacher [4.3].

The stability of the system under study can now be determined using a digital computer and the following procedure:

1. Use the results of §3.3 to determine those initial conditions that produce a periodic solution of (3.5-7).
2. Solve system (3.5-7) with these initial conditions for ψ_p, θ_p, and ϕ_p as well as their derivatives.
3. Solve the initial value problem

$$\dot{\underline{\hat{\Phi}}}(t) = \underline{\hat{A}}(t)\underline{\hat{\Phi}}(t) \ ,$$
$$\underline{\hat{\Phi}}(0) = \underline{I} \ , \text{ the identity matrix,} \qquad (4.2\text{-}6)$$

   using the stored values of the variables determined in step 2.
4. Determine the eigenvalues of $\hat{\Phi}(T, 0)$.

For the system under study this procedure leads to the eigenvalues: 3,088., 301.6, $(4 \pm i8) \times 10^{-4}$, and $-.977 \pm i\ .215$.* Thus, from Theorem 4.3, the periodic solution of (3.5-7) is in general unstable. However, the eigenvalues

*Mass data for the Skylab vehicle is given in [3.2].

Reproduced with permission of the copyright owner. Further reproduction prohibited without permission.

$-.977 \pm i\ .215$, of unit magnitude, correspond to the z-axis motion. This motion is, therefore, stable* by Theorem 4.2. Plots of the solution of the initial value problem (4.2-4) are given in Figures 15(a) through 15(f). These plots were made relative to the variable $\tau = \omega_0 t$, which makes all of the states of the system more nearly equal in magnitude and, therefore, easier to plot. The shape of the curves is unchanged by this step; only the scale is altered.

4.3 Some Thoughts on Optimal Control Laws for the Uncoupled Second Order System

It was shown in §4.2 that perturbations of solutions of the system equation away from the zero-fuel mode (4.2-5) are unstable. Thus, the reaction control system (RCS) must be used to keep the phase of the perturbed trajectory close to the phase of the desired trajectory (the zero-fuel mode). To achieve this, a control strategy (or law) must be devised.

The complicated form of the x and y axis equations of (4.2-5) suggests that any optimal control law developed for the general, three axis tracking problem will be correspondingly complicated and difficult to implement. However, since the

---

*Note that only the linearized equation for the z-axis motion is stable. Recall [4.1, pp. 127, 128] that, without asymptotic stability of the linearized equation, local stability of the corresponding non-linear equation cannot be inferred. However, Figure 14 shows that the non-linear equations describing z-axis motion produces a trajectory that, at least for durations less than T, is very similar to the trajectory obtained with the linear equations.

Reproduced with permission of the copyright owner. Further reproduction prohibited without permission.

z axis motion

i - does not depend on the motions about the x and y axes, and

ii - is more sensitive to applied torques than the motions about the axes with larger moments of inertia (see Figure 12),

there may be some advantage to an optimal control law for the partitioned second order system of (4.2-5), i.e.,

$$\dot{\underline{w}}(t) = \underline{F}(t)\underline{w}(t) + \underline{b}u(t) \ . \qquad (4.3\text{-}1)$$

In this equation: $\underline{w}' = [w_1, w_2] = [\varepsilon_5, \varepsilon_6]$ measures the deviation of the actual z axis motion from the minimum-fuel trajectory; $\underline{b}' = [0 \ b_0]$; u(t) is a scalar quantity that can assume the values 0, 1, -1; and

$$\underline{F}(t) = \begin{bmatrix} 0 & 1 \\ 2\alpha_3^2 \cos 2\omega_0 t & 0 \end{bmatrix} \ .$$

Note that the use of the variables ε_5 and ε_6 rather than x_5 and x_6 reduce the tracking problem to a form of the regulator problem. That is, the origin of the ε_5 - ε_6 phase plane is tracked instead of the moving target set formed by the trajectory of the zero-fuel solution in the x_5 - x_6 phase plane. However, we are precluded from using the powerful machinery

Reproduced with permission of the copyright owner. Further reproduction prohibited without permission.

available for the solution of the linear regulator problem* because the RCS is incapable of providing the continuous control effort required by that solution. The RCS can produce the "bang-bang" results that are obtained from minimum-time and minimum-fuel solutions to (4.3-1). Therefore, since our primary objective is to reduce fuel consumption, we will investigate the minimization of

$$J(u) = \int_{t_0}^{t_1} b_0 |u(t)| dt \qquad (4.3\text{-}2)$$

subject to the constraint imposed by (4.3-1). The method used to accomplish this investigation will be the Maximum (or Minimum [4.4]) Principle of Pontryagin, which is given by THEOREM 4.4.

Given the system (4.3-1), let $u^*(t)$ be an admissible control that transfers $(\underline{w}_0, t_0)$ to $(0, t_1)$. Let $\underline{w}^*(t)$ be the trajectory of (4.3-1) corresponding to $u^*(t)$ and which has the appropriate boundary conditions, i.e., $\underline{w}^*(t_0) = \underline{w}_0$ and $\underline{w}^*(t_1) = \underline{0}$. In order that u^* be optimal for the cost functional (4.3-2), it is necessary that there exists a function $p^*(t)$ such that

---

*Roughly speaking this problem is as follows: find the admissible control $u^*(\underline{x}, t)$ that takes the phase of (4.3-1) from some $(\underline{w}_0, t_0) \rightarrow (\underline{0}, t_1)$ and minimizes the functional

$$J(w, u) = \int_{t_0}^{t_1} [\underline{w}'\underline{Q}(t)\underline{w} + \underline{u}'\underline{R}(t)\underline{u}] dt \ .$$

Reproduced with permission of the copyright owner. Further reproduction prohibited without permission.

a. $\dot{\underline{w}}^* = \frac{\partial H}{\partial \underline{p}} [\underline{w}^*, \underline{p}^*, u^*, t] = \underline{F}(t)w^* + \underline{b}u^*$, and

(4.3-3)

$$\dot{\underline{p}}^* = - \frac{\partial H}{\partial \underline{w}} [\underline{w}^*, \underline{p}^*, u^*, t] = -F'(t)\underline{p} ,$$

with the boundary conditions specified as above and where H (the Hamiltonian of the system) is defined by

$$H(\underline{w}, \underline{p}, u, t) = |u| + \underline{p}'[\underline{F}(t)\underline{w} + \underline{b}u(t)] .$$

b. $H[\underline{w}^*, \underline{p}^*, u^*, t] \leq H[\underline{w}^*, \underline{p}^*, u, t]$.

c. The function $H[\underline{w}^*, \underline{p}^*, u^*, t]$ satisfies relations

$$H[\underline{w}^*, \underline{p}^*, u^*, t] = - \int_t^{t_1} \frac{\partial H}{\partial t} [\underline{w}^*(\tau), \underline{p}^*(\tau), u(\tau), \tau] d\tau$$

and

$$H[\underline{w}^*(t_1), \underline{p}^*(t_1), u^*(t_1), t_1] = 0$$

where t_1 is the terminal plane.

Application of condition b of the theorem leads to the control law

$$u^*(t) = \begin{cases} 0, & |p_2^*| < 1 \\ -1, & p_2^* > 1 \\ 1, & p_2^* < -1 \end{cases} = \text{cst}(p_2) , \qquad (4.3-4)$$

Reproduced with permission of the copyright owner. Further reproduction prohibited without permission.

where u* is undetermined when $p_2 = \pm 1$. If an optimal control exists, it is given by (4.3-4). To complete the problem, two more questions must be considered. First, it is necessary to establish that the u* given by (4.3-4) is the optimal solution. Secondly, a relationship must be developed between the state and the costate variables in order that u* can be given as a function of the state.

While the state and costate variables can be related at t_1 by a set of transversality conditions when a finite-dimensional target set is defined, there are no easy analytical relationships between these variables for our problem.* For these reasons, an alternate approach that demonstrates the plausibility that (4.3-3) is an optimal solution is taken. This approach also leads to a specification of the control as a function of the state.

Equation (4.3-1) is an undamped Mathieu equation whose properties are well known [4.6]. The fuel-optimal control of a system that was partly described by a lightly damped Mathieu equation was studied by Busch and Flugge-Lotz [4.7]. They showed by using a trial and error solution of the TPBVP that the RCS firings for this problem should occur in the vicinity of the vertical (i.e., $\underline{w} = \underline{0}$) axis of the state space. Further simulation studies on the location of the switching

---

*The simultaneous solution of (4.3-3) requires solution of a two-point boundary value problem (TPBVP) for which, because of the lack of transversality conditions, the boundary values are not all known.

Reproduced with permission of the copyright owner. Further reproduction prohibited without permission.

lines for various initial conditions led them to the sub-optimal control law given by (4.3-5) and shown in Figure 16.

$$u = \begin{cases} \text{cst}(x_2) & \text{for } x_2^2 \geq c_5|x_1| \\ 0 & \text{for } x_2^2 < c_5|x_1| \end{cases} \qquad (4.3\text{-}5)$$

where cst(·) is defined by (4.3-4) and c_5 is a constant determined by simulation.

These results are similar in form to the fuel optimal and time-optimal solutions for a linear harmonic oscillator. For the fuel optimal problem, Flugge-Lotz and Craig [4.8] showed that switching lines should take the form shown in Figure 17. For this case too, then, RCS firings occur when the displacement is near a minimum. A complete analysis of the time-optimal control problem for the linear harmonic oscillator (including a demonstration of sufficient as well as necessary conditions) is given by Kalman in [4.5]. For this problem the switching lines in the state space are circular as in Figure 18.

Now, for cases when the control torque produces large motions relative to those that result from perturbations away from the equilibrium, all of the above results approach each other. Also, since the control torque is large, it will be applied for a very short time relative to any of the frequencies in the plant dynamics. Then, if the control torque

Reproduced with permission of the copyright owner. Further reproduction prohibited without permission.

is represented by a Dirac delta function, the switching line is defined by the $\underline{w} = \underline{0}$ line in the state space. That it is only possible to drive the system (4.3-1) to equilibrium with a delta function if it is applied when $\underline{w} = \underline{0}$ will now be demonstrated. Following this, an example will be given to demonstrate that it is one possible fuel-optimal solution.

The representation formula for the solution of (4.3-1) is

$$\underline{w}(t) = \underline{\Phi}(t, t_0)\underline{w}_0 + \int_{t_0}^{t} \underline{\Phi}(t, \tau)\underline{b}u(\tau)d\tau \qquad (4.3\text{-}6)$$

where the system is given the perturbation $\underline{w}_0$ at initial time t_0 and $\underline{\Phi}(t, t_0)$ is the state transition matrix. Now suppose the control is a Dirac delta function applied at some time $t_c > t_0$, i.e.,

$$u(t) = \delta(t-t_c) \ . \qquad (4.3\text{-}7)$$

Then, if t_c- and t_c+ are defined, respectively, as the instants immediately before and after application of (4.3-7), we can write, using (4.3-6)

$$\underline{w}(t_c-) = \underline{\Phi}(t_c-, t_0)\underline{w}_0 \ ,$$

and

$$\underline{w}(t_c+) = \underline{\Phi}(t_c+, t_0)\underline{w}_0 + \int_{t_c-}^{t_c+} \underline{\Phi}(t_c+, \tau)\underline{b}\delta(\tau-t_c)d\tau .$$

Reproduced with permission of the copyright owner. Further reproduction prohibited without permission.

Now, because of the continuity of the state transition matrix, and

$$\underline{\Phi}(t_c-, t_0) = \underline{\Phi}(t_c+, t_0) = \underline{\Phi}(t_c, t_0)$$

and

$$\int_{t_c-}^{t_c+} \underline{\Phi}(t_c+, \tau)b\delta(\tau-t_c)d\tau = \underline{\Phi}(t_c, t_c) \int_{t_c-}^{t_c+} \underline{b}\delta(\tau-t_c)d\tau$$

$$= \underline{b} \int_{t_c-}^{t_c+} \delta(\tau-t_c)d\tau = \underline{b} \quad .$$

The change in state that is caused by $u(t) = \delta(t-t_c)$ is, then,

$$\underline{w}(t_c+) - \underline{w}(t_c-) = \begin{bmatrix} w_1(t_c+) - w_1(t_c-) \\ \\ w_2(t_c+) - w_2(t_c-) \end{bmatrix} = \begin{bmatrix} 0 \\ \\ b_0 \end{bmatrix} \qquad (4.3\text{-}8)$$

The conclusion that is drawn from (4.3-8) is that a control application of the form (4.3-7) can only change the w_2 component of system (4.3-1). Further, it is seen from Figure 15(a) that the system can never intersect the origin of the state space when $u(t) = 0$. Thus, if the control is a

Reproduced with permission of the copyright owner. Further reproduction prohibited without permission.

delta function, the only solution to the previously stated Optimal Control Problem that satisfied the boundary condition occurs when the $\underline{w} = \underline{0}$ line is the switching curve.

If the control is a delta function, it can be shown by an example that its application at $\underline{w} = \underline{0}$ results in a local "minimum-fuel" solution.* Consider the sketch in Figure 19 where the mass m and the support 0 of the pendulum are in the horizontal plane xz. That is, xz represents a table-top that will be considered frictionless with respect to the motion of m. In addition, the support will be free to move along the z axis. The rod of the pendulum is light and inextensible. The equation that describes the small, rotational motion of m in response to force f(t) in the z direction and applied at the support is

$$\ddot{w} = \frac{L}{I} f(t)\sin w \simeq \frac{L}{I} f(t)w \qquad (4.3\text{-}9)$$

where:

L = the length of the rod and

I = the moment of inertia of m about 0.

Choosing $Lf(t)/I = 2\alpha_3^2 \cos 2\omega_0 t$ yields (4.3-1). Notice that there is no applied torque when $\underline{w} = 0$. Suppose that a control is applied when $\underline{w} = \underline{0}$ in Figure 19. The amount of propellant consumption is by (2.6-5) proportional to I_t. Now suppose

---

*Of course, since this solution is the only one that satisfies the boundary conditions of the control problem when u(t) is a delta function, this solution must be optimal.

Reproduced with permission of the copyright owner. Further reproduction prohibited without permission.

the same control were applied when $\underline{w} \neq \underline{0}$. Then, even though its velocity will be nulled or reversed, the pendulum will continue to rotate. Thus, another application of the control, applied when $\underline{w}$ is again equal to zero, is necessary to satisfy the boundary conditions of the optimal control problem.

The conclusion that is drawn from the above is that, when u(t) is nearly able to be represented by a Dirac delta-function, a suboptimal control law can be generated with the switching lines given by the portion of the curves close to the ordinate in any of the Figures 16 through 18.

4.4 A Practical Control Strategy

The suboptimal strategies for minimum-fuel control of the z-axis motion discussed in §4.3, while suitable in an ideal case, share a practical shortcoming. This is best explained with the help of Figure 15(a), which is a state space trajectory of the solution of (4.3-1). By noting the times at which the trajectory intersects the $\dot{w}$ axis, it can be seen that the time interval between firing regions exceeds the orbital period. Thus, if for some reason (such as venting of an on-board fluid) the state were displaced by a relatively large amount, it could go uncorrected for a considerable length of time. Now, even though this trajectory is locally stable, (C-9) shows that it is coupled by the elements $\hat{a}_{26}$ and $\hat{a}_{46}$ into the x and y axis motions. Further, as shown in Figures 15(c) - 15(f), the latter trajectories are

Reproduced with permission of the copyright owner. Further reproduction prohibited without permission.

unstable. Therefore, the z-axis perturbation described above could result in a substantial propellant expenditure for the control of the x and y axis motions.

What is needed is a control law that keeps the actual trajectory suitably close to the desired trajectory and utilizes as much as possible the insight gained from the sub-optimal strategies; i.e., the most efficient firings occur in the vicinity of the $\dot{w}$ axis. For this reason (and because it is easily implemented) a linear deadband control law such as the one shown in Figure 9(b) is used. Of course, this policy will be relative to the zero-fuel mode trajectory rather than to the origin of the $z - \dot{z}$ phase plane. In order to avoid the chattering that can obtain because of the minimum impulse bit firing (see §2.6), the slope of the switching lines must be quite steep for a desired deadband of 0.5 degrees. Enough rate control is included, however, to ascertain that firings usually will not occur when the state is in the second or fourth quadrant.

It is obvious that the linear deadband control law does not guarantee that every firing will be optimally efficient. However, this shortcoming is counteracted by its superior stability characteristics which, in turn, are responsible for lower propellant consumption about the pitch and yaw axis.

Reproduced with permission of the copyright owner. Further reproduction prohibited without permission.

A steep linear deadband control law was also tried relative to the oscillatory trajectories about the x and y axes. This was chosen because of the similarity of the perturbed x and y axis trajectories to the unstable systems studied by Mendel [3.6] who obtained minimum-fuel solutions with the deadband shown in Figure 10.

The three-axis linear deadband control law relative to the minimum-fuel trajectory was tested on a full non-linear digital computer simulation with the following results:

1. A substantial reduction in the propellant consumption was achieved relative to the performance of the linear deadband control law without the zero-fuel mode.
2. This improvement in performance was achieved solely by the reduction in roll (z) axis propellant consumption.

Result 2 will be discussed first. The first simulation runs used to test the zero-fuel mode included only the uncoupled roll axis oscillatory trajectory as a target set. The results of these runs are discussed below. When the oscillatory trajectories of the pitch and yaw axes were added, no improvement in propellant consumption was noted. The reasons for this result are as follows:

(i) An examination of equation (C-9) shows that the perturbed equations of motion relative to the minimum-fuel solution are identical to the unperturbed equations (3.5-7) except for the replacement of the

Reproduced with permission of the copyright owner. Further reproduction prohibited without permission.

aerodynamic forcing functions by the terms $a_{26}\varepsilon_6$ and $a_{46}\varepsilon_6$. These latter terms may also be considered as forcing functions because ε_5 and ε_6 are uncoupled and may be determined separately. The fact that the perturbed equation is non-homogeneous and unstable requires a consistent application of thruster action to maintain the actual pitch and yaw motions close to the desired motions.

(ii) The width of the deadband (which is necessary because of the minimum impulse bit) also serves to obscure the difference between the performance of the systems (C-9) and (3.5-7). If a linear controller (i.e., $u = cx$) with no deadband were available to control all three axes, the perturbed trajectory would stay close to the desired solution. This would reduce the effect of both the forcing ($\hat{a}_{26}\varepsilon_6$ and $\hat{a}_{46}\varepsilon_6$) terms and the gravity-gradient torques that are proportional to the deviations ε_1 to ε_4 of the trajectory from the periodic solution of (3.5-7). A substantial improvement in minimum-fuel mode performance would be expected with this hypothetical controller. The inability of the pitch-yaw components of the minimum-fuel mode to improve system performance causes the computation necessary to generate the target set to be unjustified. Thus, only the z-axis oscillating target set will be employed.

Reproduced with permission of the copyright owner. Further reproduction prohibited without permission.

The results of three different runs of the aforementioned digital computer simulation are shown in Table 2.

TABLE 2

COMPARISON OF THE PERFORMANCE OF THREE CONTROL LAWS

Control Law	Avg. Firings per Orbit	Fuel Cons. per Orbit	84-Day Totals Firings	84-Day Totals Fuel Cons.
1	68.75	.344 lbs.	92,400	462 lbs.
2	24.1	.121 lbs.	32,340	162 lbs.
3	34.0	.170 lbs.	45,700	228 lbs.

In Case 1, the target set for the linear deadband control law was the origin of the state space. Case 2 demonstrates the results that occur when the exact z-axis zero-fuel trajectory is generated as a target set for the control law. In Case 3, as sinusoidal target set was generated to see how much propellant could be saved without incurring the computational penalty required for generating the exact trajectory in Case 2. Table 2 shows that Case 2 results in a 65% reduction and Case 3 a 50% reduction in controller activity relative to Case 1. The full impact of this reduction is demonstrated in Table 2 by the inclusion of the accumulated totals for 84 days, which was the originally scheduled duration for the first two missions of the Skylab program. Most

Reproduced with permission of the copyright owner. Further reproduction prohibited without permission.

importantly, these results constitute a practical achievement of the original goal of the research; namely, to reduce the propellant requirements so that more fuel is available for contingencies, and to enhance the reliability of the system by reducing the required number of thruster firings. Note also that even better results could have been achieved with a more subtle controller, which would have permitted efficient use of the x and y axis zero-fuel modes.

In order to analyze the stability of the closed loop system just described, it will be assumed that Case 2 has been selected for the control law. It should also be mentioned that the control law actually used for the above results differs slightly from the one shown in Figure 10. The actual control law, illustrated in Figure 20, includes small regions, Γ_{p1} and Γ_{p2}, between the full-off control and full-on control regions. If the state of the system (which is sampled at one-second intervals) is contained in one of these intermediate regions, a minimum impulse bit (MIB) will be fired by the thrusters. The firing time, Δt, for a MIB is 50 milliseconds. If the sampled state is contained in Γ_+ or Γ_-, then the thrusters are fired for the full one-second sampling interval. The latter strategy enables the thrusters to fire continuously if more than firing is needed for control. Now because the sampling interval is much smaller than any system response time, the MIB firing will be represented as a smaller torque acting over 50 milliseconds. This model of the control torques is illustrated in Figure 21 and is used for the stability analysis of Chapter 5.

Reproduced with permission of the copyright owner. Further reproduction prohibited without permission.

CHAPTER V

STABILITY OF THE CONTROLLED SYSTEM

5.1 Introduction

It remains to be shown that the system under study is stable when influenced by the control law of §4.4. In other words, we seek to determine the stability of the controlled (or closed-loop) system given in general by

$$\dot{\underline{x}} = \underline{f}(\underline{x}, t) + \underline{u}(\underline{x}, t) = \underline{g}(\underline{x}, t) \qquad (5.1\text{-}1)$$

where $\underline{f}(\underline{x}, t)$ is the mathematical model of the plant dynamics and $\underline{u}(\underline{x}, t)$ is the model of the control law.

The approach taken herein to solve this problem utilizes some recent generalizations by Yoshizawa and LaSalle of the well-known Direct Method of Lyapunov. A review of the basic (classical and modern) results of Lyapunov stability theory is presented in §5.2 prior to the application of these results in §5.3 to the system under study.

5.2 Stability in the Sense of Lyapunov

The stability analysis of dynamical systems using the so-called Direct Method of Lyapunov has been well known outside the Soviet Union only since 1960* despite the fact that

---

*Two early expository references are [5.1] and [5.2].

Reproduced with permission of the copyright owner. Further reproduction prohibited without permission.

Lyapunov's work was done before the turn of the century [5.3]. Much of the work that has been done in this area has been concerned with the stability of autonomous (i.e., unforced, stationary) systems. For this reason a rather complete exposition of the stability analysis of nonautonomous systems using the Direct Method will be given in this section. The framework for this exposition is suggested by the work of Yoshizawa [5.4] and LaSalle [5.5], [5.6], which provides a more general class of Lyapunov functions than the classical approach.

We begin with what might be called the standard introduction to the Direct Method and then use the results of [5.4] to [5.6] as a comparison. It is necessary first to provide two definitions.

Definition 5.1 An equilibrium state* $\underline{x}_e$ is stable in the sense of Lyapunov (i.s.L.) if for every real number $\varepsilon > 0$, there exists a real number $\delta(\varepsilon, t_0)$ such that $||\underline{x}_0 - \underline{x}_e|| \leq \delta$ implies that for all $t \geq t_0$,

$$||\underline{\phi}_g(t; \underline{x}_0, t_0) - \underline{x}_e|| \leq \varepsilon$$

where $\underline{\phi}_g(t; \underline{x}_0, t_0)$ is the solution to the initial value

---

*$\underline{x}_e$ is an equilibrium state for system (5.1-1) if $\underline{g}(\underline{x}_e, t) = \underline{0}$ for all $t \geq t_0$.

Reproduced with permission of the copyright owner. Further reproduction prohibited without permission.

problem that obtains when $\underline{x}_0$ and t_0 are specified in addition to system (5.1-1). The equilibrium state is <u>asymptotically stable</u> i.s.L. if

(i) it is stable, and

(ii) every motion starting sufficiently near $\underline{x}_e$ converges to $\underline{x}_e$ as $t \to \infty$.

<u>Definition 5.2</u> Let G be any set in R^n. Then the function $V(\underline{x}, t)$ on $[t_0, \infty) \times R^n$ to R is called a Lyapunov function on G if:

(i) $V(\underline{x}, t)$ has continuous first partial derivatives in $\underline{x}$ and t,

(ii) $V(\underline{x}, t) \geq 0$ for all $\underline{x} \in G$ and all $t > t_0$,

(iii) $\dot{V}(\underline{x}, t) \leq -W(\underline{x}) \leq 0$ for all $\underline{x} \in G$ and all $t > t_0$ where W is continuous on R^n to R and, using (5.1-1),

$$\dot{V} = \frac{\partial V}{\partial t} + \sum_{i=1}^{n} \frac{\partial V}{\partial x_i} g_i \quad .$$

A standard theorem for system stability using the Direct Method [5.1] takes a form similar to the following:

<u>THEOREM 5.1</u>

1. If $V(\underline{x}, t)$ is a Lyapunov function on some component* of G that includes the origin of the state space, then the null solution (or equilibrium point) of the system

---

*The set G need not be connected. Therefore, we must consider components of G; i.e., maximally connected subsets of G.

Reproduced with permission of the copyright owner. Further reproduction prohibited without permission.

$$\dot{\underline{x}} = \underline{g}(\underline{x}, t)$$

$$\underline{g}(\underline{0}, t) = \underline{0} \qquad (5.2\text{-}1)$$

is stable.

2. If the null solution of (5.2-2) is stable and if $\dot{V}(x, t) \leq -W(\underline{x}) < 0$, then the null solution of (5.2-2) is asymptotically stable.

Theorems such as Theorem 5.1 have found wide application in the past decade. Indeed, they provide a physically satisfying concept. That is, a system is stable if its energy (or an energy-like function) decreases along the system trajectory. The typical problems associated with applications of Theorem 5.1 are the generation of Lyapunov functions and the estimation of the "domain of attraction" for a particular system. These problems were reduced for autonomous systems by the introduction of the variable-gradient method [5.7] and Zubov's method [5.8].

There are two additional shortcomings with regard to the application of Theorem 5.1 to the system under study. They are:

1. the a priori specification of the origin of the state space as the limit point of all solutions to (5.1-1), and
2. the requirement that $V(\underline{x}, t)$ must possess continuous first partial derivatives in $\underline{x}$ and t.

Reproduced with permission of the copyright owner. Further reproduction prohibited without permission.

The Yoshizawa-LaSalle approach improves these conditions by providing a larger class of acceptable Lyapunov functions and limit sets. It also provides a method for estimating domains of attraction.

As before, we begin with some definitions. Let G be a set in R^n and G* be an open set of R^n containing $\bar{G}$, the closure of G. The distance between a point $\underline{x}$ and a set Q is given by

$$d(\underline{x}, Q) = \inf\{||\underline{x} - \underline{p}||, \underline{p} \in Q\} .$$

If for each $\varepsilon > 0$ there is a $T > 0$ such that for each $t > T$ there is a point $\underline{p} \in Q$ such that $d(\underline{x}, Q) < \varepsilon$, then $x(t)$ is said to approach Q ($\to Q$) as $t \to \infty$. A point $\underline{p}$ is in the positive limit set Γ^* of the solutions $\underline{x}(t)$ of (5.1-1) if, for each $\varepsilon > 0$ and each $T > 0$, there is a $t > T$ such that $||\underline{x}(t) - \underline{p}|| < \varepsilon$. Positive limit sets have the following properties [5.4]:

P1. If a solution $\underline{x}(t; \underline{x}_0, t_0)$ of (5.1-1) is bounded for $t \geq t_0$, then its positive limit set Γ^+ is a non-empty, compact set and $\underline{x}(t; \underline{x}_0, t_0) \to \Gamma^+$ as $t \to \infty$.

P2. If $\underline{x}(t; \underline{x}_0, t_0)$ is bounded for $t \geq t_0$ and if $\Gamma^+ \subset Q$, then $\underline{x}(t) \to Q$ as $t \to \infty$.

P3. Let Q be a closed set in R^n and suppose that a solution $\underline{x}(t; \underline{x}_0, t_0)$ of (5.1-1) is bounded and $\underline{x}(t) \to Q$ as $t \to \infty$. Then $\Gamma^+ \subset Q$.

Reproduced with permission of the copyright owner. Further reproduction prohibited without permission.

Finally, a function $V(\underline{x}, t)$ that takes $[0, \infty) \times G^* \to R$ is locally Lipschitzian if for each $(\underline{x}, t)$ in $G^* \times [0, \infty)$ and some neighborhood U of $(\underline{x}, t_0)$ there is a constant L such that

$$|V(\underline{x}, t) - V(\underline{x}', t)| \leq L|\underline{x}-\underline{x}'|; \quad (\underline{x}', t) \in U .$$

This lengthy preamble leads to

Definition 5.3. [5.6] $V(\underline{x}, t)$ is a Lyapunov function of (5.1-1) on G if it is continuous and locally Lipschitzian on $G^* \times [0, \infty)$ and if

(i) given $x \in \overline{G}$ there is a neighborhood U of $\underline{x}$ such that $V(\underline{x}, t)$ is bounded from below for all $t \geq 0$ and all $\underline{x}$ in $U \cap G$, and

(ii) $\dot{V}(\underline{x}, t) \leq W(\underline{x}) \leq 0$ for all $t \geq 0$ and all $\underline{x}$ in G, where W is continuous on G.

REMARKS

1. The requirement that $V(\underline{x}, t)$ be continuous and locally Lipschitzian guarantees its differentiability.
2. The definitions preceding 5.3 should suggest that the Lyapunov function of Definition 5.3 will be used to get information on the asymptotic behavior of solutions of (5.1-1). In fact, we will be investigating that behavior whether it suggests stability or instability. This statement requires another definition. Let $R^n_\infty = R^n \cup \{\infty\}$ be the compactification ([5.5]) of R_n and define $d(\underline{x}, \infty) = 1/||\underline{x}||$. Then,

Reproduced with permission of the copyright owner. Further reproduction prohibited without permission.

if $Q \subset R^n_\infty$, the statement that $d(\underline{x}, Q) = \inf\{d(\underline{x}, \underline{p}); \underline{p} \in Q\} \to 0$ as $t \to \infty$ can, depending on the set Q, give quite different information about the asymptotic behavior of solutions of (5.1-1). For example:

(a) If Q consists of the single point $\underline{p} = \underline{0}$, then $d(\underline{x}, Q) \to 0$ as $t \to \infty$ is a statement of asymptotic stability of solutions of (5.1-1) that remain in G.

(b) If Q is a compact subset in R^n, then $d(\underline{x}, Q) \to 0$ as $t \to \infty$ is a statement of boundedness for solutions of (5.1-1) that remain in G.

(c) If $Q = \{\infty\}$, then $d(\underline{x}, \infty) = ||\underline{x}||^{-1} \to 0$ as $t \to \infty$ is a statement of the instability of solutions of (5.1-1).

Definition 5.4. If V is a Lyapunov function of (5.1-1) on G, then

$$E \triangleq \{\underline{x} \in G: \ W(\underline{x}) = 0\} \ . \tag{5.2-2}$$

If E is an unbounded set in R^n, then

$$E_\infty \triangleq E \cup \{\infty\} \ . \tag{5.2-3}$$

These definitions lead to

THEOREM 5.2

Let V be a Lyapunov function for (5.1-1) on G and let $\underline{x}(t)$ be a solution of (5.1-1) that remains in G for $t \geq t_0 \geq 0$. Then $\underline{x}(t) \to E$ as $t \to \infty$ if one of the following

Reproduced with permission of the copyright owner. Further reproduction prohibited without permission.

conditions is satisfied:

(a) For each $\underline{p} \in \overline{G}$ there is a neighborhood U of $\underline{p}$ such that $||\underline{g}(\underline{x}, t)||$ is bounded for all $t \geq 0$ and all $\underline{x} \in U \cap G$.

(b) $W(\underline{x})$ is absolutely continuous and its derivative is bounded from above (or below).

For our purposes E will always be chosen as a bounded (compact) subset of R^n. Thus, the following trivial corollary of Theorem 5.2 will be the relevant result.

Corollary 5.1

If the set E is bounded, i.e., given by (5.2-2) then Theorem 5.2 implies that $\underline{x}(t) \to E$ as $t \to \infty$.

The usual application of Theorem 5.2 consists of trying to find the positive limit set $\Gamma^+ \subset E_\infty$. One way to accomplish this is to try several Lyapunov functions $V_i(\underline{x}, t)$; $i = 1,2,\ldots,N$, of (5.1-1) that correspond respectively to sets $E_{i\infty}$. Then

$$E_\infty = E_{1\infty} \cap E_{2\infty} \cap \cdots \cap E_{N\infty} \quad .$$

This procedure is most useful when the system (5.1-1) is autonomous. In that case, Γ^+ is an invariant set. That is, every solution of (5.1-1) that enters Γ^+ remains there.

The application of Theorem 5.2 to the system under study, which is discussed in §5.4, adopts a different philosophy. Since the open-loop stability properties of the

Reproduced with permission of the copyright owner. Further reproduction prohibited without permission.

system under study have already been determined in §4.2, only the closed-loop stability properties are sought. Moreover, it is only necessary to show that the controller drives the system towards the deadband or uncontrolled region.* Therefore, a Lyapunov function which makes the deadband a subset of E_∞ is used. By property P3 of positive limit sets, if a solution $\underline{x}(t; \underline{x}_0, t_0)$ of (5.1-1) is bounded and if $\underline{x}(t) \to Q$ as $t \to \infty$, then $\Gamma^+ \subset Q$. The set Q is taken to be a bounded subset of the deadband, and we will generate sufficient conditions that $d(\underline{x}, Q) \to 0$ as $t \to \infty$.

Finally, note that Theorem 5.2 requires assurance that all solutions $\underline{x}(t)$ of (5.1-1) remain in G, and P3 requires that $\underline{x}(t)$ be bounded. The method that is used to provide this information also establishes a domain of attraction for the set Q.

5.3 Lyapunov Functions for Systems with a Dead-Zone

In this section we investigate the stability of systems given by

$$\begin{aligned} \underline{\dot{x}} &= \underline{f}(\underline{x}, t) - B\,\underline{u}(\underline{y}) \\ \underline{y} &= \underline{g}(\underline{x}, t) \end{aligned} \qquad (5.3\text{-}1)$$

where $\underline{x} \in R^n$, $\underline{u} \in R^r$, and $\underline{y} \in R^m$. $\underline{u}(\underline{y})$ is, in general, a

---

*See Figures 20 and 21.

Reproduced with permission of the copyright owner. Further reproduction prohibited without permission.

bounded, nonlinear function containing a dead zone,* and the uncontrolled system $\dot{\underline{x}} = \underline{f}(\underline{x}, t)$ may not be asymptotically stable or may be unstable. Note that because of the dead zone in $\underline{u}(\underline{y})$, the origin of the state space is not a limit point of any nontrivial solution of (5.3-1). Also, if the uncontrolled system is unstable, the boundedness of $\underline{u}(\underline{y})$ implies that the controlled system will be unstable for large $\underline{y}$. Thus, we seek to determine stability in some region $G \subset R^n$ that does not include the origin and which may be finite. It is clear that standard Lyapunov theorems, which determine stability relative to either an equilibrium point or a non-trivial solution† of (5.3-1) are not applicable. It is the purpose of this section to show that the framework of Theorem 5.2 is ideally suited for the analysis of the stability of such systems. We begin by considering the stability of the uncoupled second order equation of roll motion, proceed to an investigation of the coupled pitch and yaw equations, and conclude with some generalizations.

The result of adding a controller of the form shown in Figures 20 and 21 to the open-loop roll equations included in (C-9)

---

*See Figures 20 and 21 for example.

†Stability i.s.L. with respect to a solution reduces to a stability analysis of an equilibrium point by such perturbational techniques as those of Appendix D.

Reproduced with permission of the copyright owner. Further reproduction prohibited without permission.

$$\dot{x}_5 = x_6$$

$$\dot{x}_6 = (a_5^2 \cos 2t)\, x_5 - b_6\, u(y_3) \qquad (5.3\text{-}2)$$

$$y_3 = c_{35}\, x_5 + c_{36}\, x_6$$

where the independent variable has been normalized by letting $\omega_0 = 1$, and where

$$u(y_3) = \begin{cases} 0; & |y_3| < 1 \\ .05; & 1 \le |y_3| < 1.6 \\ 1; & 1.6 \le |y_3| \end{cases} .$$

It was shown in §4.2 that the linearized equation (5.3-2) is stable i.s.L. and has the representative trajectories shown in Figure 15. Our interest in this section is whether or not the controller of (5.3-2) drives the system toward the deadband (see Figure 20). This is accomplished with the aid of the following candidate Lyapunov function:

$$V(\underline{x}) = \begin{cases} 0; & |y_3| < a_3 \\ \frac{1}{2}(y_3 - a_3)^2; & y_3 \ge a_3 \\ \frac{1}{2}(y_3 + a_3)^2; & y_3 \le -a_3 \end{cases} . \qquad (5.3\text{-}3)$$

Reproduced with permission of the copyright owner. Further reproduction prohibited without permission.

With respect to Definition 5.3, $V(\underline{x})$ is continuous and locally Lipschitzian over any finite $G \subset R^n$. Further, since $V(\underline{x})$ is positive semidefinite and, therefore, bounded from below by zero everywhere in R^n. The definition of $V(\underline{x}) = 0$ for $|y_3| < a_3$ amounts to a discarding of any stability information about the open-loop system, but this information is already known. This definition also helps assure the differentiability of V along solutions of (5.3-1) or (5.3-2).

$\dot{V}$ is given for the general system (5.3-1) by

$$\dot{V} = [\frac{\partial V}{\partial \underline{y}}]' [\underline{\nabla}_x \underline{y}]' [\underline{f}(\underline{x}, t) - \underline{B}\, \underline{u}(\underline{y})] \qquad (5.3\text{-}4)$$

where the prime indicates the transpose of a matrix and

$$[\underline{\nabla}_x \underline{y}]' = [\frac{\partial \underline{y}}{\partial \underline{x}}]' = [\underline{\text{grad}_x}\ \underline{y}]' \quad .$$

For system (5.3-2): $\partial V/\partial y$ is a scalar, $[\underline{\nabla}_x y]' = [c_{35}\ c_{36}]$, and

$$\dot{V}(\underline{x}, t) = \begin{cases} 0; & |y_3| < a_3 \\ (y_3 - a_3)[c_{35}x_6 + c_{36}\{(a_5^2 \cos 2t)x_5 - b_6 u(y_3)\}]; & y_3 \geq a_3 \\ (y_3 + a_3)[c_{35}x_6 + c_{36}\{(a_5^2 \cos 2t)x_5 - b_6 u(y_3)\}], & y_3 \leq -a_3 \end{cases} \qquad (5.3\text{-}5)$$

In order to comply with (ii) in Definition 5.3, it is necessary to specify a region $G \subset R^n$ and a continuous $W(\underline{x}) \leq 0$ for all t and all $\underline{x} \in G$ such that $\dot{V}(\underline{x}, t) \leq W(\underline{x})$.

Reproduced with permission of the copyright owner. Further reproduction prohibited without permission.

To this end, define

$$W(\underline{x}) = \begin{cases} 0; \ |y_3| < a_3 \\ (y_3-a_3)[c_{35}x_6+c_{36}a_5^2|x_5|-c_{36}b_6u(y_3)]; \ y_3 \geq a_3 \\ (y_3+a_3)[c_{35}x_6-c_{36}a_5^2|x_5|-c_{36}b_6u(y_3)]; \ y_3 \leq -a_3 \end{cases} , \quad (5.3\text{-}6)$$

or, more concisely,

$$W(\underline{x}) = \begin{cases} 0; \ |y_3| < a_3 \\ (\partial V/\partial y_3)W_+(x); \ y_3 \geq a_3 \\ (\partial V/\partial y_3)W_-(x); \ y_3 \leq -a_3 \end{cases} . \quad (5.3\text{-}7)$$

Note that:

1. $\text{sgn}[\partial V/\partial y_3] = \text{sgn}[y_3]$ when $|y_3| > |a_3|$.
2. when $|y_3| = a_3$, $(\partial V/\partial y_3) = 0$ and the discontinuity of $u(y_3)$ at that point does not result in a discontinuity of $W(\underline{x})$,
3. for $V(\underline{x})$ in (5.3-3) to be a Lyapunov function for system (5.3-2), it is sufficient that $W_+(\underline{x}) \leq 0$ and $W_-(\underline{x}) \geq 0$ for all $\underline{x} \in G$.

Next, we establish a first estimate of outer boundaries of G by setting $W_-(\underline{x}) = W_+(\underline{x}) = 0$. For the case when $a_3 = 1.6$ and $u(y_3) = \text{sgn}(y_3)$, these boundaries are the lines in the x_5 - x_6 state space given by

Reproduced with permission of the copyright owner. Further reproduction prohibited without permission.

$$\partial G_1: \quad x_6 = -\frac{c_{36}}{c_{35}} a_5^2 |x_5| + \frac{c_{36}}{c_{35}} b_6; \quad y_3 \geq a_3$$

$$\partial G_2: \quad x_6 = \frac{c_{36}}{c_{35}} a_5^2 |x_5| - \frac{c_{36}}{c_{35}} b_6; \quad y_3 \leq -a_3$$

and illustrated in Figure 22. The set G in which $W_+ \leq 0$ $W_- \geq 0$ for all $\underline{x} \in G$ can be described as the union of three sets G_1, G_2 and G_3 where, if $\bar{Q}$ = the closure of set Q,

$$\bar{G}_1 = \{x_5, x_6: \quad c_{35}x_6 + c_{36}[a_5^2|x_5| - b_6] \leq 0, \; y_3 \geq a_3\}$$

$$\bar{G}_2 = \{x_5, x_6: \quad c_{35}x_6 - c_{36}[a_5^2|x_5| + b_6] \geq 0; \; y_3 \leq a_3\} \quad .$$

$$\bar{G}_3 = \{x_5, x_6: \quad |c_{35}x_5 + c_{36}x_6| \leq a_3\}$$

Now the construction of G as above also produces the set

$$E = \{x_5, x_6: \quad W(\underline{x}) = 0, \; x_5, x_6 \in \bar{G}\}$$

which can be written as $E = \partial G_1 \cup \partial G_2 \cup \bar{G}_3$, where ∂G_1 and ∂G_2 represent respectively the set of all boundary points of G_1 and G_2.

We are, at last, ready to apply Corollary 5.1. Since the candidate function, $V(\underline{x})$, given by (5.3-3) has been shown to be a Lyapunov function on G, and since hypotheses (a) and (b) of the theorem can be verified, then it may be concluded that every solution $\underline{x}(t)$ of system (5.3-2) that remains in G will approach E_∞ as t approaches ∞. The procedure for showing

Reproduced with permission of the copyright owner. Further reproduction prohibited without permission.

which solutions remain in G also yields an estimate of the domain of attraction and a reduction in the extent of the possible limit set.

Assume that system (5.3-1) is activated by an initial condition $\underline{x}_0 \in G_1$. The instantaneous rate of change of the state vector is just $\underline{f}(\underline{x}, t) - \underline{Bu}(\underline{y})$. The establishment of set ∂G_1 by setting $\dot{V} = 0$ can be seen from (5.3-4) to be equivalent to determining the set of vectors $\dot{\underline{x}}$ that are in the null space of $[\underline{\nabla}_x \; y]'$. For system (5.3-2), $[\underline{\nabla}_x \; y]' = [C_{35} \; C_{36}]$ is a vector perpendicular to the switching surfaces. This information along with the system function equation (5.3-2) and the condition that $\dot{V} < 0$ for $\underline{x} \in G$ will now be used to show that solutions of (5.3-2) that begin in G_1 (G_2) tend toward the set G_3 and away from the possible limit set on the boundary ∂G_1 (∂G_2). Consider the set of interior points of G_1 in the neighborhood of boundary ∂G_1 in Figure 22. From (5.3-2), $x_5 = x_6 \geq 0$ for all trajectories of (5.3-2) in the first and second quadrants. Now, the only way this condition is consistent with $\dot{V} < 0$ is for $\dot{x}_6 < 0$ in this neighborhood. Thus, since Theorem 5.2 guarantees that solutions of (5.3-2) that remain in G approach $E_\infty = \overline{G}_3 \cup \partial G_1 \cup \partial G_2$, then the above analysis (which proceeds in exactly the same manner mutatis mutandis in the neighborhood of ∂G_2) shows that solutions in fact approach $\overline{G}_3$.

Reproduced with permission of the copyright owner. Further reproduction prohibited without permission.

The above argument, however, does not yet provide sufficient conditions for stability of solutions of (5.3-2) because the set $G_3 \subset E_\infty$, which includes the positive limit set for all solutions of (5.3-2) that remain in G, is unbounded. Note also from Figure 22 that any point in the set $G_{1a} = G_{11} \cup G_{12}$ where:

$$G_{11} = \{\underline{x}: \quad x_6 \in G_1 < -1150\}$$

$$G_{12} = \{\underline{x}: \quad x_6 \in G_2 > 1150\}$$

is likely to proceed through G_3 and enter region S. Region S is outside G and solutions of (5.3-2) that pass through points in S do not necessarily approach G_3 as $t \to \infty$. The problem of defining the region G in such a way that all solutions of (5.3-2) remain in G is remedied by the following reduction of G and $G_3 \subset E_\infty$.

Consider the set $G^* = G_1^* \cup G_2^* \cup G_3^* \subset G$ that is enclosed by the polygon ABCDEFGHA in Figure 23. We wish to show that (at least) interior points of G^* are in the domain of attraction for the set

$$G_3^* = G_3 \cap G^* \subset E^* = E_\infty \cap G^* = \{\underline{x} \in G^*: \quad W(\underline{x}) \leq 0\} .$$

This requires only a demonstration that all solutions of (5.3-2) that begin in G^* remain in G^*. Then Corollary 5.1 implies that these solutions approach $E^* = G_3^* \cup (\partial G_1 \cap G^*)$.

Reproduced with permission of the copyright owner. Further reproduction prohibited without permission.

Finally, we show that the solutions of (5.3-2) really $\to G_3^*$ as $t \to \infty$ by showing that they cannot $\to G_1 \cap G^*$,

1. Solutions of (5.3-2) beginning on line segments DE and HA (which represent boundary sets $\partial G_1 \cap G^*$ and $\partial G_2 \cap G^*$, respectively) must proceed into the interior of the polygon in Figure 23 because for these points:

(a) $\dot{V}(\underline{x}, t) \leq W(\underline{x}) = 0$.

(b) $\dot{x}_5 = x_6 > 0$ (<0) along DE (HA).

The combination of (a) and (b) imply that $\dot{x}_6 < 0$ in the vicinity of DE and $\dot{x}_6 > 0$ near HA because no solution for which (b) holds can proceed outward (away from G^*) without increasing V, which is prohibited by (a). This conclusion is verified by noting that at these boundaries,

(c) $\dot{x}_6$ has the appropriate sign since, from (5.3-2), $|b_6 u(y_3)| > a_5^2 |x_5|$ for all $\underline{x} \in G_1^* \cup G_2^*$.

2. Points along the vertical lines EG and AC (purposely selected for this property) proceed to the interior of G^* because along EG (AC) $\dot{x}_5 = x_6 > 0$ (<0). Note especially that this property ensures the proper passage of trajectories of (5.3-2) from G_1^* or G_2^* into G_3^* even at the points F and A.

3. Finally, solutions of (5.3-2) passing through points along the constant V lines CD and GH $\to G_3^*$ as $t \to \infty$ by Corollary 5.1 since they are interior points of the larger set G and, because by step 1 above, they cannot $\to \partial G_1 \cup \partial G_2$.

Reproduced with permission of the copyright owner. Further reproduction prohibited without permission.

In summary, the philosophy of this approach is as follows:

1. Since it is desired to show that the set $G_3 \subset E_\infty$ enclosed by the switching lines contains the positive limit set Γ^+ of all solutions of (5.3-2) that remain in some region $G \subset R^2$, the Lyapunov function, $V(\underline{x}, t)$, should be constructed such that the value of V for $\underline{x} \in G_3$ is the lower bound of V in G and such that the lines of constant V are parallel to the switching lines.
2. Then, using properties of system trajectories that are evident from the system equation and the equation for $W(\underline{x})$, a boundary which encloses $G^* \subset G$ can be constructed such that G^* and therefore $E^* = E_\infty \cap G^*$ and $G_3^* = G_3 \cap G^*$ are finite.

Before considering the application of these principles to the coupled pitch and yaw equations, it is necessary to consider the stability of the roll equation in the MIB region of Figure 20 wherein $u(y_3) = .05$ as in Figure 21. The approach to this problem differs from the above only in details that will be discussed in the study of domains of attraction. Therefore, only the results will be given for system (5.3-2) in this region. As shown in Figure 24 with G^* defined to be the interior of polygon ABDCEFA, the sets G_1^* and G_2^* are in the domain of attraction for set G_3^*. Two points are

Reproduced with permission of the copyright owner. Further reproduction prohibited without permission.

noteworthy about this construction:

1. If the line segments AB and DE were placed such that $|x_5| > .65$ at these boundaries, it could be shown that the slope of $\underline{\dot{x}}$ along segments CD and FA is such that points in G_3^* could leave G*.
2. G* could be made much larger by increasing the rate feedback coefficient c_{66}. This is explained in more detail in the sequel.

The stability analysis of the pitch-yaw equations requires considerations of two additional problems: coupling between equations and the presence of a forcing function. These equations are given by (3.57 (b) and (c)) and are repeated below as (5.3-8) with the following changes:

(i) (5.3-8) is the state-variable representation of (3.5-7) with $\phi = x_1$ and $\theta = x_3$,

(ii) the independent variable has been normalized by setting $\omega_0 = 1$,

(iii) the forcing functions are temporarily omitted.

$$\dot{x}_1 = x_2$$

$$\dot{x}_2 = P_{21}(t)x_1 + P_{23}(t)x_3 + P_{24}(t)x_4 - b_2u(y_1) \qquad (5.3\text{-}8)$$

$$\dot{x}_3 = x_4$$

$$\dot{x}_4 = P_{41}(t)x_1 + P_{42}(t)x_2 + P_{43}(t)x_3 - b_4u(y_2)$$

Reproduced with permission of the copyright owner. Further reproduction prohibited without permission.

where:

$$y_2 = c_{21}x_1 + c_{22}x_2 \quad ,$$

$$y_4 = c_{43}x_3 + c_{44}x_4 \quad ,$$

$$P_{21}(t) = \omega_0^{-2}[|k_1|\dot{\psi}^2+\alpha_1^2(1-\cos 2(t-\psi)] \quad ,$$

$$P_{23}(t) = -\omega_0^{-2}(\alpha_1^2+\alpha_3^2)\sin 2(t-\psi) \quad ,$$

$$P_{24}(t) = \omega_0^{-1}(1+|k_1|)\dot{\psi} \quad ,$$

$$P_{41}(t) = -\omega_0^{-2}(\alpha_2^2-\alpha_3^2)\sin 2(t-\psi)$$

$$P_{42}(t) = -\omega_0^{-1}(1+k_2)\dot{\psi} \quad , \text{ and}$$

$$P_{43}(t) = \omega_0^{-2}[k_2\dot{\psi}^2+\alpha_2^2(1+\cos 2(t-\psi))]$$

Even though (5.3-8) is coupled, the switching lines and deadbands are designed as though the motion about each axis were uncoupled (as in Figures 20 and 21). Since we want to show that motions within a given region $G \subset R^4$ approach these deadbands, we select the candidate Lyapunov function, $V = V_1 + V_2$ where

$$V_i = \begin{cases} 0; & |y_i| \leq a_i \\ \frac{1}{2}(y_i-a_i)^2; & a_i \leq y_i, \ i = 1,2 \\ \frac{1}{2}(y_i+a_i)^2; & y_i \leq -a_i, \ i = 1,2 \end{cases} \quad . \qquad (5.3\text{-}9)$$

Now, using

Reproduced with permission of the copyright owner. Further reproduction prohibited without permission.

$$\dot{V} = [\underline{\partial V/\partial y}]' \; [\underline{\nabla_x} \; y]'[\underline{f}(\underline{x}, t) - \underline{Bu}(\underline{y})]$$

where:

$$[\underline{\partial V/\partial y}]' = [(y_1-a_1)(y_2-a_2)] \text{ , and}$$

$$[\underline{\nabla_x} \; \underline{y}]' = \begin{bmatrix} c_{21} & c_{22} & 0 & 0 \\ 0 & 0 & c_{43} & c_{44} \end{bmatrix} .$$

Finally, if the elements of the vector $f(\underline{x}, t)$ are given by f_i, then

$$\dot{V}_1(\underline{x}, t) = \begin{cases} 0; \; |y_1| \leq a_1 \\ (y_1-a_1)[c_{21}x_2+c_{22}(f_2(x,t)-b_2u(y_1)]; \; a_1 \leq y_1 \\ (y_1+a_1)[c_{21}x_2+c_{22}(f_2(x,t)-b_2u(y_1)]; \; y_1 \leq -a_1 \end{cases} ,$$

$$\dot{V}_1(\underline{x}, t) = \begin{cases} 0; \; |y_2| \leq a_2 \\ (y_2-a_2)[c_{43}x_4+c_{44}(f_4(x,t)-b_4u(y_2))]; \; a_2 \leq y_2 \\ (y_2+a_2)[c_{43}x_4+c_{44}(f_4(x,t)-b_4u(y_2))]; \; y_2 \leq -a_2 \end{cases}$$

As with the roll equation, we seek a $W(\underline{x}) = W_1(\underline{x}) + W_2(\underline{x}) \leq 0$ such that for all t and all $\underline{x}$ in the (as yet undefined) region G, $\dot{V}(\underline{x}, t) \leq W(\underline{x})$. This function is defined as follows:

Reproduced with permission of the copyright owner. Further reproduction prohibited without permission.

$$W_i(\underline{x}) = \begin{cases} 0; & |y_i| \le a_i \\ (\partial V/\partial y_i)W_{i+}; & a_i \le y_i \\ (\partial V/\partial y_i)W_{i-}; & y_i \le -a_i \end{cases} \quad ; i = 1,2, \qquad (5.3\text{-}10)$$

where

$$W_1(\underline{x}) = (\partial V/\partial y_1)\{c_{21}x_2+c_{22}\omega_0^{-2}[|k_1|\sup_t[\dot{\psi}^2]+\alpha_1^2]x_1 - c_{22}b_2u(y_1)$$

$$+ \operatorname{sgn}[y_1]\omega_0^{-2}c_{22}[\alpha_1^2|x_1|+(\alpha_1^2+\alpha_3^2)|x_3| + \omega_0(1+|k_1|)\sup_t[\dot{\psi}]|x_4|]\}$$

$$W_2(\underline{x}) = (\partial V/\partial y_2)\{c_{43}x_4+c_{44}[\omega_0^{-2}(k_2\sup_t[\dot{\psi}^2]+\alpha_2^2)x_3-b_4u(y_2)]$$

$$+ \operatorname{sgn}[y_2]\omega_0^{-2}c_{44}[\alpha_2^2|x_3|+(\alpha_2^2-\alpha_3^2)|x_1|+\omega_0(1+k_2)\sup_t[\dot{\psi}]|x_2|]\}$$

In other words, equation (5.3-10) represents W_{i+} when $y_i \ge a_i$ and W_{i-} when $y_i \le -a_i$ for i = 1, 2.

REMARKS

1. A sufficient condition that solutions of system (5.3-8) $\to E_\infty$ as $t \to \infty$ is that $W_1(\underline{x})$ and $W_2(\underline{x})$ be negative semidefinite for all $\underline{x} \in G \subset R^4$.
2. Since $\operatorname{sgn}[\partial V/\partial y_i] = \operatorname{sgn}[y_i]$, the sufficiency condition is reduced to the condition that $W_{i+}(\underline{x}) \le 0$ or, which is equivalent, $W_{i-}(\underline{x}) \ge 0$ for i = 1,2.
3. The supremum of $\dot{\psi}(\omega_0 t)$ or $\dot{\psi}^2(\omega_0 t)$ is taken relative to the origin of the x_5-x_6 state-space rather than relative to the minimum-fuel mode. Further, the

Reproduced with permission of the copyright owner. Further reproduction prohibited without permission.

supremum of the perturbation of $\dot{\psi}$ relative to the minimum-fuel mode, i.e, x_6, is taken to be the largest value that x_6 assumes within the MIB of Figure 23 since this region has already been shown to be stable.

For the coupled equations (5.3-8) the domain of attraction for the MIB region of Figures 20 and 21 will be sought. Having established the basic ideas, the stability properties of (5.3-8) when $u(y_i) = 1$ (i = 1 and/or 2) follow immediately. When $u(y_i) = 0.05$ the region $G \subset R^4$ is defined as

$$G = G_{41} \cup G_{42}$$

where

$$G_{41} = \{x_1, x_2: \ |y_1| < a_4 - \varepsilon\}$$

and (5.3-11)

$$G_{42} = \{x_3, x_4: \ |y_2| < a_4 - \varepsilon\} \ .$$

For this problem a_4 is taken to be 1.6. The inclusion of the parameter $\varepsilon > 0$ in Definitions (5.3-11) is necessary to avoid the discontinuity of $u(y_i)$ at $y_i = a_4$, which results in a discontinuity of $W_i(\underline{x})$ and violates hypothesis (b) of Theorem 5.2. Also, for this problem, the coefficients c_{22} and c_{44} will be set equal to 0.2 instead of the value 0.02266 used for c_{66} in the uncoupled equation. This ten-fold increase in the rate feedback will be shown below to give a much larger domain of attraction. Note that, since

Reproduced with permission of the copyright owner. Further reproduction prohibited without permission.

c_{21} and c_{43} are kept equal to 2, the rate feedback coefficient still is only one-tenth the value of the position (attitude) feedback coefficient.

For reasons of clarity $W_{1+}(\underline{x})$ and $W_{2+}(\underline{x})$ are written with the numerical values of the system under study. For $1 = a_i \leq y_i \leq a_4 - \varepsilon = 1.6 - \varepsilon$,

$$W_{1+}(\underline{x}) = 2x_2 + .29x_1 + .27|x_1| + (.4|x_3| + .15|x_5|) - 242$$

$$W_{2+}(\underline{x}) = 2x_4 + .31x_3 + .29|x_3| + (.15|x_1| + .15|x_2|) - 125 \qquad (5.3\text{-}12)$$

We suppose for the moment that there is no coupling in order to get a first estimate for G_{41} and G_{42}, denoted by $\hat{G}_{41}$ and $\hat{G}_{42}$. This is done by neglecting the terms in parentheses in (5.3-12) and setting the remaining terms to zero as in (5.3-13)

$$\hat{W}_{1+}(\underline{x}) = .29x_1 + .27|x_1| + 2x_2 - 242 = 0$$

$$\hat{W}_{2+}(\underline{x}) = .31x_3 + .29|x_3| + 2x_4 - 125 = 0 \qquad (5.3\text{-}13)$$

The boundaries ∂G_{41} and ∂G_{42} that obtain from the solution of (5.4-13) are shown in Figures 25 and 26. Note:

1. that the boundaries are extended beyond the deadband to avoid the case where an element of $G_5 \subset \hat{G}_{41}$ could proceed into region G_6, which is not included in the domain of attraction;

Reproduced with permission of the copyright owner. Further reproduction prohibited without permission.

2. that the elements of $\hat{G}_{41}$ and $\hat{G}_{42}$ that are not within the MIB region, (shown shaded in Figures 25 and 26) are superfluous since $u(y_i) = 1$ in those regions; and
3. that the magnitudes of the rates x_2 and x_4 near the boundaries $\overset{\gamma}{G}_{41}$ and $\overset{\gamma}{G}_{42}$ are much greater than the range of values for which the linearization procedure used for the derivation of (5.3-8) are valid.

Proceeding from the last point, we assume that the variables for both axis are constrained to stay within the region $G_i^* = G_{1i}^* \cup G_{2i}^*$; $i = 1,2$, of the polygon ABCDEFA in Figure 27. This assumption is justified by observing typical trajectories of the uncontrolled motion of (5.3-8) in the vicinity of $\underline{x} = \underline{0}$ (see for example Figures 15(c-f)). Next, we get a worst case estimate of coupling by assuming that all variables take on their maximum values within G_i^*[†]. For this case $W_{i+}(\underline{x})$ of (5.4-12) becomes

$$W_{1+}(\underline{x}) = 2x_2 + .29x_1 + .27|x_1| + 4.5 - 242$$
$$W_{2+}(\underline{x}) = 2x_4 + .31x_3 + .29|x_3| + 4.1 - 125 \quad . \tag{5.3-14}$$

[†]For example, we assume that, when we are analyzing the $x_1 - x_2$ system, the $x_3 - x_4$ system is taking on its most adverse value.

Reproduced with permission of the copyright owner. Further reproduction prohibited without permission.

In this context the effects of coupling can be considered as a disturbance torque that opposes the control torque. The boundaries $\hat{G}^*_{41}$ and $\hat{G}^*_{42}$ of the new estimates, $\hat{\hat{G}}_{41}$ and $\hat{\hat{G}}_{42}$, of G_4 that result from this dimunition of control effort are also shown in Figures 25 and 26.

Now the regions G^*_i shown in Figure 28 and superimposed on the other estimates in Figures 26 and 27 will be called reduced estimates of the domain of attraction for the set

$$E^*_i = \{\underline{x} \in G^*_i: \quad W_i(\underline{x}) = 0\}$$

which, it will be recalled, includes the positive limit set Γ^+ of solutions of (5.3-8) that remain in $G^* = G^*_1 \cup G^*_2$. We now proceed to verify that G^* is a domain of attraction for $E^* = E^*_1 \cup E^*_2$.

1. Trajectories of (5.4-8) beginning at points on the constant V line segments BC and EF tend toward E^* because they are interior points of the larger estimate G_4 for which $\dot{V}(\underline{x}, t) \leq W(\underline{x}) < 0$.
2. Line segments CD and FA are also interior points of G_4. In addition, from the system equation (5.3-8), it can be shown that $\dot{x}_2$ and $\dot{x}_4$ are negative for $\underline{x} \in G^*_{1i}$ and positive for $\underline{x} \in G^*_{2i}$. These conditions hold even for the most adverse values of the $P_{ij}(t)$ in (5.3-8).

Reproduced with permission of the copyright owner. Further reproduction prohibited without permission.

3. Trajectories crossing line segments AB and DE also tend towards the interior of G_i^* because $\dot{x}_1$ or $\dot{x}_3$ are negative on AB and positive on DE.

These three steps guarantee that all solutions of (5.4-8) beginning in $G^* = G_1^* \cup G_2^*$ remain in G^*. Therefore, by Corollary 5.1, these solutions will all approach $E^* = E_1^* \cup E_2^*$ as $t \to \infty$.

The stability properties of system (5.3-8) when $u(y_i) = 1$ proceeds along the same lines as the analyses that led to the domains of attraction of

(a) the uncoupled system (5.3-2) with $u(y_3) = 1$, and

(b) the coupled system (5.3-8) with $u(y_i) = 0.05$.

More specifically, first estimates for the domain of attraction G are made by temporarily neglecting the coupling effects in $W_i(\underline{x})$ in (5.3-10). These estimates are shown in Figures 28 and 29 where, for reasons of scale, the deadband and the MIB region are represented by a line through $\underline{x} = \underline{0}$. Next, a suitable reduced estimate, $G^* = G_1^* \cup G_2^*$, of G is made as in Figure 30. A second estimate of G, which should have G^* as a subset, is then made by reconsidering the effects of coupling as an adverse disturbance torque. If properly constructed, all points on the boundary of G^* can easily be shown to be in the domain of attraction of the set $E^* = E_1^* \cup E_2^*$, where

$$E_i^* = \{\underline{x} \in G_i^* : \ W_i(\underline{x}) = 0\} \ ; \ i = 1,2.$$

Reproduced with permission of the copyright owner. Further reproduction prohibited without permission.

Then, by property P3 of §5.2, the positive limit set of $\Gamma^+ \subset E^*$.

REMARKS

1. Note that the sets E^* can be made smaller if reductions in G^* are acceptable for a given problem.
2. The manner in which coupling was considered does not differ in any essential way from the direct analysis of system (5.3-8) for a four-dimensional G^*. This is because the two-dimensional systems are analyzed simultaneously.
3. The first estimate, $\hat{G}$, of the domain of attraction for the yaw (x_1, x_2) axis portion of (5.3-8) when the rate feedback coefficient is $c_{22} = 0.02266$ instead of 0.2 is shown in Figure 31. It will be recalled that this lower value was used for c_{66}, the rate feedback coefficient of the uncoupled system (5.3-2). Note from Figure 31 that the intersection of the boundary $\tilde{G}$ of $\hat{G}$ with the x_2 axis occurs at $x_2 = 270$ as compared with the value $x_2 = 2418$ obtained in Figure 28 when $c_{22} = 0.2$. Further, since the switching lines are given by

$$c_{21}x_1 + c_{22}x_2 = a_4$$

$$a_4 = 1 \text{ or } 1.6 \ ,$$

Reproduced with permission of the copyright owner. Further reproduction prohibited without permission.

an increase in c_{22} reduces their slope. The combination of these effects results in a much larger domain of attraction for the larger value of c_{22}.

4. The approach used above for the consideration of the effects of coupling suggest a format for the discussion of the input-output stability [5.9-5.17] of system (5.3-8) as well as a for a whole class of systems.

It will be recalled that the defining equations (5.3-8) used for the stability analysis of the coupled pitch-yaw equations differed from the actual equations of motion (3.5-7) in that the forcing functions were not included in the former. We now show that they can be handled very simply. Proceeding in a more general way, rewrite (5.3-1) with the inclusion of these functions, i.e.,

$$\dot{\underline{x}} = \underline{f}(\underline{x}, t) + \underline{z}(t) - \underline{B}\ \underline{u}(\underline{y})$$

$$\underline{y} = \underline{g}(\underline{x}, t) \qquad (5.3\text{-}12)$$

where $\underline{z}(t)$ is an n x 1 vector whose properties will become obvious in the sequel. Proceeding exactly as before with the Lyapunov function defined by (5.3-9), we get for $\dot{V}$

$$\dot{V}(\underline{x}, t) = [\underline{\partial V/\partial y}]'[\underline{\nabla_x y}]'[\underline{f}(\underline{x}, t) + \underline{z}(t) - \underline{Bu}(\underline{y})]. \qquad (5.3\text{-}13)$$

Reproduced with permission of the copyright owner. Further reproduction prohibited without permission.

The next step is to select a $W(\underline{x}) \leq 0$ such that $\dot{V}(x, t) \leq W(\underline{x})$ for all $\underline{x}$ in $G \subset R^n$, our region of interest. In the homogeneous system (5.3-8), $W(\underline{x})$ was formed by replacing all time-varying coefficients by a function of their maximum values. The forcing function is handled the same way. Recall that $\underline{u}(y_i)$ is defined such that $\underline{y}_i \cdot \underline{u}(y_i) \geq 0$ for all $\underline{x} \in G$. Another way of saying the same thing is that $\text{sgn}[\underline{u}(y_i)] = \text{sgn}[y_i]$ for all $\underline{x} \in G$. This is a sensible requirement for any controller that seeks to stabilize a system. Under these conditions, the $\underline{z}(t)$ that guarantee the domination of $\dot{V}(\underline{x}, t)$ by $W(\underline{x})$ is

$$\hat{z}_i = \max_t |z_i(t)| \text{sgn}[y_i], \quad i = 1, \ldots, N$$

where the $z_i(t)$ are elements of the vector $\underline{z}(t)$. In this framework, the forcing function is considered to be an effect that reduces the stabilizing power of the controller. For systems such as those considered above, the effect is to reduce the size of the domain of attraction. If the $\underline{z}(t)$ is taken to be the model of the aerodynamic torque derived in Chapter II and described by the forcing terms in (3.5-7b) and (3.5-7c), it can be shown that $|z_i(t)| << b_i$; $i = 2,4$. The result of this is that the hyperplanes specified by setting $W(\underline{x}) = 0$ in R^n differ only inconsequentially from those in Figures 28 and 29.

Reproduced with permission of the copyright owner. Further reproduction prohibited without permission.

The importance of the concepts presented above is less ad-hoc than might appear at first glance. Indeed, they provide a framework for the consideration of the bounded-input, bounded-output stability of systems that are not open-loop asymptotically stable in the large. That this is a non-trivial problem is evident from a study of [5.9 - 5.17].

Reproduced with permission of the copyright owner. Further reproduction prohibited without permission.

CHAPTER VI

CONCLUSIONS AND SUGGESTIONS FOR FUTURE RESEARCH

The primary results of this research are:

1. the establishment of the zero-fuel mode as a first step in the determination of a minimum-fuel control law for linear multidimensional dynamical systems with uncontrolled periodic inputs, and
2. the development of a method for analyzing the closed-loop stability of a class of multidimensional feedback systems:

(a) whose linear plants have arbitrary open-loop stability properties,

(b) that may have a deadband (region of zero torque) incorporated in its control law, and

(c) that may have any bounded uncontrolled input.

The method for achieving the second result, an application of some recent generalizations of the Lyapunov stability theory by Yoshizawa and LaSalle, also provides the domain of attraction for the system; i.e., the region G* in which all solutions of the system equation converge to a compact set E* that contains the positive limit set of the solution.

Reproduced with permission of the copyright owner. Further reproduction prohibited without permission.

The approach taken herein to the problem of developing periodic solutions of the open-loop system equation as target sets for an optimal control problem could be extended to nonlinear systems with periodic inputs. This extension, however, would be at the expense of the elegance and generality of Theorem 3.1 and its associated algorithm for determining the initial condition that yields the periodic solution. One possibility for achieving this extension is to develop the required initialization criteria using the method of successive approximations (MSA). This approach was taken for the linear system studied herein in [3.2]. The main shortcoming of the MSA approach is the expected inability to generalize the results to a whole class of systems. Further generalizations of the first result, say to systems with bounded aperiodic inputs, may also be possible using MSA. However, a more fruitful possibility than obtaining the exact solution of the system equation that is to be used as a target set, might be to use as a target set some invariant, compact set E^* that includes the exact solution. One way to generate E^* is discussed below as an extension of our second result.

The generalization of the second result to nonlinear, nonstationary, multidimensional systems is complicated only by the geometry involved. That is, the regions E^*, which contains the positive limit set, and G^*, which is contained in the domain of attraction, might be n-dimensional and be enclosed by complicated boundary surfaces. This problem could be alleviated, however, by accepting a $G_1^* \subset G^*$ and an $E_1^* \supset E^*$ whose boundaries are more easily described.

Reproduced with permission of the copyright owner. Further reproduction prohibited without permission.

A more general extension of the second result is the application of the theory of Lyapunov to the study of the bounded-input bounded-output (b.i.b.o.) stability of nonlinear systems. This extension need not be confined to systems containing a deadband controller where the E* was known in advance. Rather, a series of estimates E^*_{1i}; i = 1,2,..., N could be made. Then, if some subset E^*_{2j}; j = 1,2,..., M ≤ N of E^*_{1i} can be shown to contain the positive limit set of solutions of the system equation originating in regions G^*_j, then

$$E^* = E^*_{21} \cap E^*_{22} \cap \cdots \cap E^*_{2M} \quad .$$

Some advantages of this approach to b.i.b.o. stability analysis are now given.

1. The nonlinearities need not be imbedded within a larger class of nonlinear functions and should, therefore, yield larger G*'s and smaller E*'s than more general methods.
2. The boundedness of the output need not be expressed as a function of any particular norm although the boundedness of the Euclidean norm will be implied. This admits a wider class of admissible input and output functions than, for example, analyses of systems that are b.i.b.o. stable in the L_2 norm.
3. This method can be applied to feedback systems with arbitrary open-loop stability properties by the simple device of limiting the magnitude (but not the form) of admissible input functions to be

Reproduced with permission of the copyright owner. Further reproduction prohibited without permission.

somewhat less than the magnitude of the controller in G*. Of course, this condition must exist in any well-designed feedback system.

Reproduced with permission of the copyright owner. Further reproduction prohibited without permission.

APPENDIX A

ILLUSTRATIONS

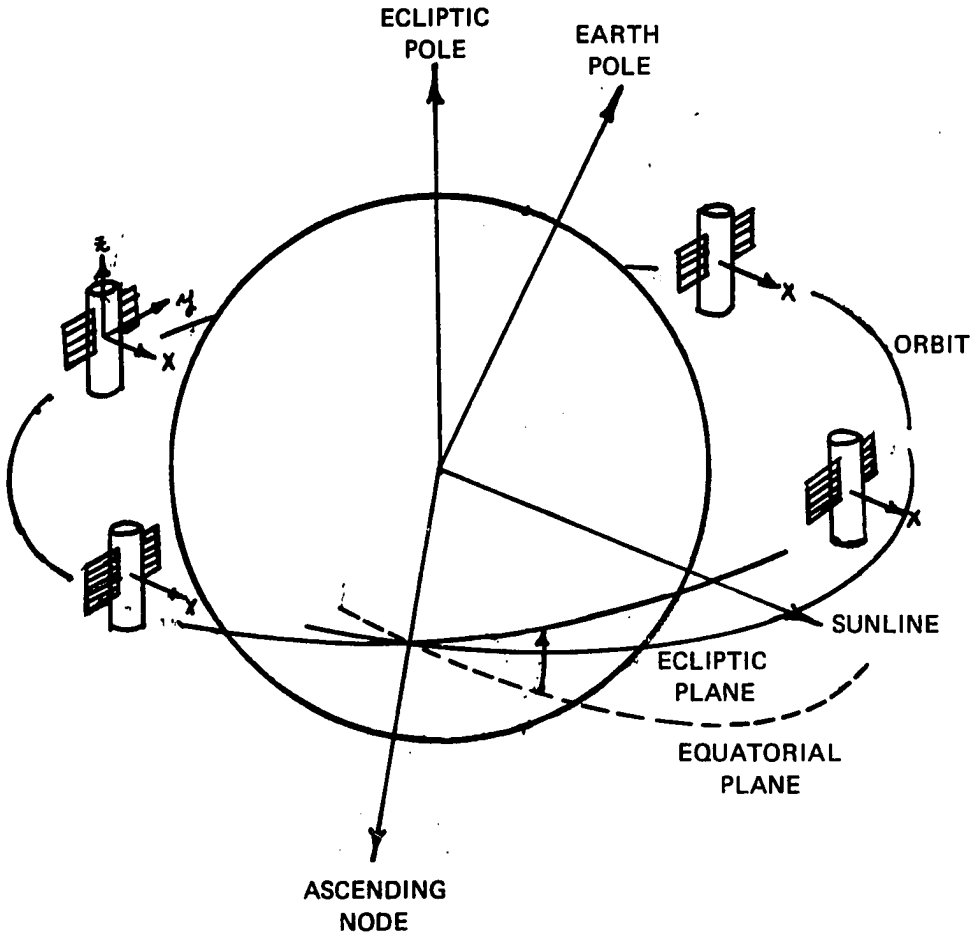

FIGURE 1 - NOMINAL SPACECRAFT ATTITUDE

Reproduced with permission of the copyright owner. Further reproduction prohibited without permission.

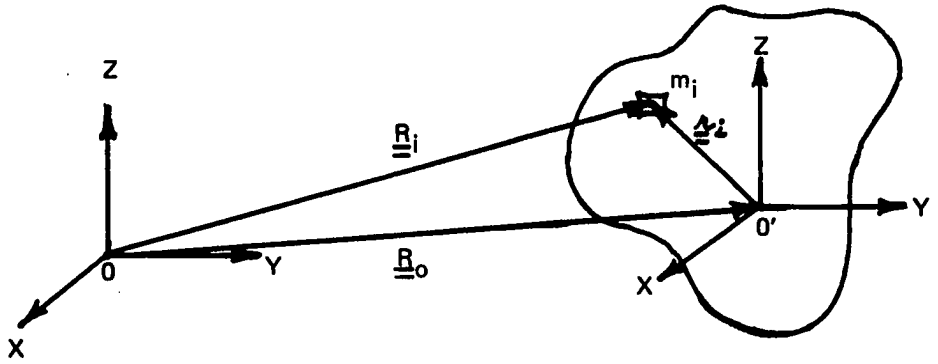

FIGURE 2 - DYNAMICS OF n BODIES

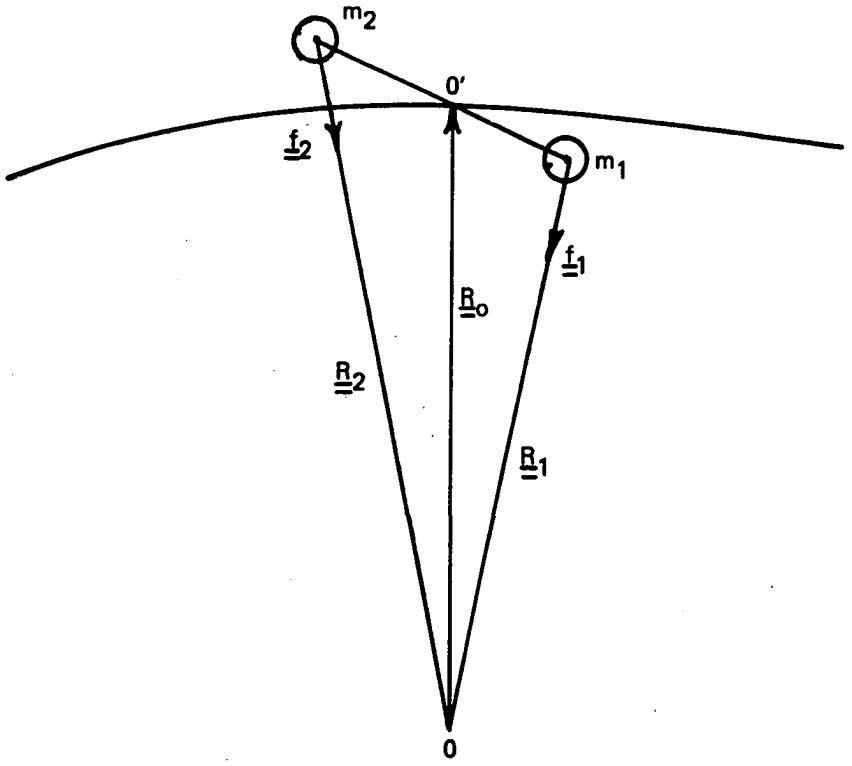

FIGURE 3 - GRAVITY-GRADIENT TORQUE ABOUT THE CENTER OF MASS OF A DUMBBELL

Reproduced with permission of the copyright owner. Further reproduction prohibited without permission.

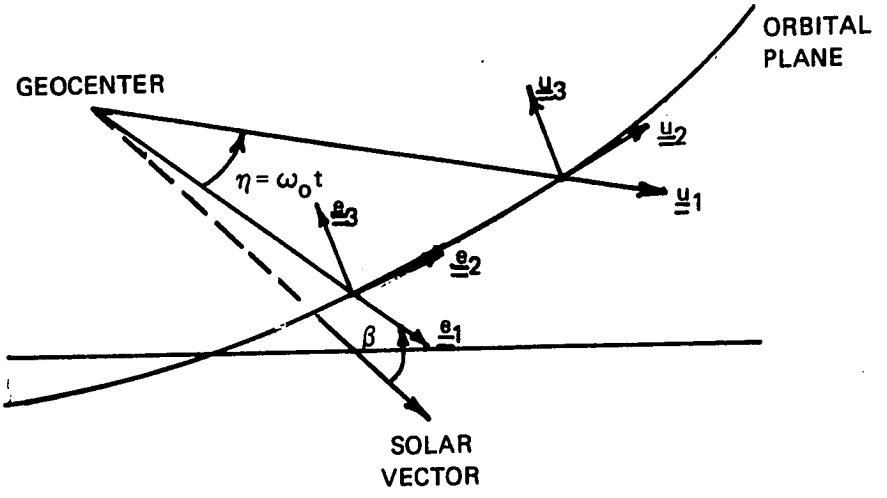

FIGURE 4 - THE LOCAL VERTICAL AND THE INERTIAL COORDINATE SYSTEMS

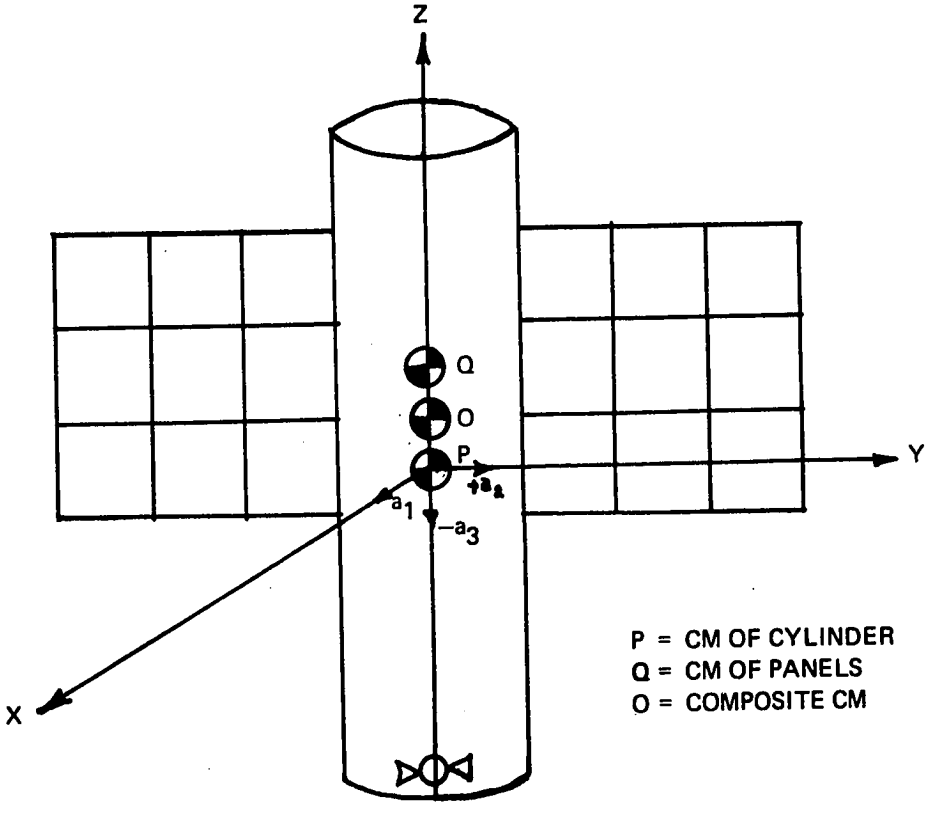

FIGURE 5 - SPACECRAFT COORDINATE SYSTEM (BODY AXES)

Reproduced with permission of the copyright owner. Further reproduction prohibited without permission.

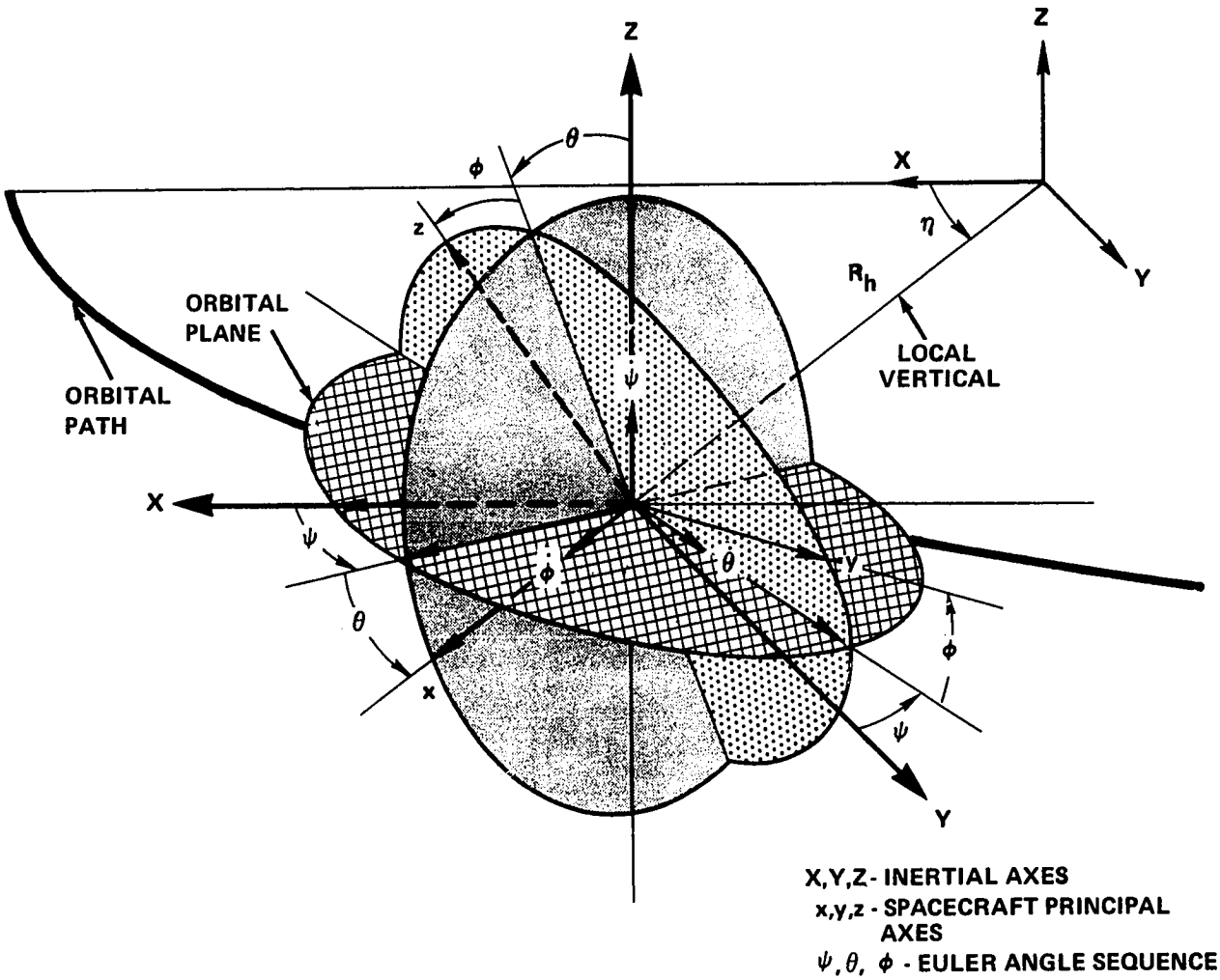

FIGURE 6 - RELATIONSHIPS BETWEEN BODY AXES, BODY RATES AND INERTIAL AXES

Reproduced with permission of the copyright owner. Further reproduction prohibited without permission.

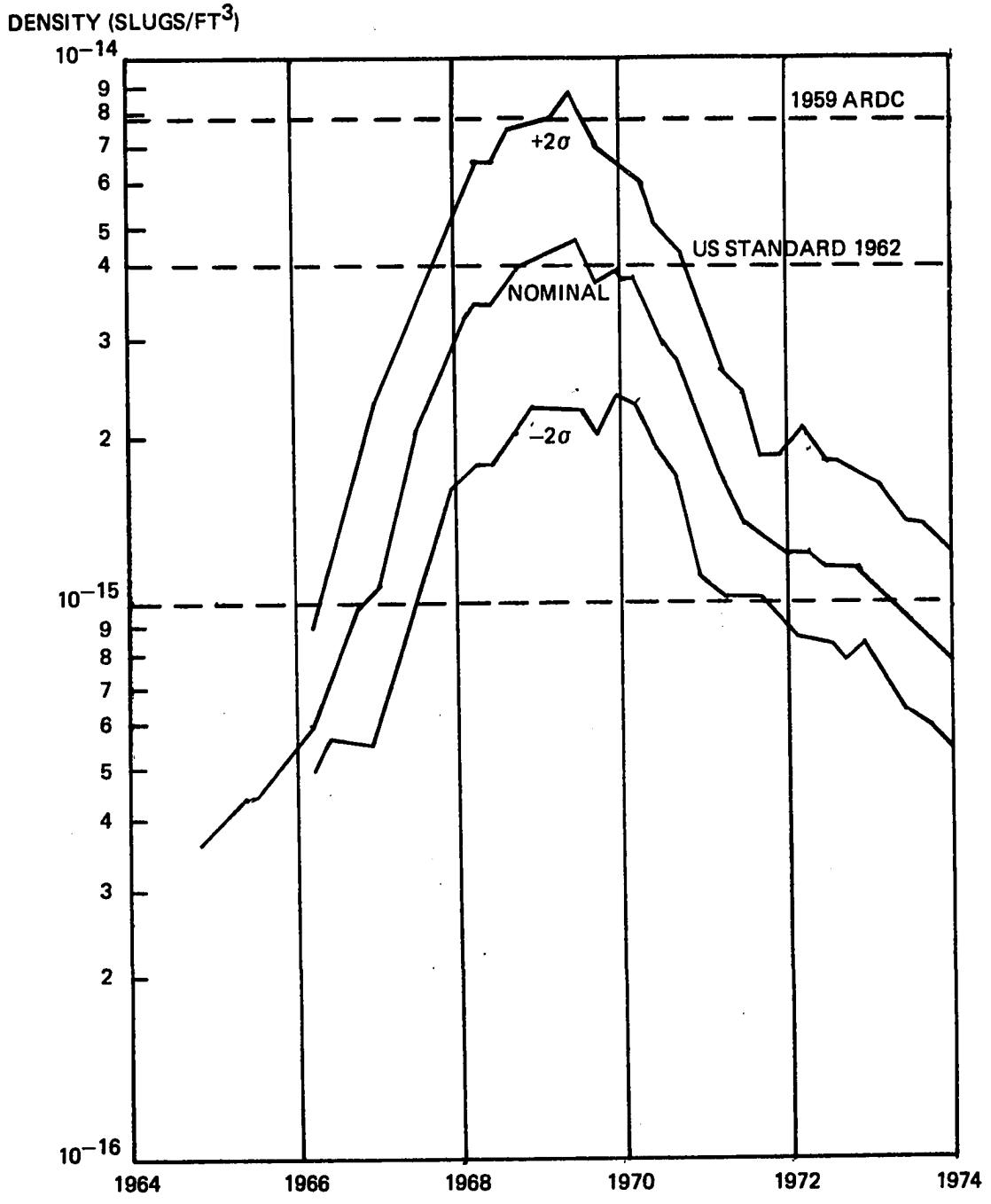

FIGURE 7 - ATMOSPHERIC DENSITY AS A FUNCTION OF SOLAR ACTIVITY

Reproduced with permission of the copyright owner. Further reproduction prohibited without permission.

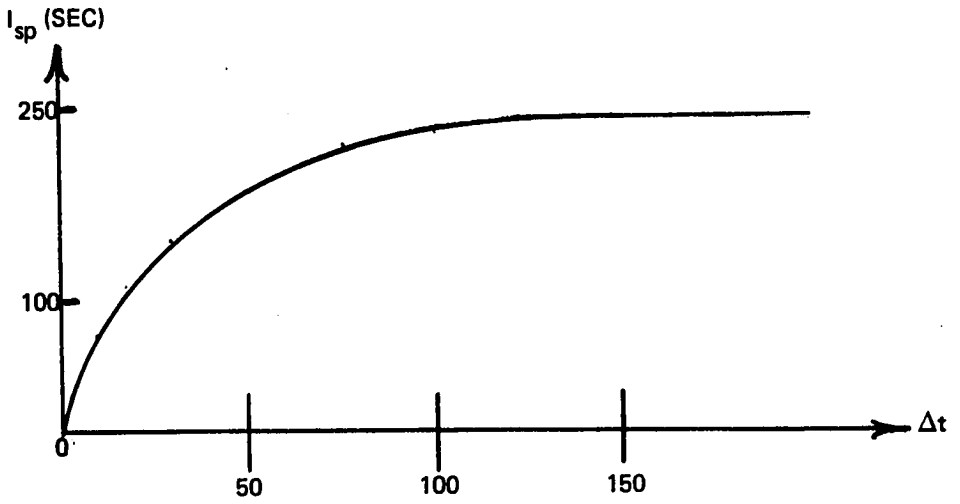

FIGURE 8 - SPECIFIC IMPULSE (I_{sp}) VS THRUSTER ON-TIME (Δt) FOR BIPROPELLANT THRUSTERS

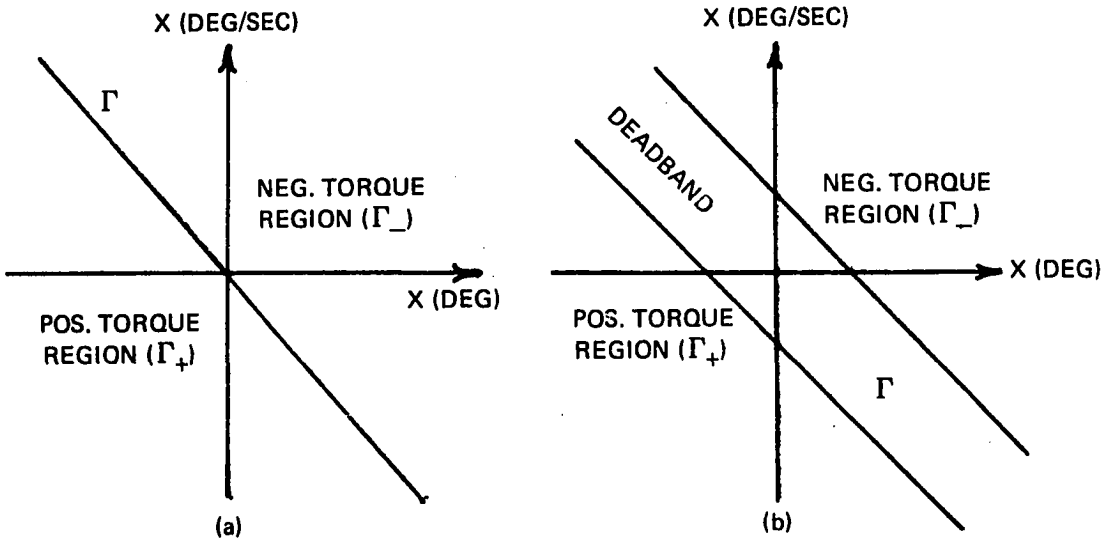

FIGURE 9

Reproduced with permission of the copyright owner. Further reproduction prohibited without permission.

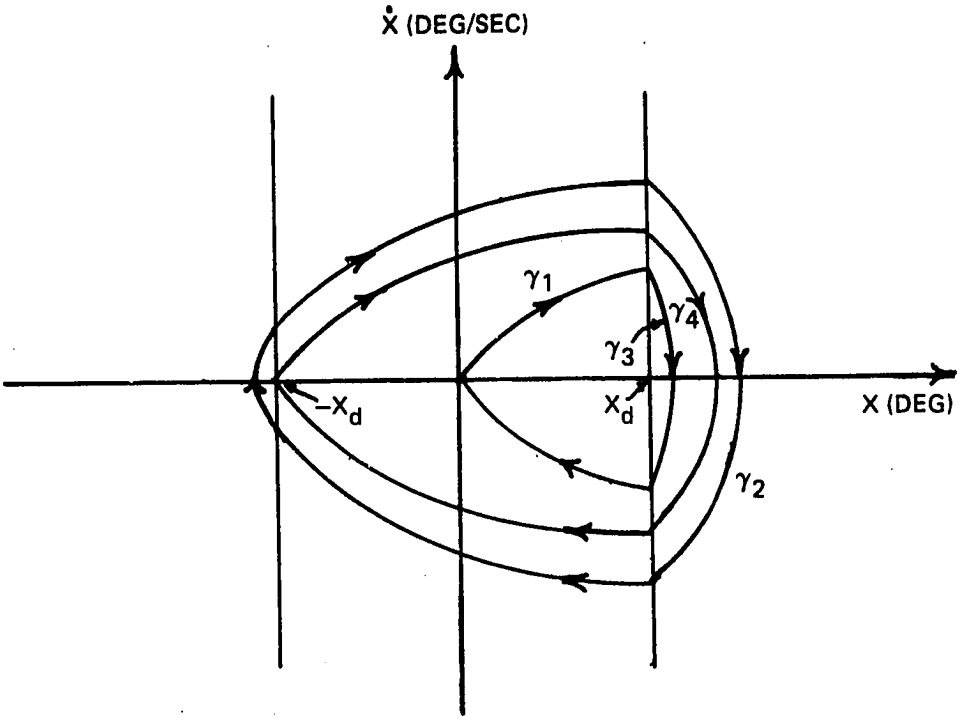

FIGURE 10 - TRAJECTORIES FOR SYSTEM $X = \lambda_o + \lambda_c (X)$

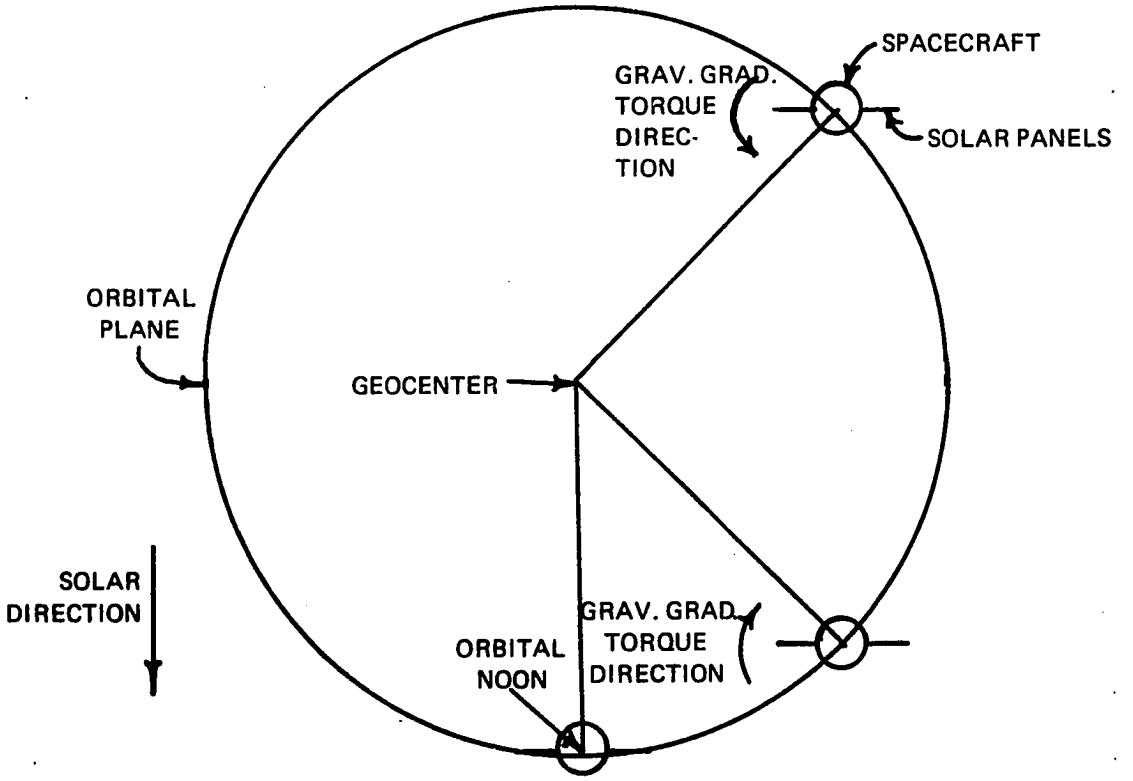

FIGURE 11 - SCHEMATIC REPRESENTATION OF SOLAR PANEL ORIENTATION

Reproduced with permission of the copyright owner. Further reproduction prohibited without permission.

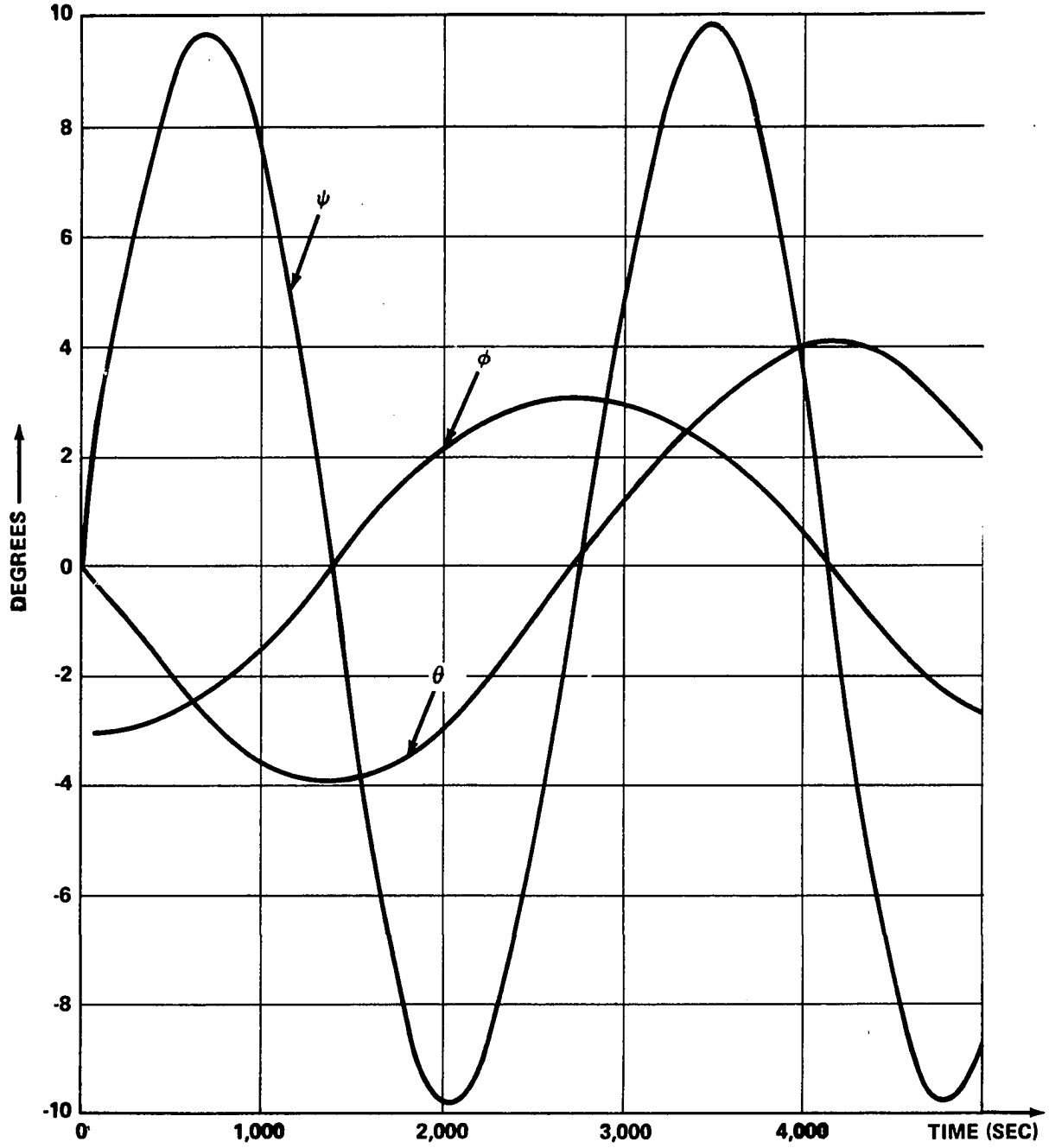

FIGURE 12 - ZERO-FUEL MOTION FOR LINEARIZED SYSTEM

Reproduced with permission of the copyright owner. Further reproduction prohibited without permission.

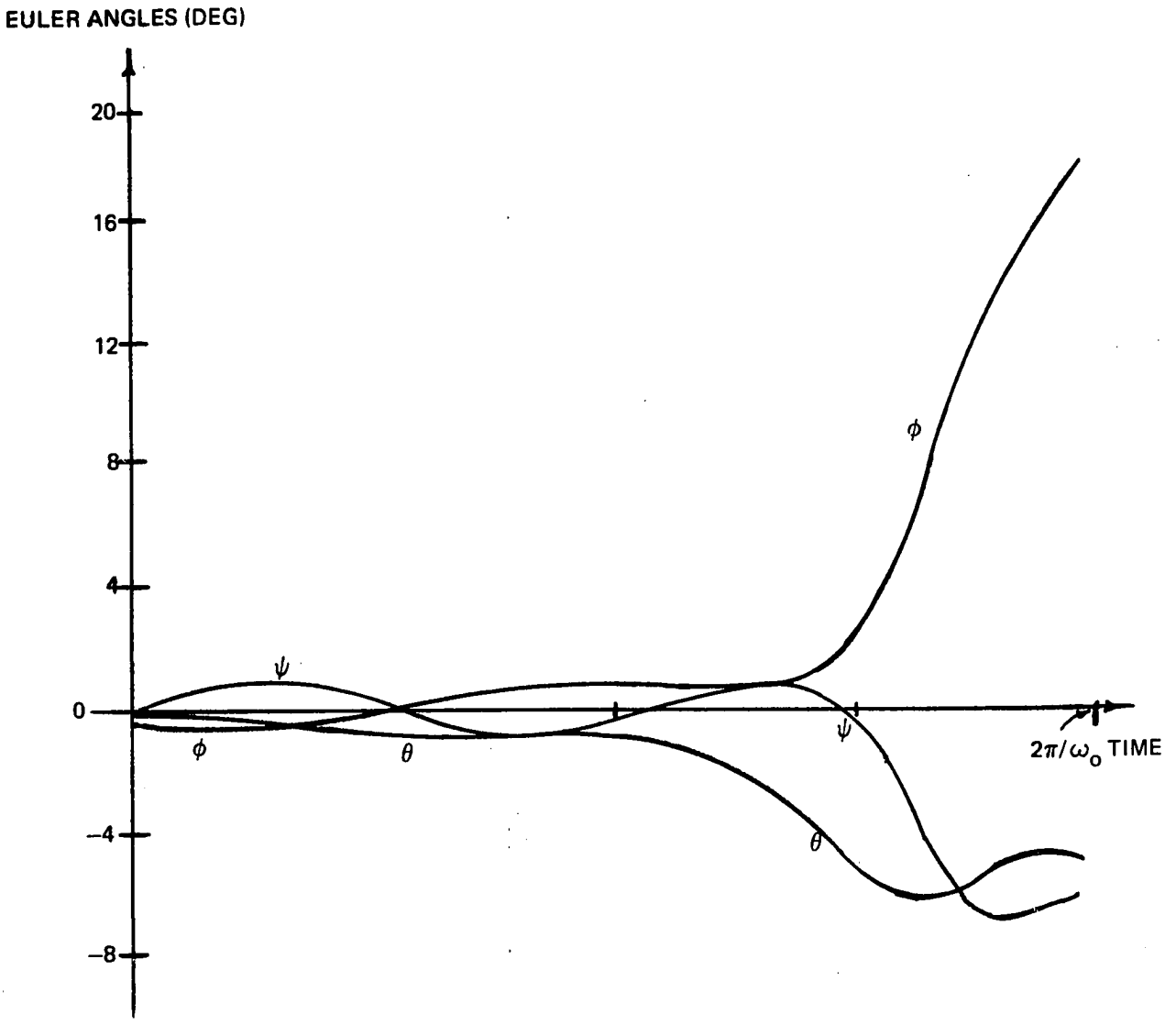

FIGURE 13 - RESPONSE OF NON-LINEAR SYSTEM EQUATIONS TO INITIALIZATION BASED ON LINEAR SYSTEM (2.7-4)

Reproduced with permission of the copyright owner. Further reproduction prohibited without permission.

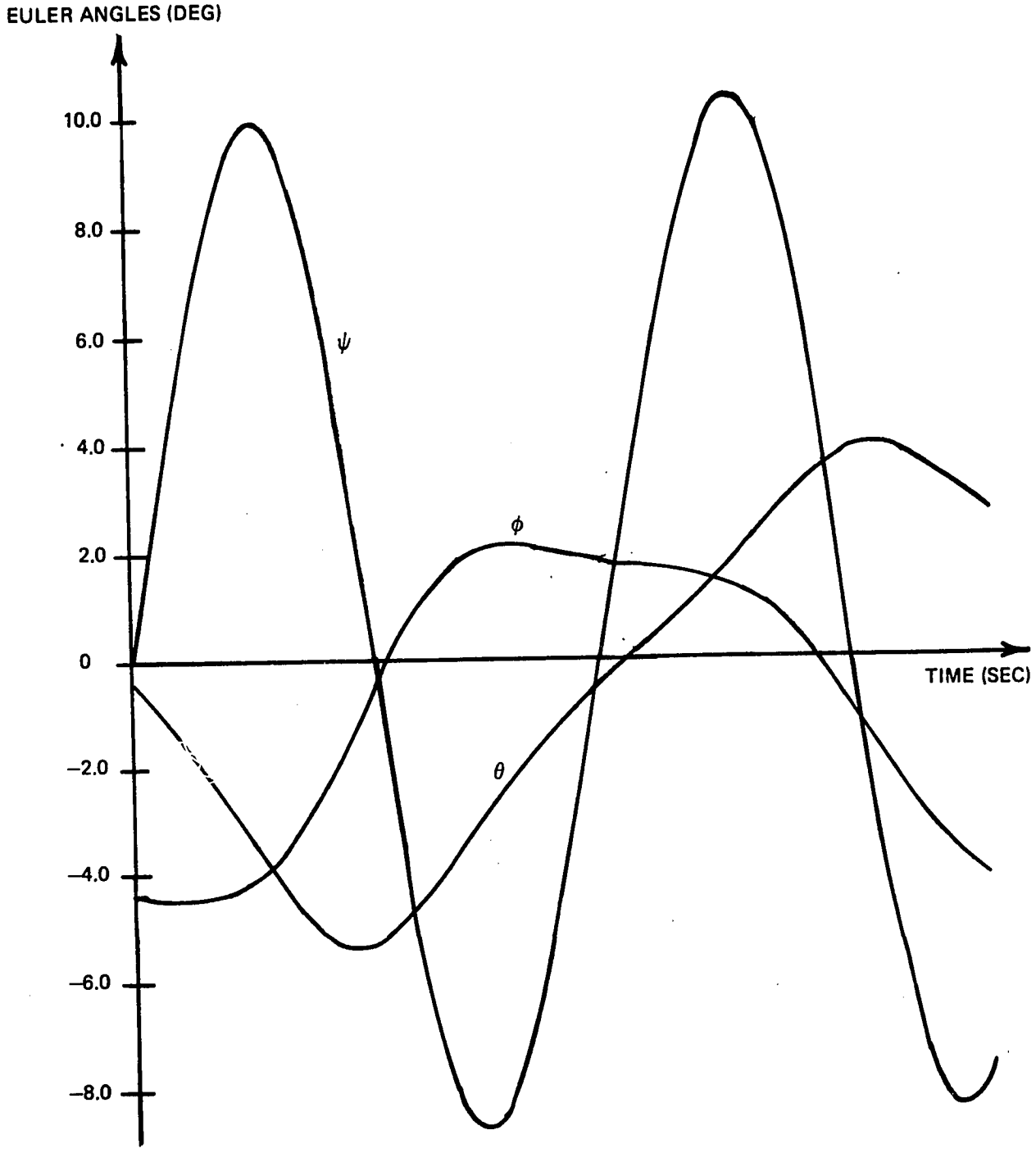

FIGURE 14 - RESPONSE OF NON-LINEAR SYSTEM EQUATIONS TO INITIALIZATION BASED ON LINEAR SYSTEM (3.5-7)

Reproduced with permission of the copyright owner. Further reproduction prohibited without permission.

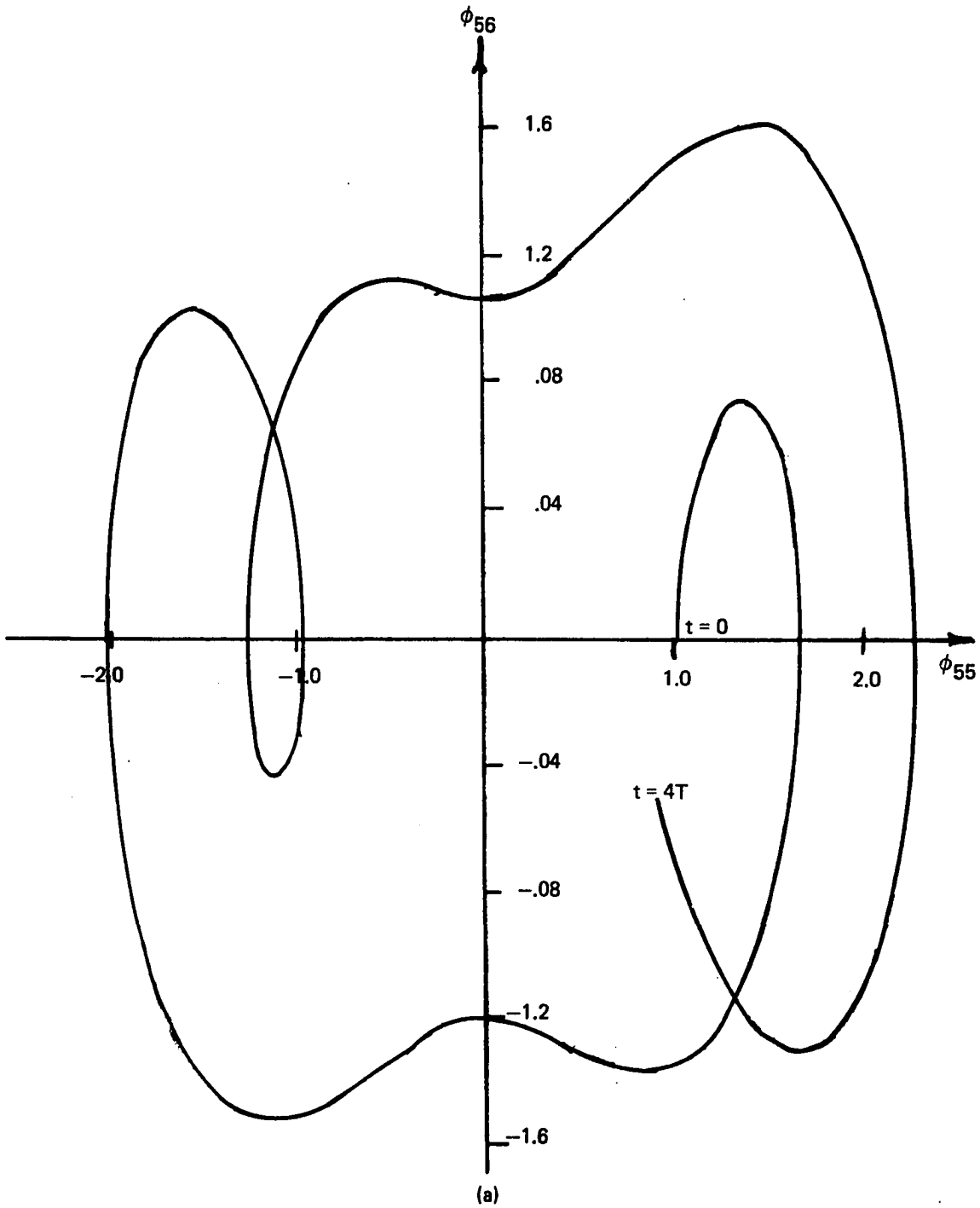

FIGURE 15a - UNCONTROLLED Z-AXIS MOTION VS. TIME (ϕ_{55} VS. ϕ_{56} OF SYSTEM TRANSITION MATRIX)

Reproduced with permission of the copyright owner. Further reproduction prohibited without permission.

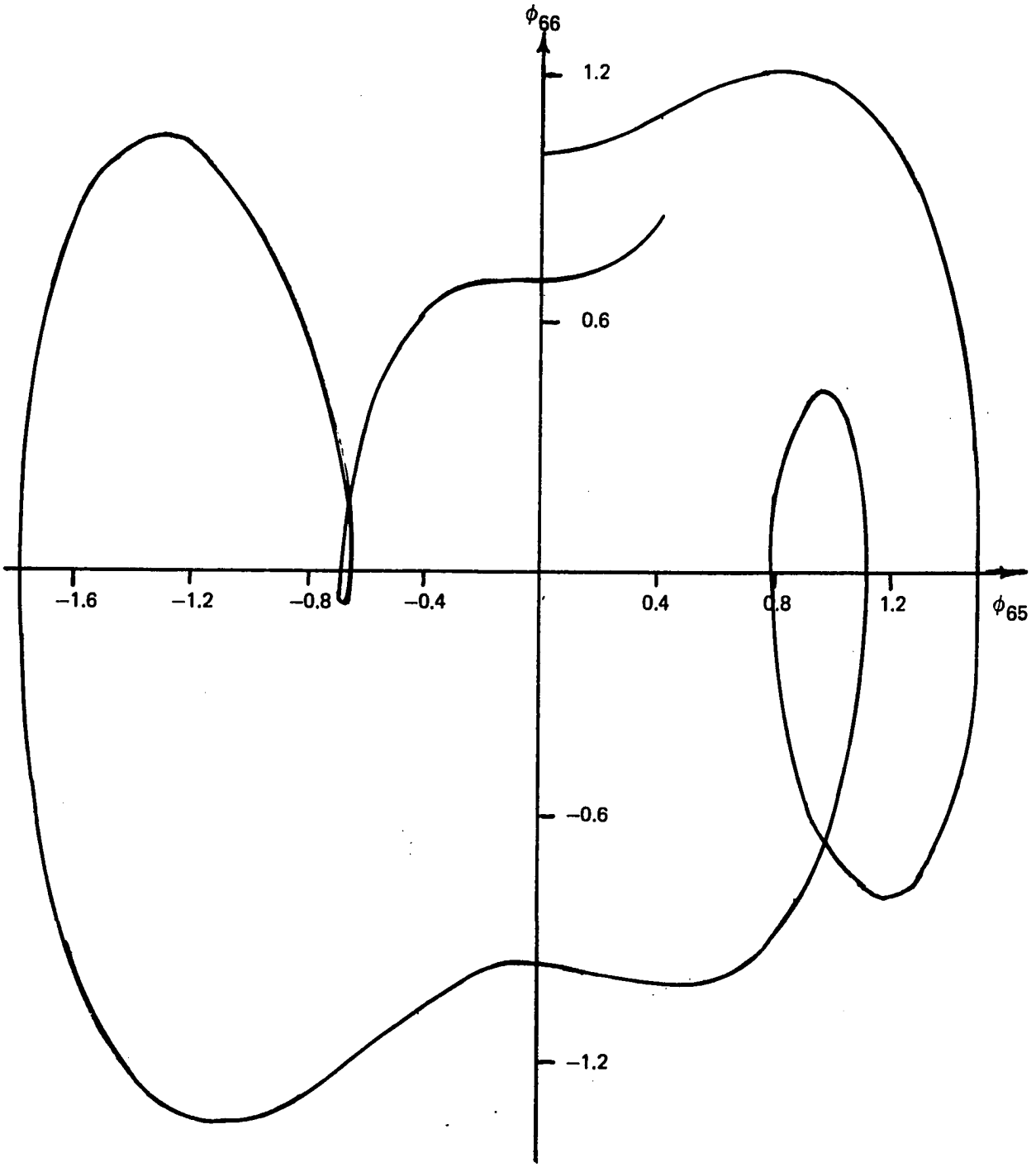

FIGURE 15b - UNCONTROLLED Z-AXIS MOTION VS. TIME (ϕ_{66} VS. ϕ_{65} OF SYSTEM TRANSITION MATRIX)

Reproduced with permission of the copyright owner. Further reproduction prohibited without permission.

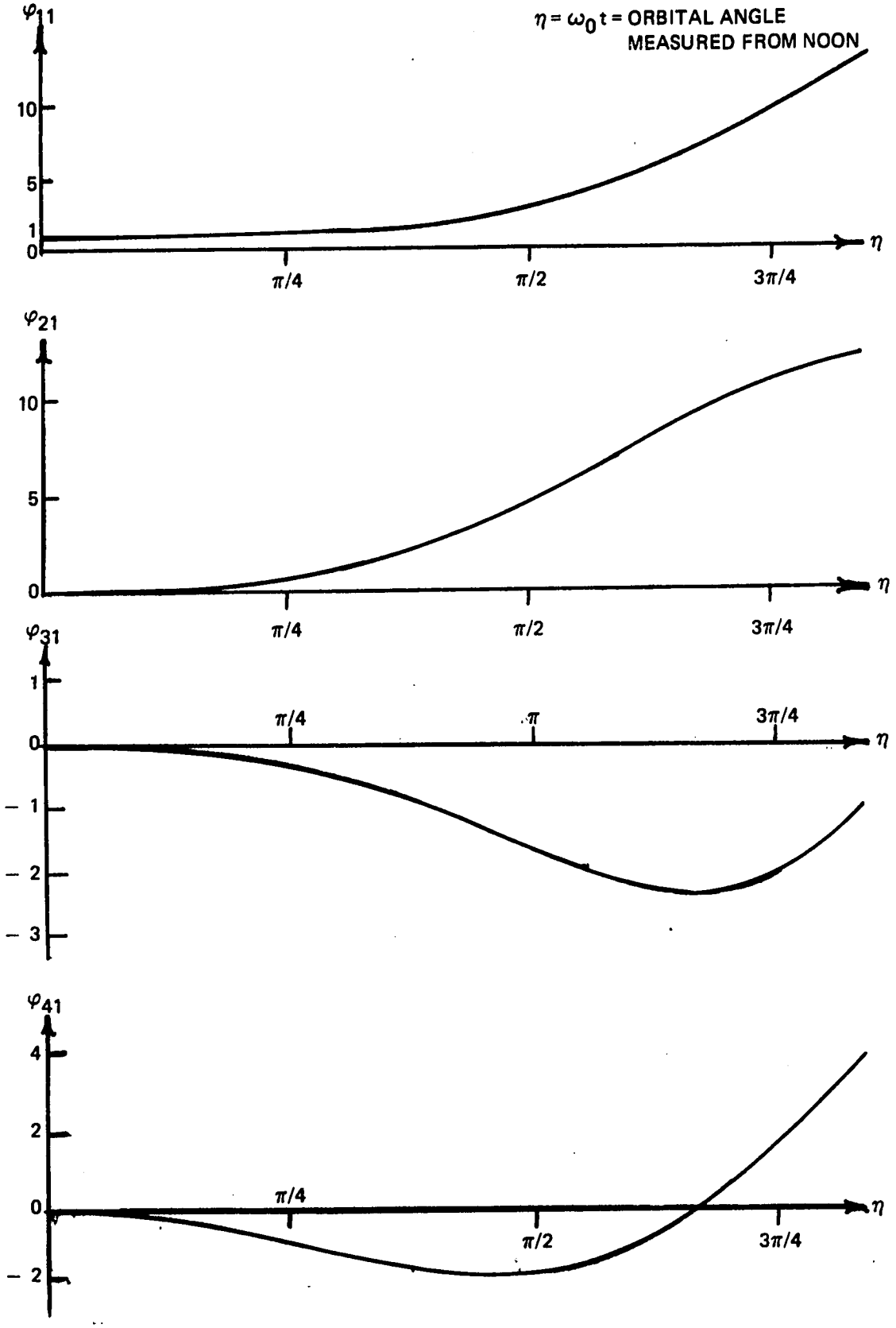

FIGURE 15c - ELEMENTS $\phi_{11} - \phi_{41}$ OF SOLUTION OF (4.2-4) VS. η

Reproduced with permission of the copyright owner. Further reproduction prohibited without permission.

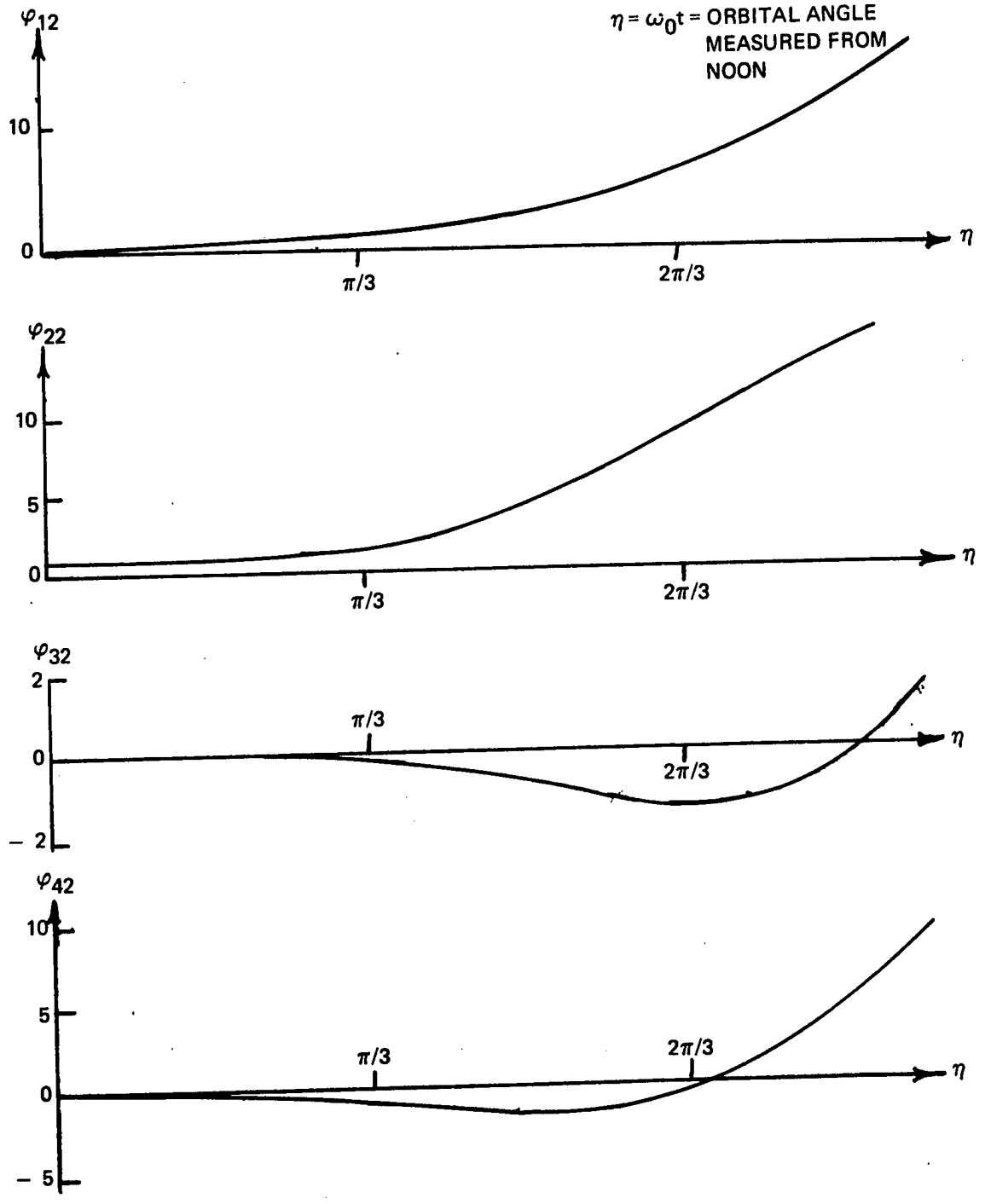

FIGURE 15d - ELEMENTS $\phi_{12} - \phi_{42}$ OF SOLUTIONS OF (4.2-4) VS. η

Reproduced with permission of the copyright owner. Further reproduction prohibited without permission.

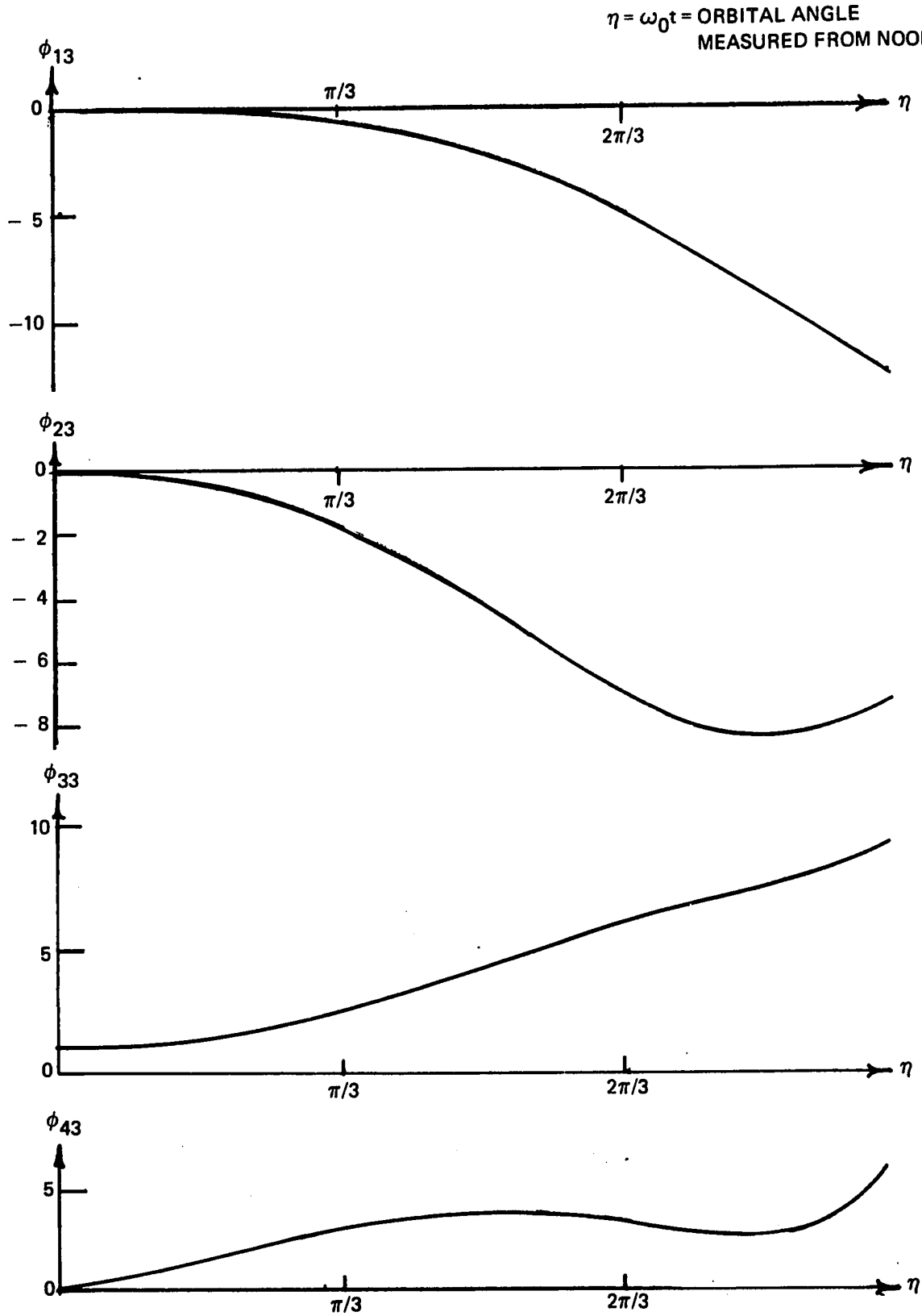

FIGURE 15e - ELEMENTS $\phi_{13} - \phi_{43}$ OF SOLUTIONS OF (4.2-4) VS. η

Reproduced with permission of the copyright owner. Further reproduction prohibited without permission.

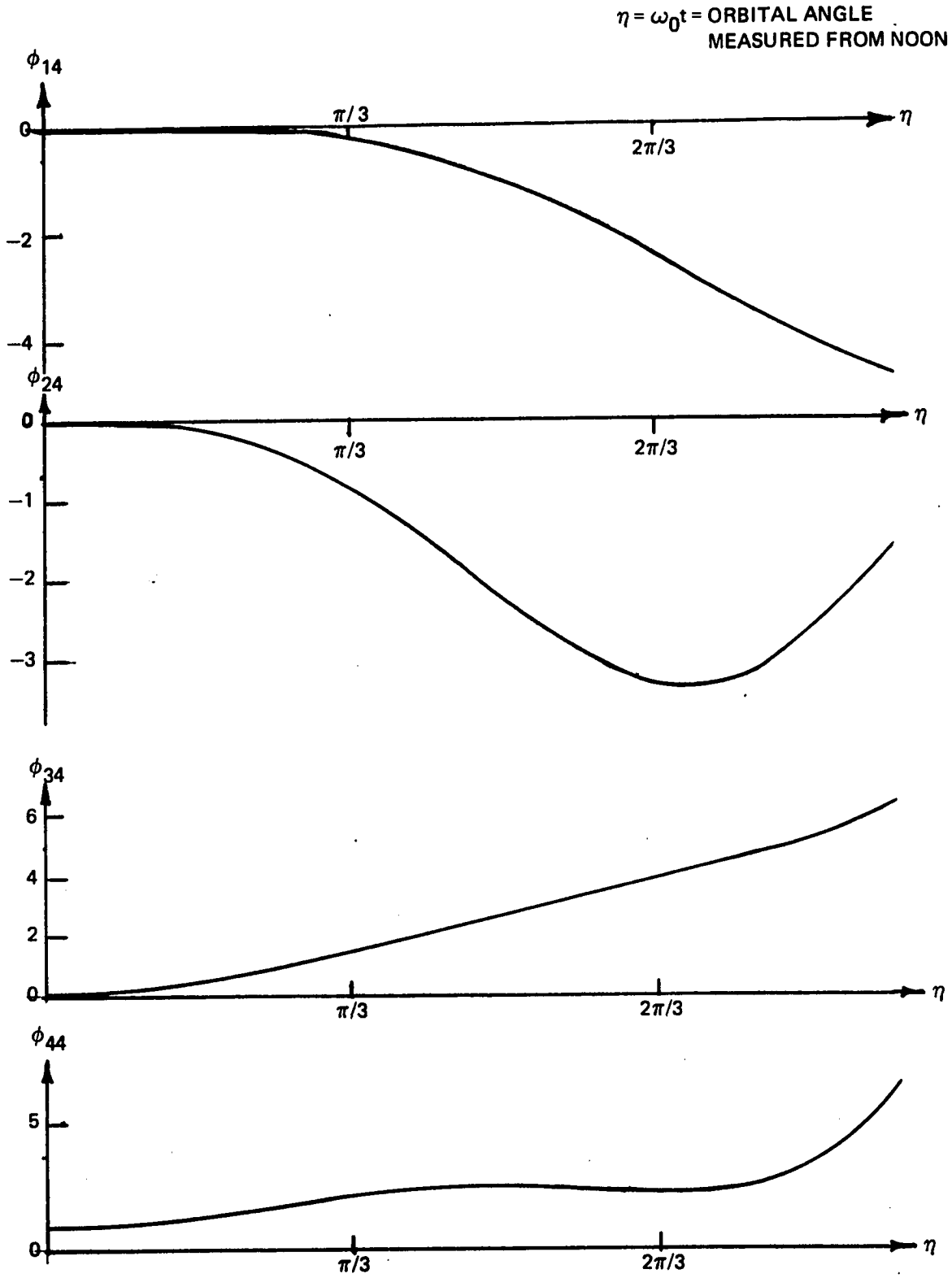

FIGURE 15f - ELEMENTS $\phi_{14} - \phi_{44}$ OF SOLUTIONS OF (4.2-4) VS. η

Reproduced with permission of the copyright owner. Further reproduction prohibited without permission.

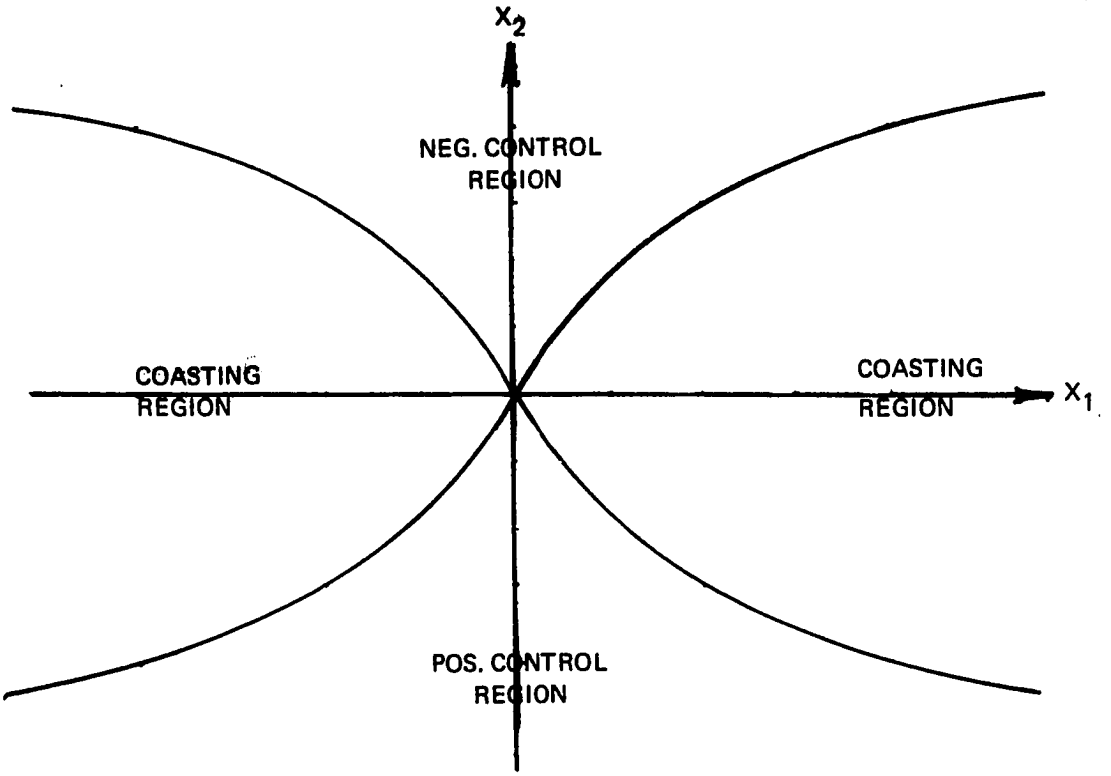

FIGURE 16 - SWITCHING LINES FOR SUB-OPTIMAL CONTROL OF A SYSTEM DESCRIBED BY A "DAMPED" MATHIEU EQUATION

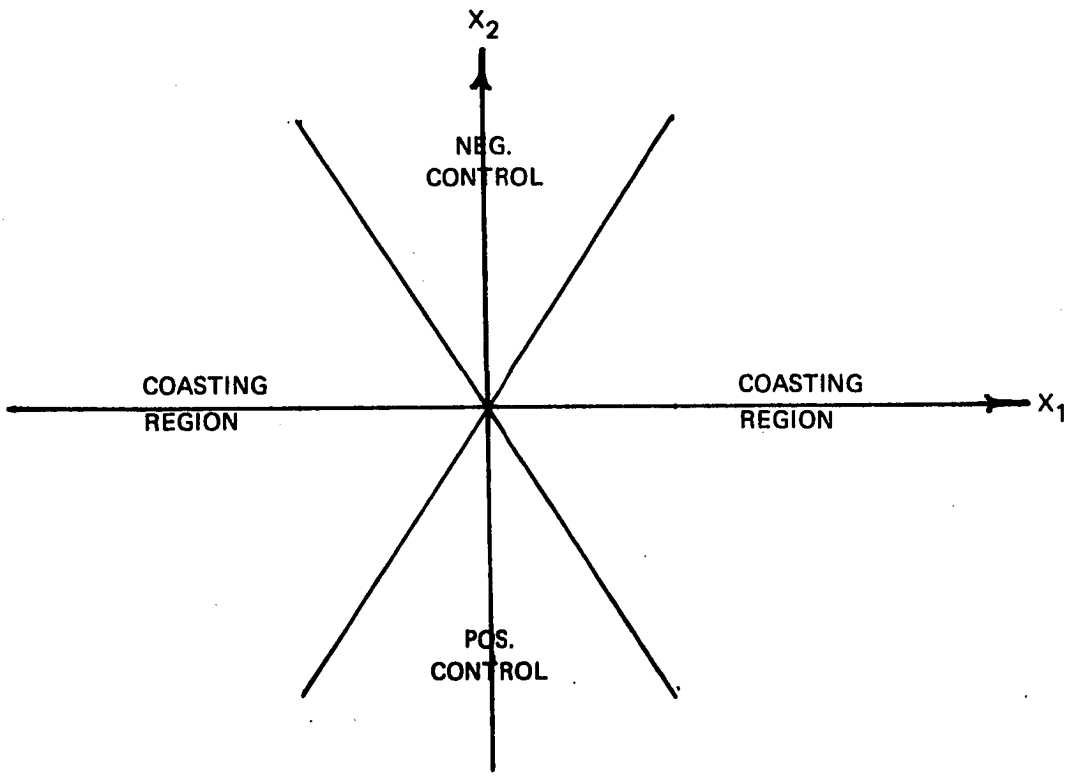

FIGURE 17 - SWITCHING LINES FOR MINIMUM-FUEL CONTROL OF 2nd ORDER LINEAR HARMONIC OSCILLATOR (FLUGGE-LOTZ & CRAIG)

Reproduced with permission of the copyright owner. Further reproduction prohibited without permission.

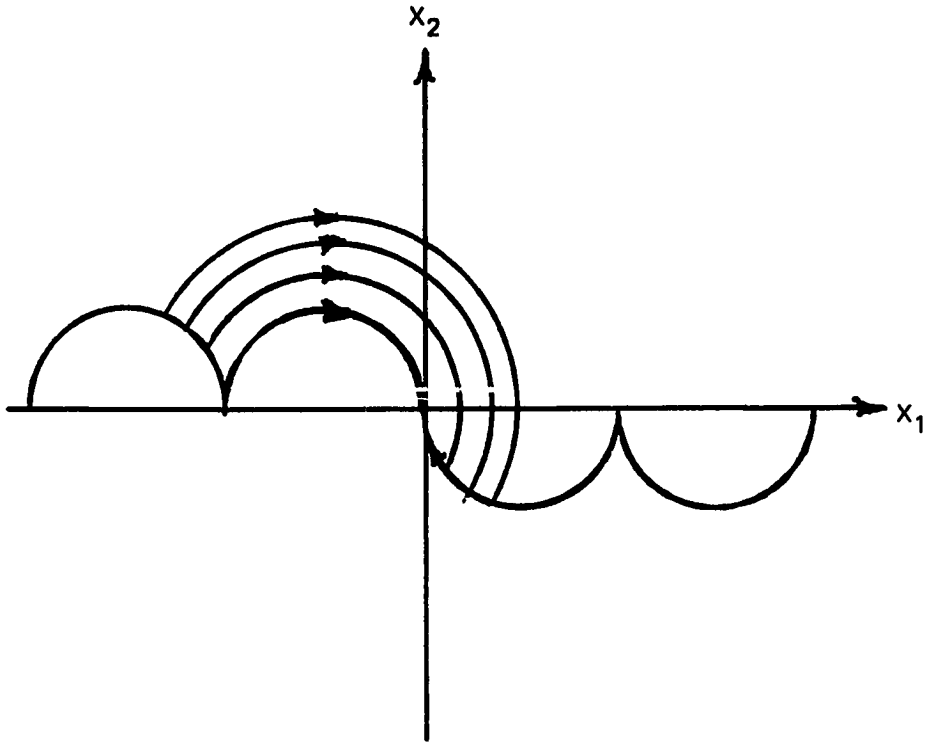

FIGURE 18 - SWITCHING CURVES FOR TIME-OPTIMAL CONTROL OF A 2nd ORDER LINEAR HARMONIC OSCILLATOR

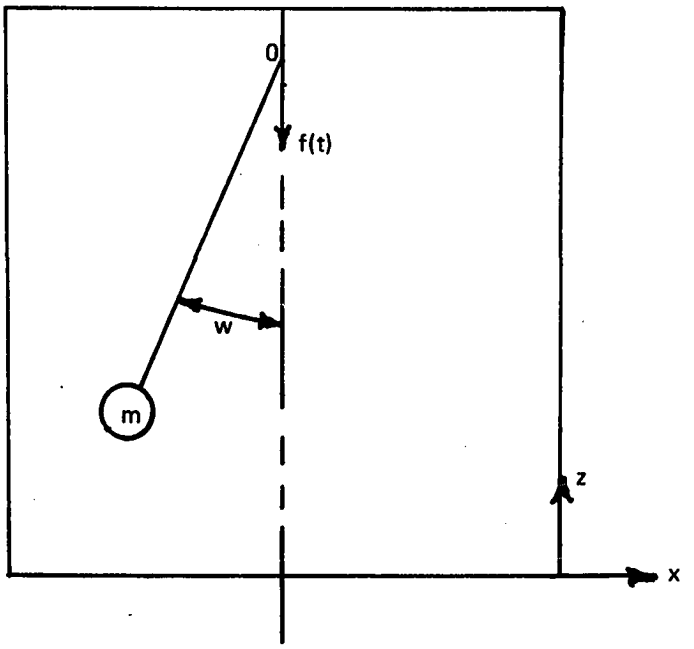

FIGURE 19 - EXAMPLE OF A SYSTEM DESCRIBED BY AN UNDAMPED MATHIEU EQUATION

Reproduced with permission of the copyright owner. Further reproduction prohibited without permission.

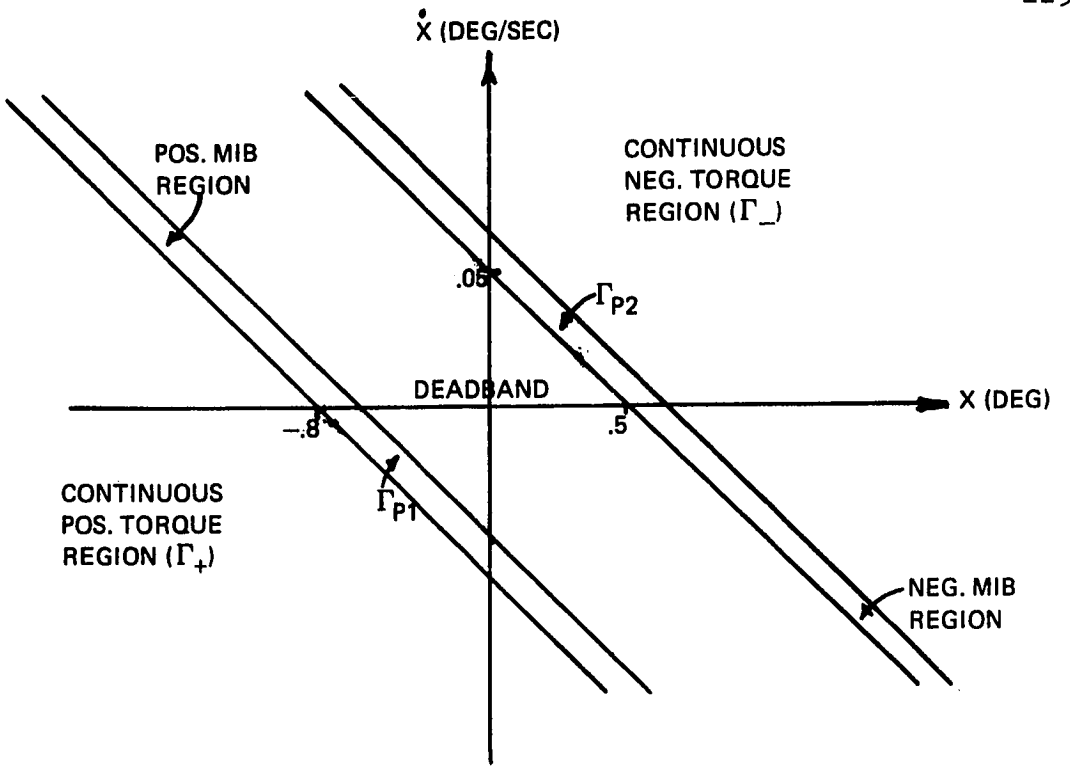

FIGURE 20 - LINEAR DEADBAND CONTROL WITH MIB REGIONS

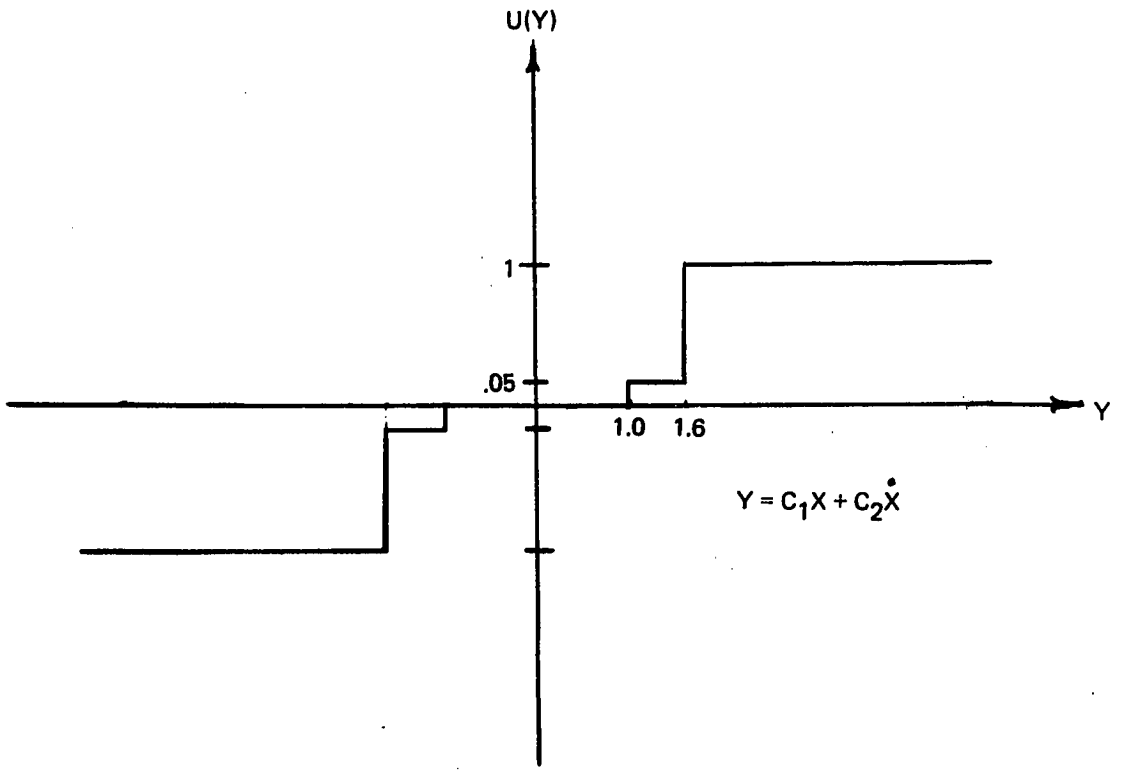

FIGURE 21 - CONTROL TORQUE VS. OUTPUT ERROR Y

Reproduced with permission of the copyright owner. Further reproduction prohibited without permission.

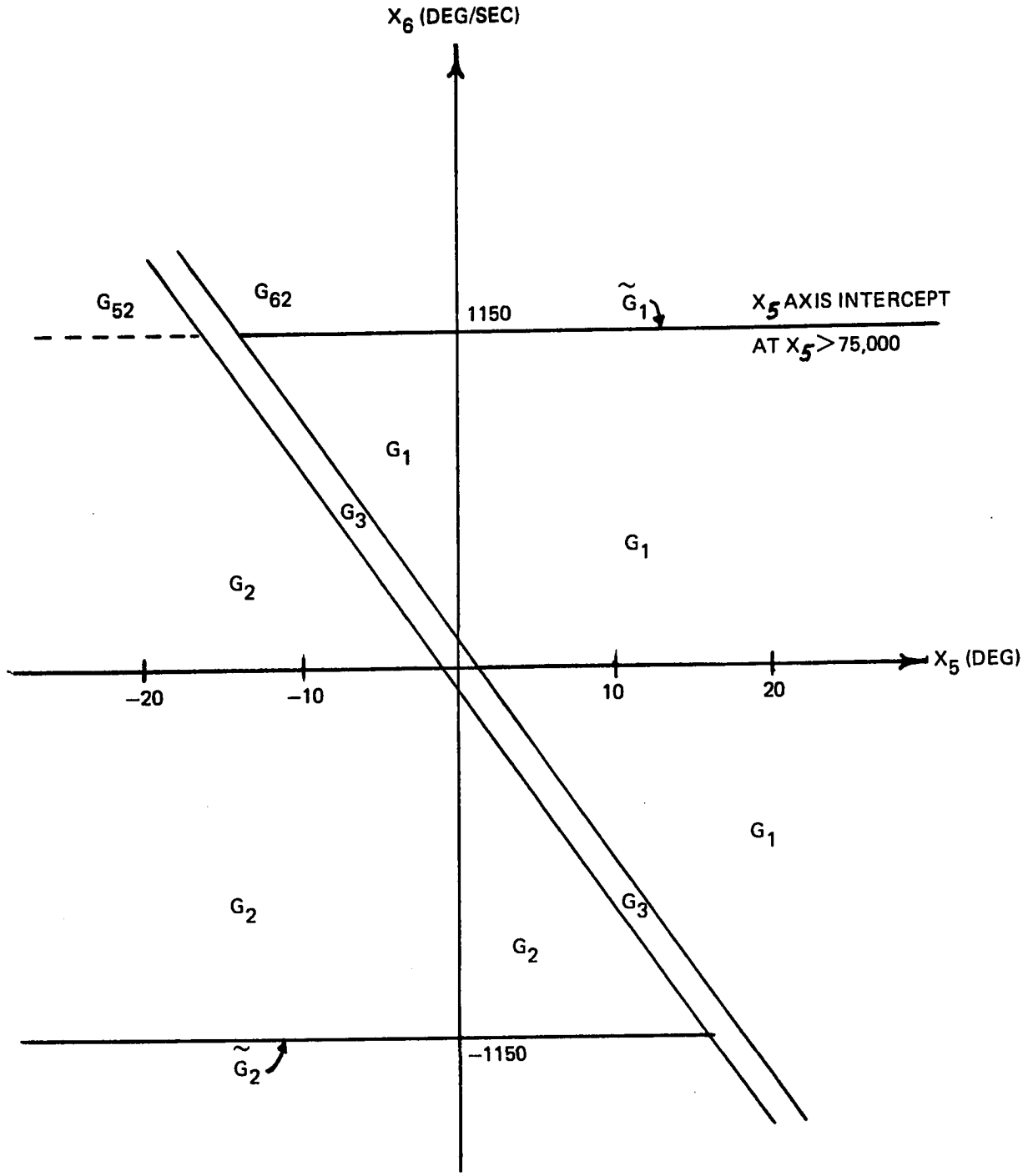

FIGURE 22 - FIRST ESTIMATE OF THE DOMAIN OF ATTRACTION OF SYSTEM (5.4-2) WHEN $U(Y_3) = 1$

Reproduced with permission of the copyright owner. Further reproduction prohibited without permission.

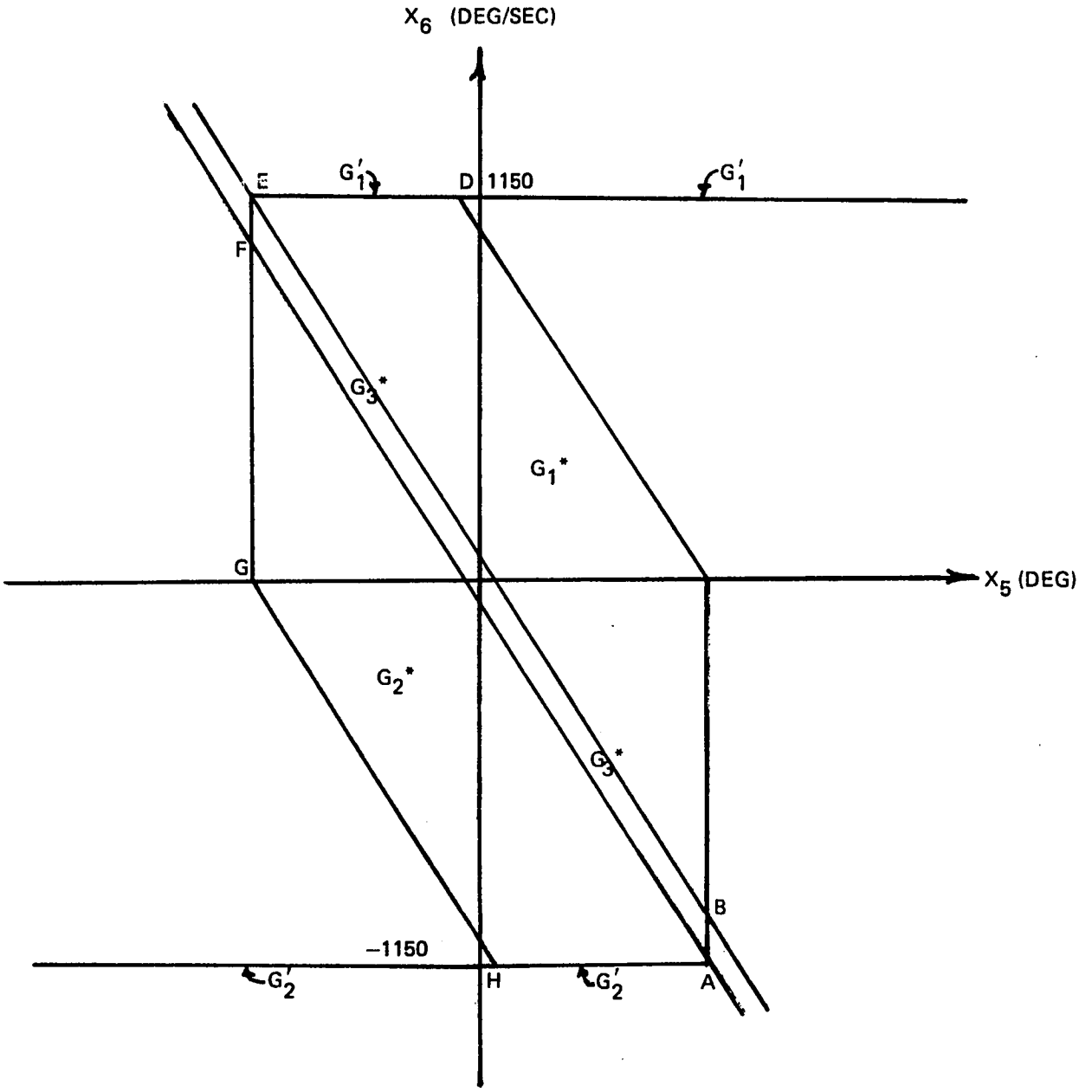

FIGURE 23 - A BOUNDED DOMAIN OF ATTRACTION FOR SYSTEM (5.3-2) WHEN $U(Y_3) = 1$

Reproduced with permission of the copyright owner. Further reproduction prohibited without permission.

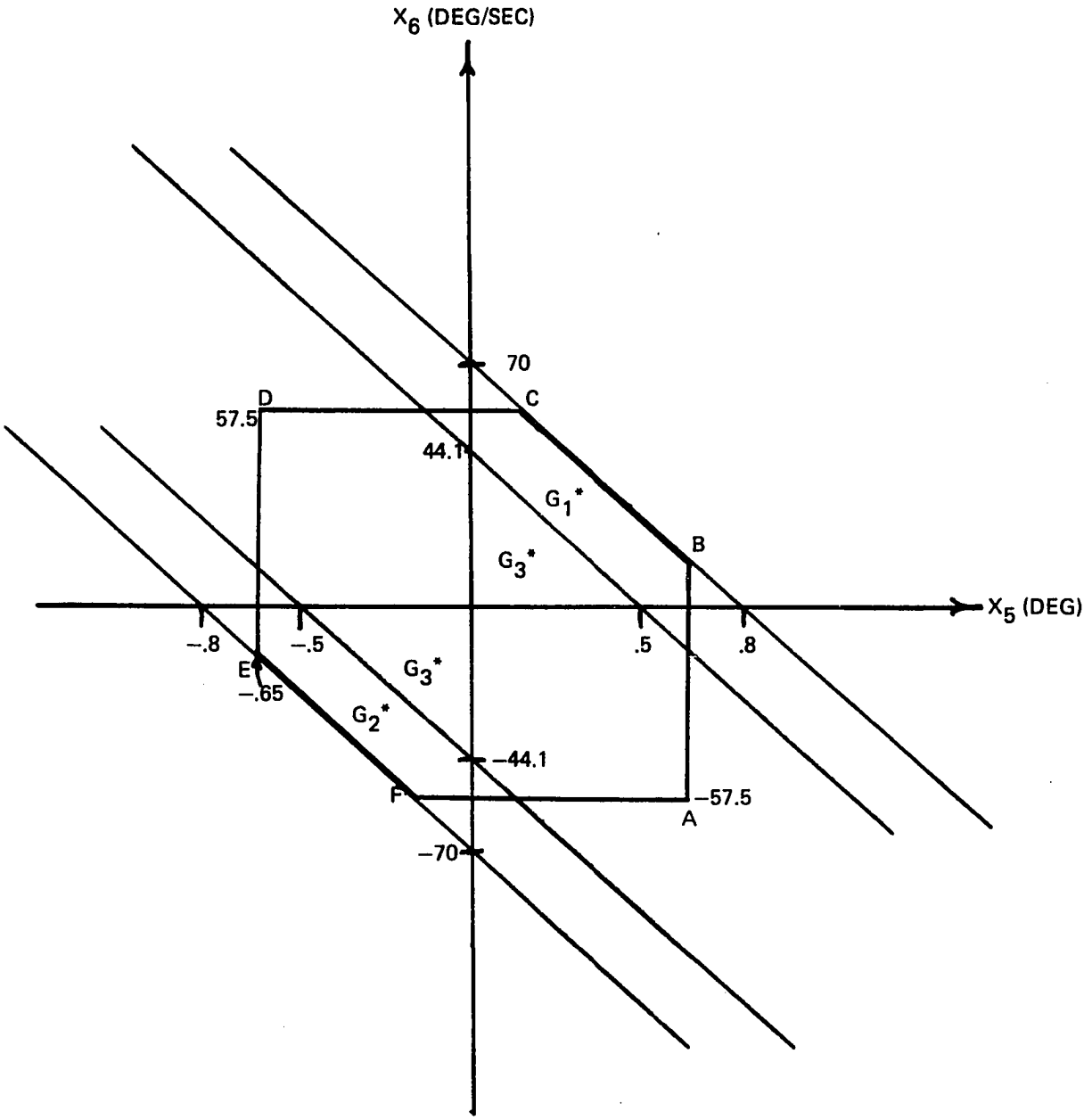

FIGURE 24 - DOMAIN OF ATTRACTION FOR SYSTEM (5.3-2) WHEN $U(Y_3) = 0.05$

Reproduced with permission of the copyright owner. Further reproduction prohibited without permission.

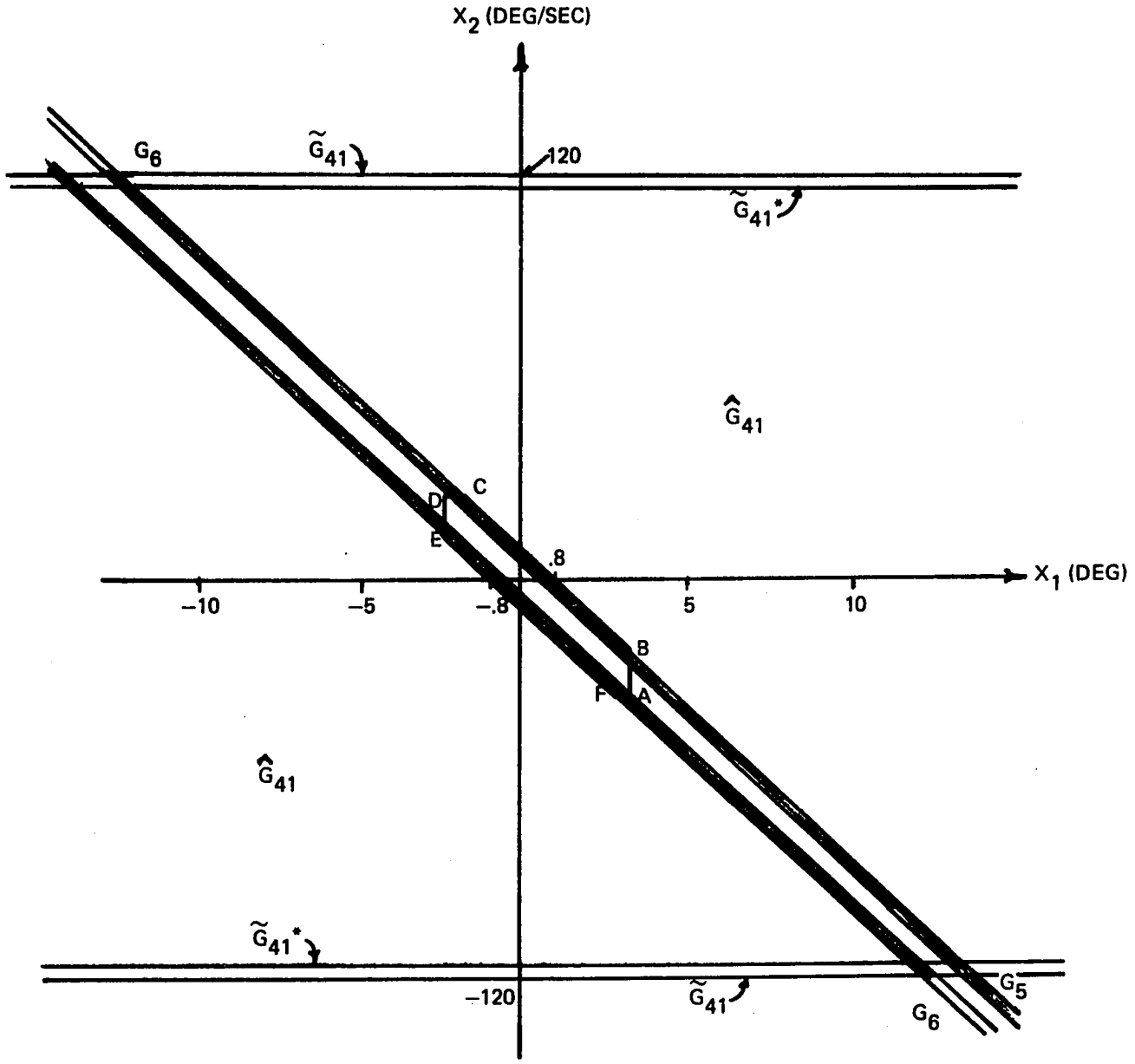

FIGURE 25 - VARIOUS ESTIMATES FOR $X_1 - X_2$ DOMAIN OF ATTRACTION FOR SYSTEM (5.3-8); $U(Y_1) = .05$

Reproduced with permission of the copyright owner. Further reproduction prohibited without permission.

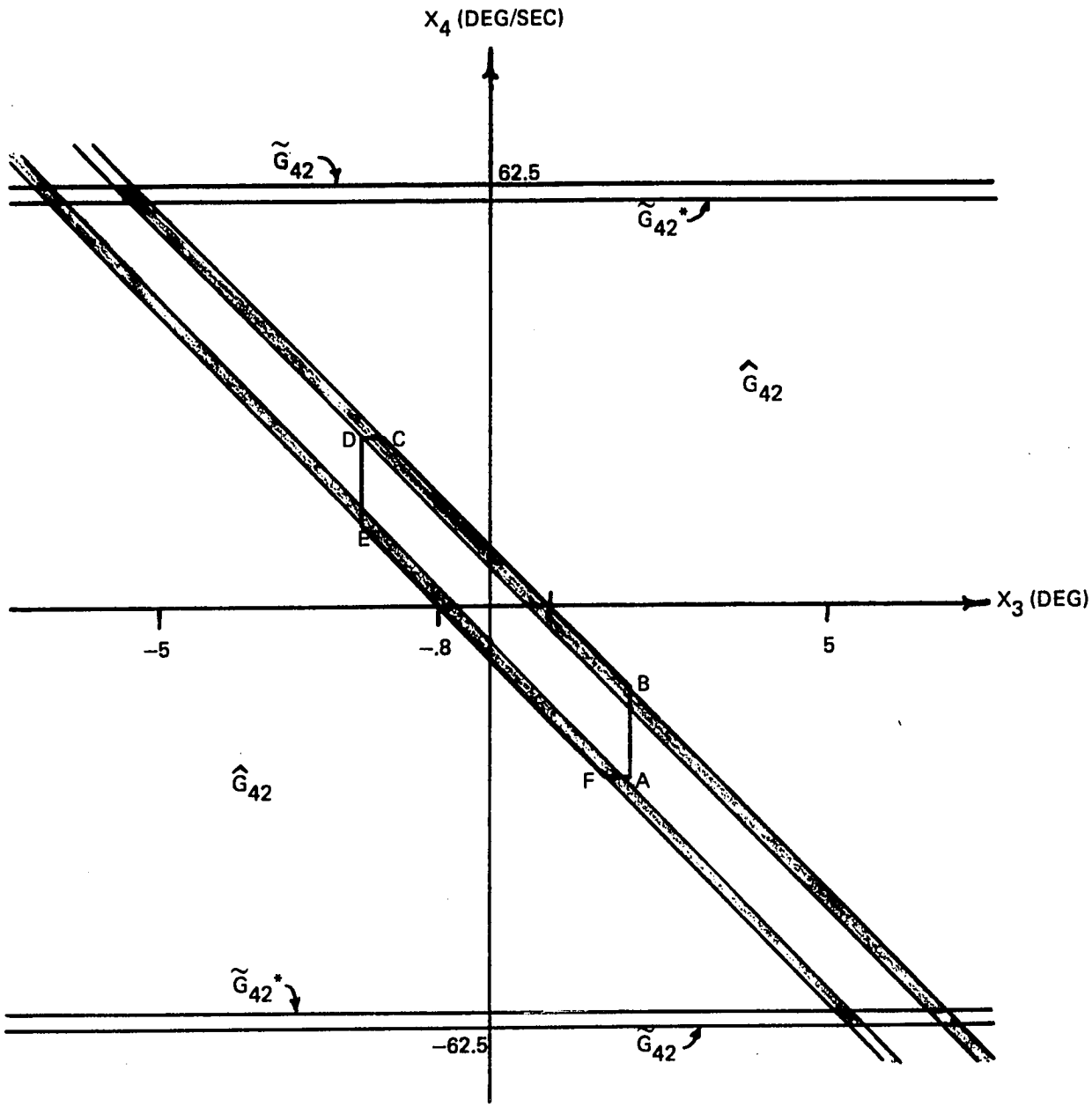

FIGURE 26 - VARIOUS ESTIMATES FOR $X_3 - X_4$ DOMAIN OF ATTRACTION FOR SYSTEM (5.3-8); $U(Y_2) = .05$

Reproduced with permission of the copyright owner. Further reproduction prohibited without permission.

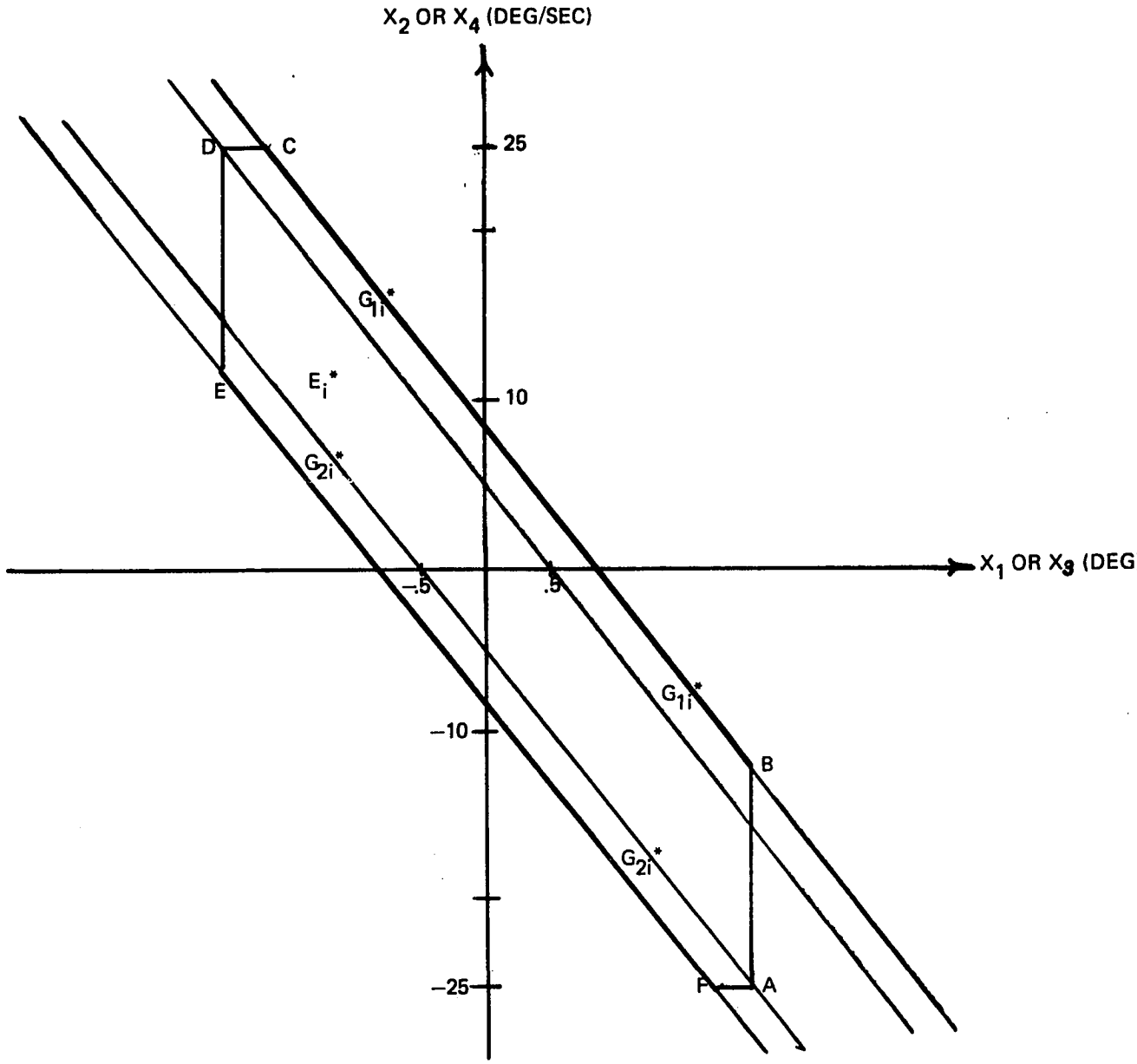

FIGURE 27 - REDUCED ESTIMATE OF DOMAIN OF ATTRACTION FOR EITHER AXIS OF (5.3-8) WHEN $U(Y_i) = .05$

Reproduced with permission of the copyright owner. Further reproduction prohibited without permission.

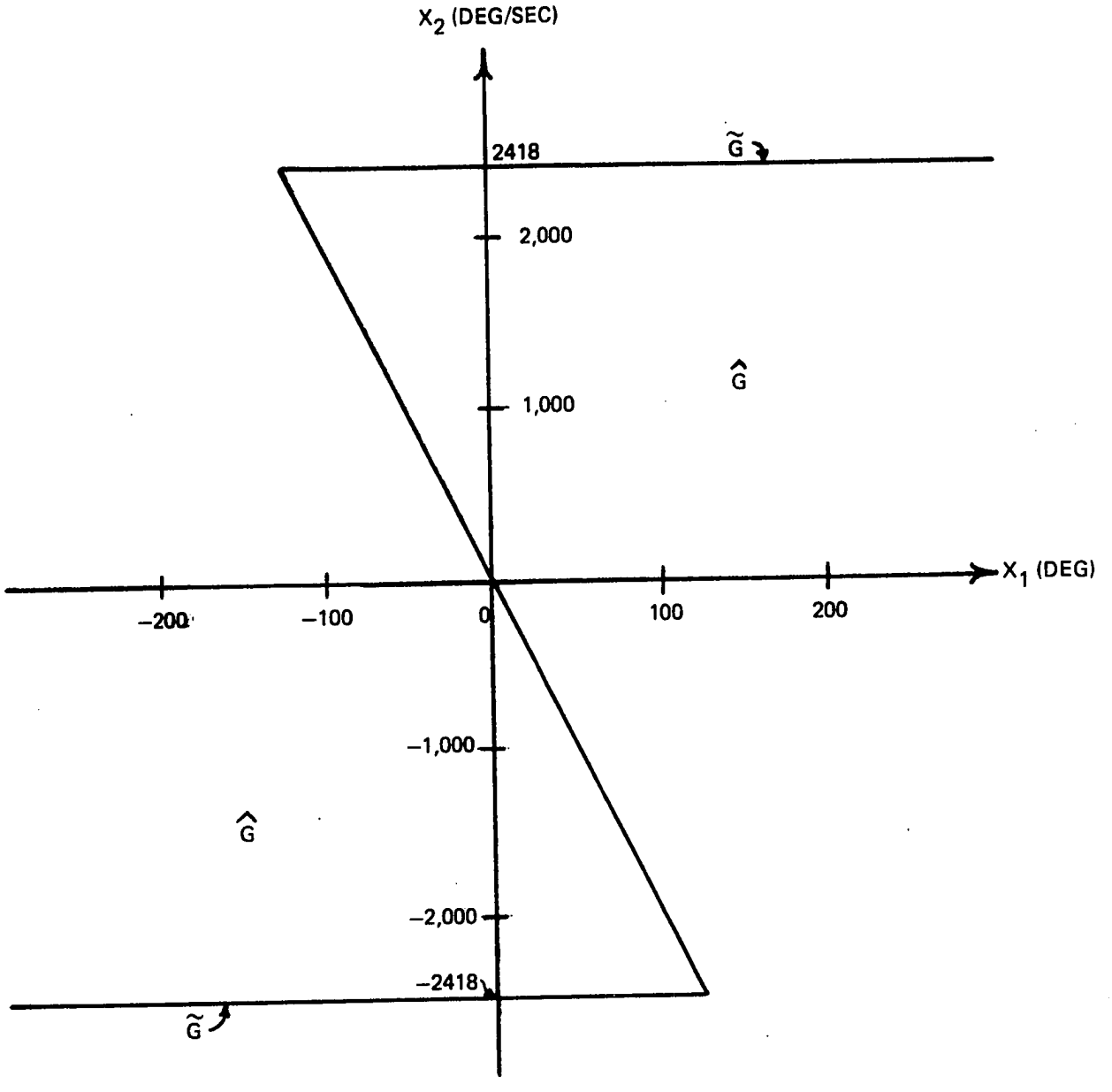

FIGURE 28 - FIRST ESTIMATE FOR THE $X_1 - X_2$ DOMAIN OF ATTRACTION FOR SYSTEM (5.3-8); $U(Y_1) = 1$, $C_{22} = .2$

Reproduced with permission of the copyright owner. Further reproduction prohibited without permission.

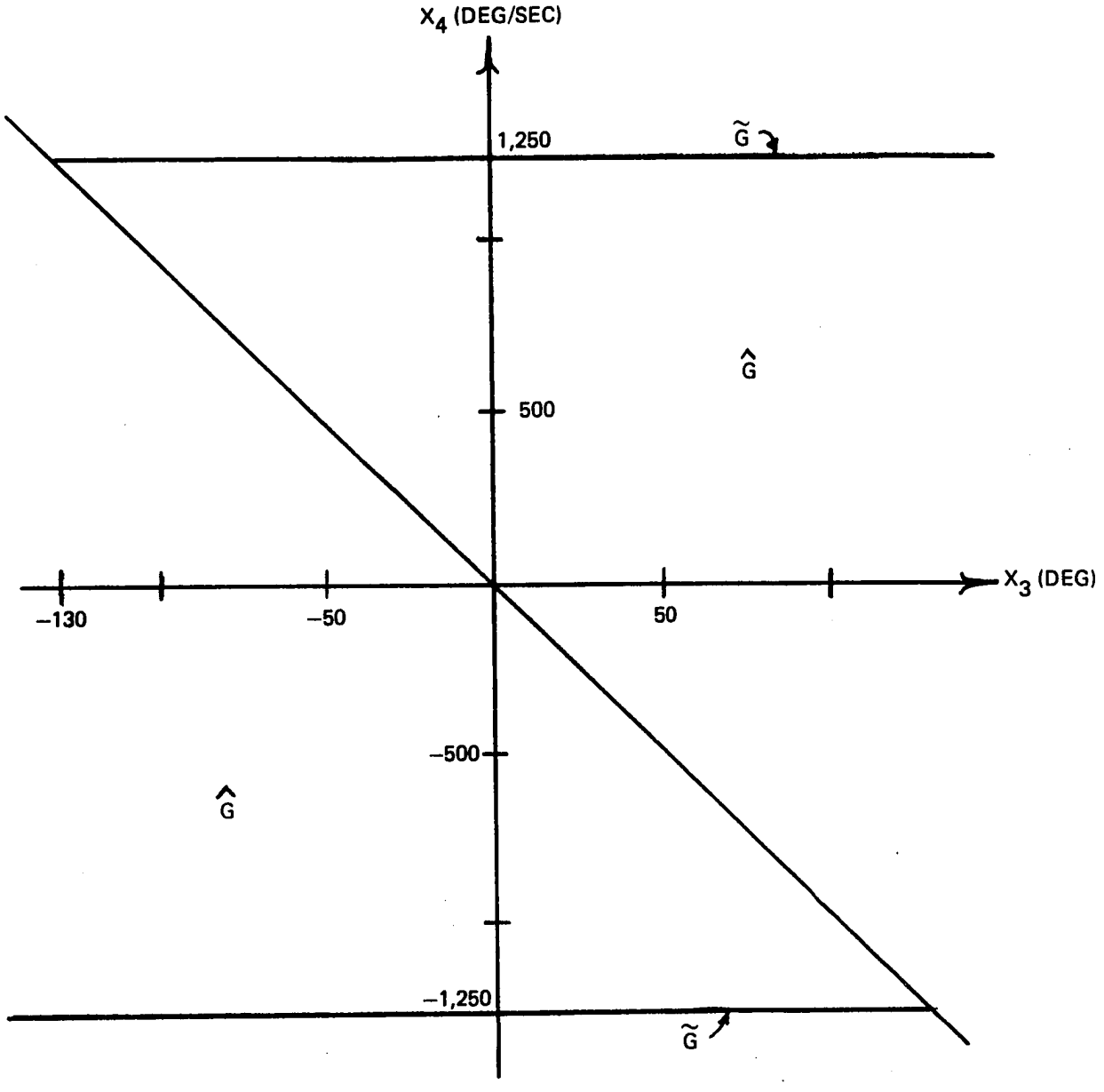

FIGURE 29 - FIRST ESTIMATE FOR THE $X_3 - X_4$ DOMAIN OF ATTRACTION FOR SYSTEM (5.3-8); $U(Y_2) = 1$, $C_{44} = .2$

Reproduced with permission of the copyright owner. Further reproduction prohibited without permission.

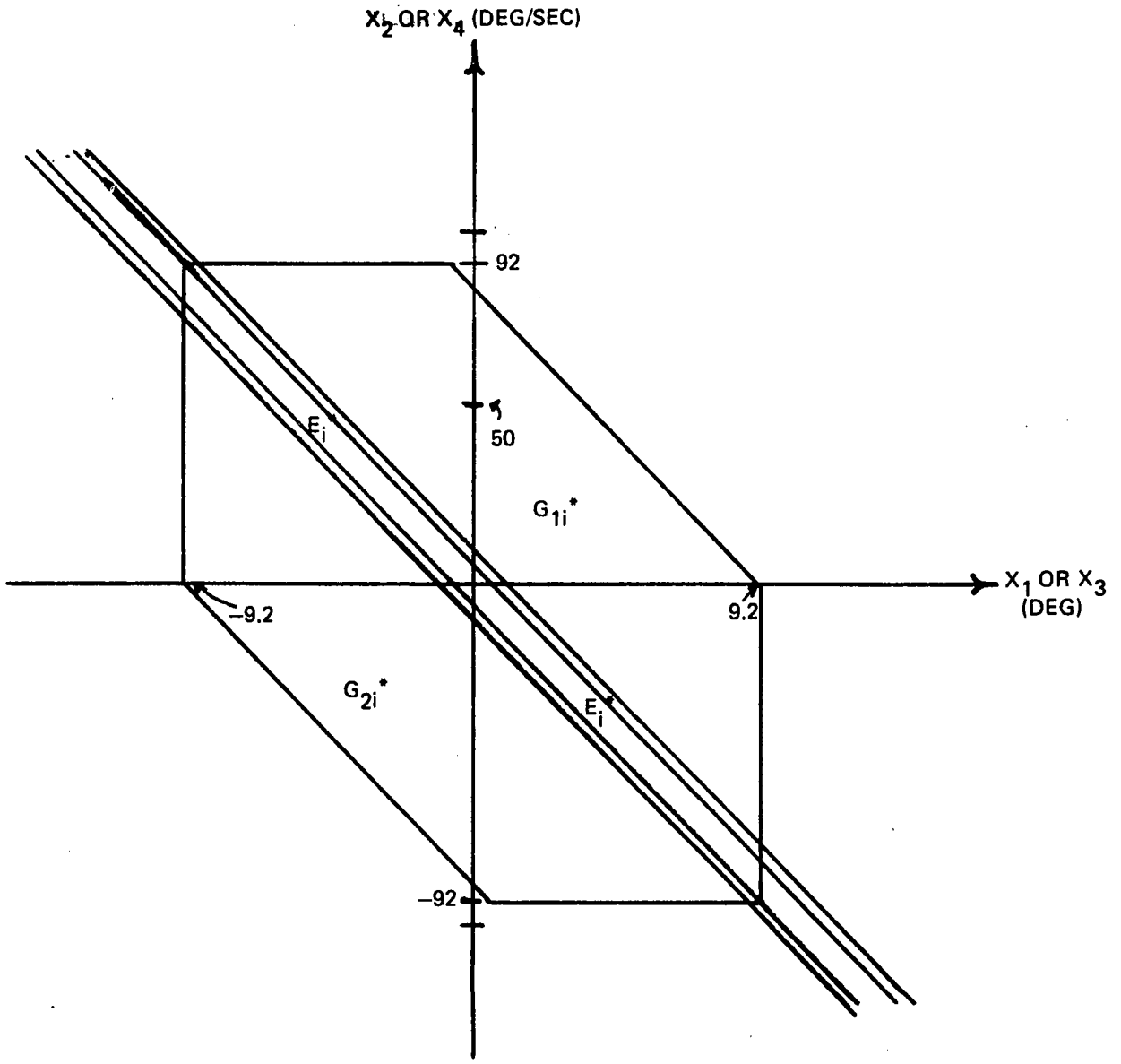

FIGURE 30 - REDUCED ESTIMATE FOR DOMAIN OF ATTRACTION OF EITHER AXIS OF (5.3-8) WHEN $U(Y_i) = 1; C_{2i,2i} = .2$

Reproduced with permission of the copyright owner. Further reproduction prohibited without permission.

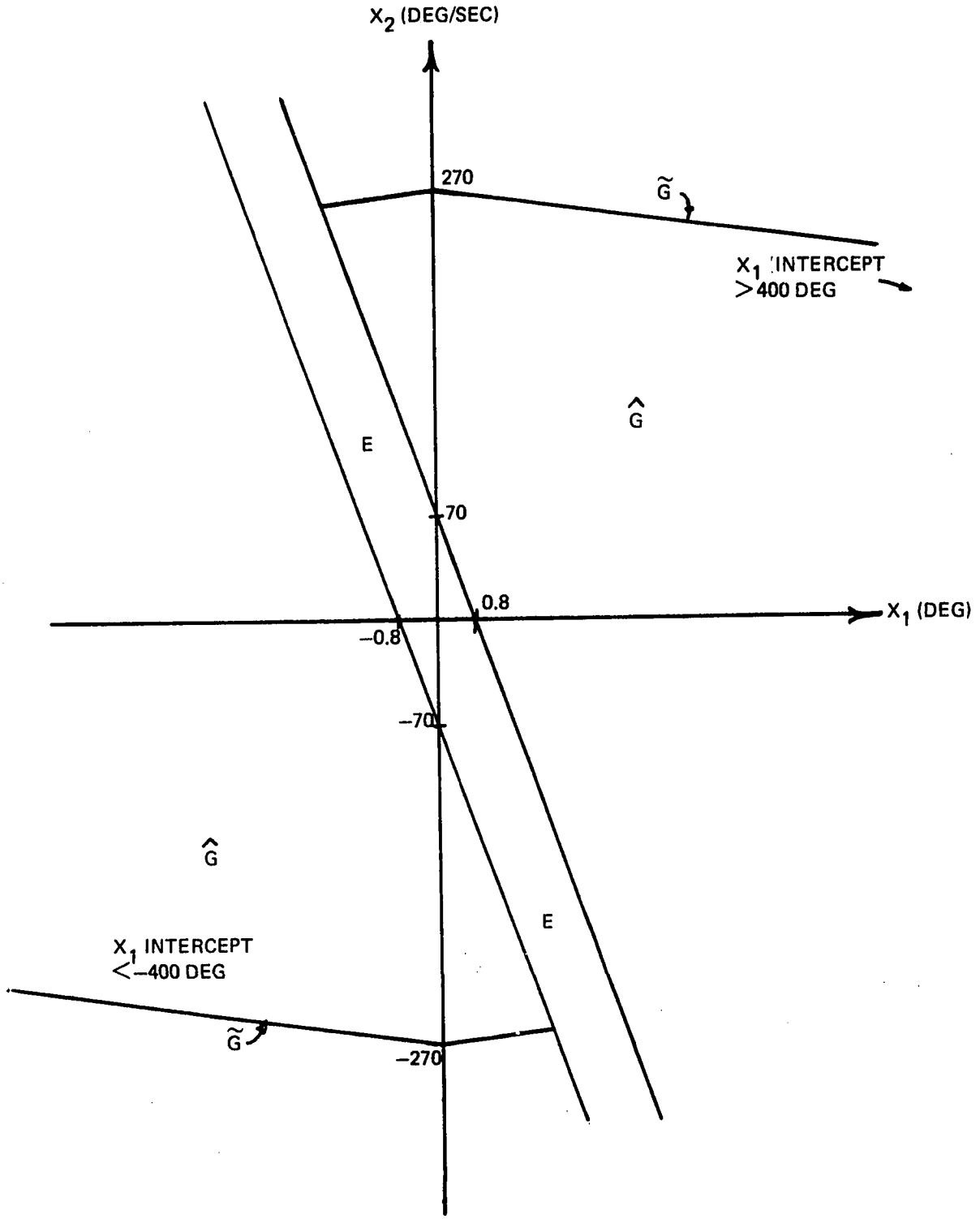

FIGURE 31 - FIRST ESTIMATE FOR THE $X_1 - X_2$ DOMAIN OF ATTRACTION FOR SYSTEM (5.3-8), $U(Y_1) = 1$, $C_{22} = .02266$

Reproduced with permission of the copyright owner. Further reproduction prohibited without permission.

APPENDIX B

THE DISTURBANCE TORQUES ON A SATELLITE IN LOW, CIRCULAR EARTH ORBIT

1. Derivation of the Gravity Gradient Torque

The torque acting about the CM of a rigid satellite in a circular orbit due to the effects of the gravitational "pull" of the Earth is derived with the help of Figure B-1.

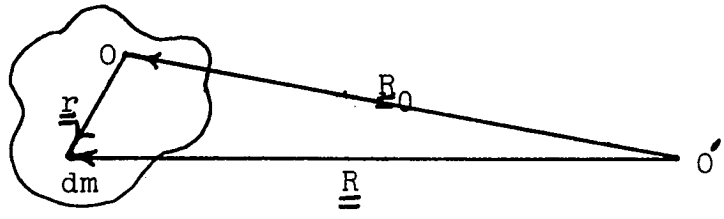

FIGURE B-1

The gravitation force, $\underline{dF}$, acting on an element of mass, dm, is given by (B-1) if the Earth is considered to be a sphere.

$$\underline{dF} = - \frac{GMdm}{R^3} \underline{R} \qquad \text{(B-1)}$$

where:

Reproduced with permission of the copyright owner. Further reproduction prohibited without permission.

G = the universal gravitational constant,

M = the mass of the Earth, and

m = the mass of the spacecraft.

$\underline{R}$ and dm are evident from the figure.

Using the law of cosines and the fact that $|\underline{R}_0| >> |\underline{r}|$ leads to

$$R^2 = (R_0^2 + r^2 + 2\underline{R}_0 \cdot \underline{r}) \quad ,$$

or

$$R^2 \simeq R_0^2\left(1 + \frac{2\underline{R}_0 \cdot \underline{r}}{R_0^2}\right) \quad . \qquad \text{(B-2)}$$

(B-1) and (B-2) together with the definition of the torque relative to the CM imply

$$\underline{N}_{gg} = \int_m \underline{r} \times d\underline{F} = -\frac{GM}{R_0^3} \int_m \underline{r} \times \left(\frac{(\underline{R}_0+\underline{r})dm}{1 + \frac{2\underline{R}_0 \cdot \underline{r}}{R_0^2}}\right) \qquad \text{(B-3)}$$

Now if the term in parentheses in the denominator of (B-3) is approximated by the first two terms of a geometric series and if the cross-product identity $\underline{r} \times \underline{r} = 0$ is noted, then

Reproduced with permission of the copyright owner. Further reproduction prohibited without permission.

$$\underline{N}_{gg} \simeq -\frac{GM}{R_0^3} \int_m \underline{r} \times \underline{R}_0 \left(1 - \frac{3\,\underline{R}_0 \cdot \underline{r}}{R_0^2}\right) dm \tag{B-4}$$

$$\simeq \frac{GM}{R_0^3} \left\{ \underline{R}_0 \times \left[\int_m \underline{r}\,dm - \int_m \frac{3(\underline{R}_0 \cdot \underline{r})}{R_0^2}\, dm\, \underline{r} \right] \right\}$$

Now, by definition of the CM, $\int_m \underline{r}\, dm = \underline{0}$, therefore

$$\underline{N}_{gg} \simeq -\frac{3GM}{R_0^5} \int_m (\underline{R}_0 \times \underline{r})(\underline{r} \times \underline{R}_0)\, dm \quad . \tag{B-5}$$

A more useful form of (B-5) can be constructed with some vector identities and the definition of the inertia dyadic. For example, if the vector identities

$$(\underline{R}_0 \times \underline{r})(\underline{r} \cdot R_0) = -\underline{R}_0 \times [\underline{r} \times (\underline{R}_0 \times \underline{r})]$$

and

$$\underline{r} \times (\underline{R}_0 \times \underline{r}) = [\underline{r} \cdot \underline{r}\,\underline{E} - \underline{r}\,\underline{r}] \cdot \underline{R}_0$$

where $\underline{E}$ is the unit dyadic defined such that $\underline{E} \cdot \underline{R}_0 = \underline{R}_0$, are substituted into (B-5), then

Reproduced with permission of the copyright owner. Further reproduction prohibited without permission.

$$\underline{N}_{gg} \simeq \frac{3GM}{R_0^5} \{\underline{R}_0 \times \int_m [(\underline{r} \cdot \underline{r})\underline{E} - \underline{r} \cdot \underline{r}]dm \cdot \underline{R}_0\}$$

or,

$$\underline{N}_{gg} = \frac{3GM}{R_0^5} \{\underline{R}_0 \times \underline{\underline{I}}\, \underline{R}_0\} \tag{B-6}$$

where $\underline{\underline{I}} = \int_m [(\underline{r} \cdot \underline{r})\underline{E} - \underline{r}\,\underline{r}]dm$ is the definition of the inertia dyadic.

If the dyadics and vectors of (B-6) are written in matrix form to an implied set of coordinates, then (B-6) is written as

$$\underline{N}_{gg} = \frac{3GM}{R_0^5} \tilde{\underline{e}}_{ns}\, \underline{\underline{I}}\, \underline{e}_{ns} = 3\omega_0^2\, \tilde{\underline{e}}_{ns}\, \underline{\underline{I}}\, \underline{e}_{ns} \tag{B-7}$$

where, for circular orbits, the relationship $\omega_0^2 = GM/R_0^3$ has been used.

2. The Aerodynamic Torque

The expression for the total aerodynamic torque acting on the spacecraft is derived as the sum of the individual aero torques acting on its cylindrical and rectangular portions. The cylindrical component is considered first. According to Yu and Elrod, [2.13], [2.14], the aerodynamic torque, $\underline{N}_a$, acting about the CM of a rigid cylindrical body in Earth orbit can be represented by

Reproduced with permission of the copyright owner. Further reproduction prohibited without permission.

$$\underline{N}_{ac} = N_{MC}\{(2-\sigma-\sigma')[\frac{4}{3}|\underline{v} \times \underline{s}| - \frac{\pi\sigma D}{2L}|\underline{v} \cdot \underline{s}|](\underline{v} \cdot \underline{s})(\underline{r} \times \underline{s}) \tag{B-8}$$

$$+ [(2-\sigma'+\frac{\sigma}{2})\ \frac{4}{3}|\underline{v} \times \underline{s}| + \frac{\pi\sigma D}{2L}|\underline{v} \cdot \underline{s}|](\underline{v} \times \underline{r})\}$$

where:

$N_{MC} = DLqr_c$,

D = the diameter of the cylinder,

L = the length of the cylinder,

q = the dynamic pressure = $\frac{1}{2}\rho V^2$

ρ = the atmospheric density,

V = the magnitude of the instantaneous orbital velocity,

r_c = distance from the composite CM to the center of geometry of the cylinder,

σ,σ' = the tangential and normal force reflection coefficient, respectively,

$\underline{v}$ = a unit vector in direction of $\underline{V}$,

$\underline{s}$ = a unit vector along the cylinder's axis of symmetry ($\underline{a}_3$), and

$\underline{r}$ = a unit vector in the direction of $\underline{r}_c$.

Because of the symmetry of the spacecraft under consideration, $\underline{r} \times \underline{s} = \underline{0}$ and the first term inside the curly brackets of (B-8) is ignorable. This term represents the aerodynamic torque acting about the axis of symmetry (the roll axis).

Reproduced with permission of the copyright owner. Further reproduction prohibited without permission.

Since $\underline{r} = \underline{s} = \underline{a}_3$ in spacecraft coordinates, the expansion of (B-8) depends on the transformation of $\underline{v}$ into that system. From §2.2, $\underline{v} = \underline{a}_2$ for circular orbits. If equation (2.2-4), which relates vectors in the local vertical coordinate system to vectors in the spacecraft system, is used, then, relative to the implied basis vectors $\underline{a}_i$, and using $\eta = \omega_0 t$

$$\underline{v} = \begin{bmatrix} -\sin(\eta-\psi) \\ \cos(\eta-\psi) \\ -\phi\cos(\eta-\psi) - \theta\sin(\eta-\psi) \end{bmatrix} . \qquad \text{(B-9)}$$

Note that (B-9) makes use of the approximations that were discussed in §2.3. Prior to the substitution of (B-9) into the matrix form of (B-8), however, the term $|\underline{v} \cdot \underline{s}|$ in (B-8) will be considered. It is easy to show that the error in (B-8) of neglecting this term is at most 0.2 percent. For this reason we take $|\underline{v} \cdot \underline{s}| \simeq 0$ and (B-8) is rewritten as

$$\underline{N}_{ac} = N_{MC}[(2-\sigma'+\tfrac{\sigma}{2})\tfrac{4}{3}|\tilde{\underline{v}}\ \underline{s}|](\tilde{\underline{v}}\ \underline{r}) \quad . \qquad \text{(B-10)}$$

The substitution of the matrix form of $\underline{r} = \underline{s} = \underline{a}_3$ and (B-9) into (B-10) yields

Reproduced with permission of the copyright owner. Further reproduction prohibited without permission.

$$\underline{N}_{ac} \simeq \frac{4}{3}(2 - \sigma' + \frac{\sigma}{2})N_{MC} \begin{bmatrix} \cos(\eta-\psi) \\ \sin(\eta-\psi) \\ 0 \end{bmatrix} . \qquad \text{(B-11)}$$

Using $\sigma = \sigma' = .885$ [2.10] results in (B-12), the expression to be used for the mathematical model of the aero torque acting on the cylindrical portion of the spacecraft.

$$\underline{N}_{c} = 2.08\ N_{MC} \begin{bmatrix} \cos(\eta-\psi) \\ \sin(\eta-\psi) \\ 0 \end{bmatrix} . \qquad \text{(B-12)}$$

Note that the expression for the atmospheric density is kept perfectly general.

The torque on the solar panels is given in spacecraft coordinates by

$$\underline{N}_{P} = N_{MP}\{2(2-\sigma')|\underline{v} \cdot \underline{n}|(\underline{v} \cdot \underline{n})(\tilde{\underline{n}}\ \underline{k}) + 2\sigma|\underline{v} \cdot \underline{n}||\tilde{\underline{v}}\ \underline{n}|(\tilde{\underline{t}}\ \underline{k})\} \qquad \text{(B-13)}$$

where:

$N_{MP} = qr_P A_P$,

r_P = the magnitude of the vector distance from the composite CM to the center of pressure of the solar panels,

Reproduced with permission of the copyright owner. Further reproduction prohibited without permission.

$\underline{n}$ = the unit vector normal to the plane of the panels (positive direction taken towards the Sun),

$\underline{k}$ = unit vector in the direction of $\underline{r}_P$, and

$$\underline{t} = \frac{\tilde{\underline{n}}(\tilde{\underline{v}}\ \underline{n})}{|\tilde{\underline{v}}\ \underline{n}|} \quad .$$

σ, σ', q and $\underline{v}$ are defined in (A-8).

Some simplifications are immediately apparent and others become apparent when expressed in spacecraft coordinates. Therefore, rewriting the vectors in (B-13) in terms of the spacecraft coordinate system defined in §2.2 gives $\underline{k} = \underline{a}_3$, $\underline{n} = \underline{a}_1$ for the worst case when the maximum panel area is exposed to the "wind", and

$$\begin{aligned} (\underline{v} \cdot \underline{n}) &= -\sin(\eta-\psi) \\ \underline{n} \times \underline{k} &= -\underline{a}_2 \ , \\ (\underline{v} \times \underline{n}) &\simeq -\cos(\eta-\psi)\underline{a}_3, \text{ and} \\ \underline{n} \times (\underline{v} \times \underline{n}) &= \cos(\eta-\psi)\underline{a}_2 \quad . \end{aligned} \tag{B-14}$$

These expressions depend on the $\underline{v}$ defined in (B-9). Note also that $\underline{n} \times (\underline{v} \times \underline{n}) = |\underline{v} \times \underline{n}|\underline{t}$ and that the $\underline{a}_2$ component of $(\underline{v} \times \underline{n})$, i.e., $[-\phi \cos(\eta-\psi) - \theta \sin(\eta-\psi)]$ was dropped. This component can be shown to be small for any practical direction for $\underline{n}$.

Reproduced with permission of the copyright owner. Further reproduction prohibited without permission.

The substitution of (B-14) into (B-13) yields

$$\underline{N}_P = 2(2-\sigma')N_{MP}|\sin(\eta-\psi)| \begin{bmatrix} -r\cos(\eta-\psi) \\ \sin(\eta-\psi) \\ 0 \end{bmatrix} \qquad \text{(B-15)}$$

relative to the implied set of spacecraft coordinates.

The total aerodynamic torque $\underline{N}_A$ acting on the spacecraft is then

$$\underline{N}_a = \underline{N}_{ac} + \underline{N}_P \quad . \qquad \text{(B-16)}$$

Note that there is no $\underline{a}_3$ component of aero torque in $\underline{N}_a$. This is because centers of pressure for both the cylinder and the solar panels are collinear with the composite CM along $\underline{a}_3$. This fact, along with the definitions of some of the vectors used in these derivations, is illustrated in Figure 5.

Reproduced with permission of the copyright owner. Further reproduction prohibited without permission.

APPENDIX C

DERIVATION OF SYSTEM EQUATIONS FOR THE TRACKING PROBLEM

For convenience, the general non-linear equation of motion for the system under study will be written

$$\dot{\underline{x}}(t) = \underline{h}(\underline{x}, t) + \underline{N}(\underline{x}, t) \qquad \text{(C-1)}$$

where $\underline{h}(\underline{x}, t)$ and $\underline{N}(\underline{x}, t)$ are, respectively, the mathematical models of the plant dynamics and the total external torques acting on the plant.* Expanding $\underline{h}$ and $\underline{N}$ in a Taylor series about $\underline{x} = \underline{0}$ yields

$$\underline{h}(\underline{x}, t) = \underline{J}_1(t)\underline{x} + \underline{\ell}(\underline{x}, t)$$

and

$$\underline{N}(\underline{x}, t) = \underline{z}(t) + \underline{J}_2(t)\ \underline{x}(t) + \underline{m}(\underline{x}, t)$$

where:

$\underline{h}(\underline{0}, t) = \underline{0}$ because $\underline{x} = \underline{0}$ is an equilibrium point;

$\underline{J}_1$ and $\underline{J}_2$ are matrices of first partial derivatives of $\underline{h}$ and $\underline{N}$ with respect to $\underline{x}$ and evaluated at $\underline{x} = \underline{0}$; and

---

*See Chapter II, Appendix B and §3.5.

Reproduced with permission of the copyright owner. Further reproduction prohibited without permission.

$$\lim_{\underline{x}\to\underline{0}} \frac{||\underline{\ell}(\underline{x}, t)||}{||\underline{x}||} = 0$$

and

$$\lim_{\underline{x}\to 0} \frac{||\underline{m}(\underline{x}, t)||}{||\underline{x}||} = 0 \quad . \tag{C-2}$$

Defining $\underline{J}_1(t) + \underline{J}_2(t) = \underline{A}(t)$ and $\underline{\ell}(\underline{x}, t) + \underline{m}(\underline{x}, t) = \underline{n}(\underline{x}, t)$ permits the rewriting of (C-1) as

$$\dot{\underline{x}}(t) = \underline{A}(t)\underline{x}(t) + \underline{z}(t) + \underline{n}(x, t) \tag{C-3}$$

where $\underline{n}(\underline{x}, t)$ has property (C-2).

For the initial development of the zero-fuel mode, the linear part of (C-3), i.e.,

$$\dot{\underline{x}}(t) = \underline{A}(t)\underline{x}(t) + \underline{z}(t) \tag{C-4}$$

was analyzed.* In particular, the unique initial condition $\underline{x}_p(0)$ was obtained that resulted in a periodic solution of the initial value problem corresponding to (C-4). As mentioned in §3.5, when $\underline{x}_p(0)$ was used as an initial value for the solution of (C-3), the results were unsatisfactory (see Figure 13). The led† to the analysis of (C-3) in the form

---

*Remember that, for the system under study, $\underline{A}(t)$ and $\underline{z}(t)$ were periodic with period T.

†Also in §3.5.

Reproduced with permission of the copyright owner. Further reproduction prohibited without permission.

$$\dot{\underline{x}}(t) = \underline{A}(t)\underline{x}(t) + \underline{z}(t) + \underline{p}(\underline{x}, t) + \underline{q}(\underline{x}, t) \qquad \text{(C-5)}$$

where $\underline{p}(\underline{x}, t) = \underline{n}(\underline{x}, t) - \underline{q}(\underline{x}, t)$ could not be neglected. Fortunately, one of the scalar equations (the ψ equation) of (C-5) was uncoupled and, when $\psi_p(t)$ was known, a more refined set of linear equations for ϕ and θ obtained. When the $\underline{x}_p(0)$ that was calculated by these equations was used to solve (C-3), it produced excellent results (see Figure 14). Thus, for motions in the vicinity of the zero-fuel mode, an adequate mathematical model of the plant is given by

$$\dot{\underline{x}}(t) = \underline{A}(t)\underline{x}(t) + \underline{z}(t) + \underline{p}(\underline{x}, t) \quad . \qquad \text{(C-6)}$$

For the purpose of analyzing the stability of the minimum-fuel solution, let $\underline{x} = (\underline{x}_p + \underline{\varepsilon})$ in (C-6) where $\underline{x}_p(t)$ is the periodic solution of (C-6). Thus,

$$(\dot{\underline{x}}_p + \dot{\underline{\varepsilon}}) = \underline{A}(t)\underline{x}_p + \underline{A}(t)\underline{\varepsilon} + \underline{z}(t) + p(\underline{x}_p + \underline{\varepsilon}, t) \; . \qquad \text{(C-7)}$$

If $\underline{p}(\underline{x}_p + \underline{\varepsilon}, t)$ is now expanded in a Taylor series about $\underline{x}_p(t)$, (C-7) becomes

$$\dot{\underline{x}}_p + \dot{\underline{\varepsilon}} = \underline{A}(t)\underline{x}_p + \underline{A}(t)\underline{\varepsilon} + \underline{z}(t) + p(\underline{x}_p, t) + \underline{J}_3(\underline{x}_p, t)\underline{\varepsilon} + 0(\varepsilon^2) \qquad \text{(C-8)}$$

Reproduced with permission of the copyright owner. Further reproduction prohibited without permission.

where $\underline{J}_3$ is the matrix of first partial derivatives, i.e.,

$$\underline{J}_3(\underline{x}_p, t) = \partial \underline{p}/\partial \underline{x}\big|_{\underline{x} = \underline{x}_p} \quad \text{and } 0(\varepsilon^2) \text{ has property (C-2)} .$$

However, using equality (C-6), we can write (C-8) as

$$\dot{\underline{\varepsilon}}(t) = [\underline{A}(t) + \underline{J}_3(\underline{x}_p(t), t)]\underline{\varepsilon} + 0(\varepsilon^2)$$

$$\triangleq \hat{\underline{A}}(t)\underline{\varepsilon} + 0(\varepsilon^2) \qquad \text{(C-9)}$$

where

$$\hat{\underline{A}}(t) = \begin{bmatrix} 0 & 1 & 0 & 0 & 0 & 0 \\ \hat{a}_{21} & 0 & \hat{a}_{23} & \hat{a}_{24} & 0 & \hat{a}_{26} \\ 0 & 0 & 0 & 1 & 0 & 0 \\ \hat{a}_{41} & \hat{a}_{42} & \hat{a}_{43} & 0 & 0 & \hat{a}_{46} \\ 0 & 0 & 0 & 0 & 0 & 1 \\ 0 & 0 & 0 & 0 & \hat{a}_{65} & 0 \end{bmatrix}$$

and

$$\hat{a}_{21} = \alpha_1^2[1 - \cos 2(\omega_0 t - \psi_p)] + |K_1|\dot{\psi}_p^2 ,$$

$$\hat{a}_{23} = -(\alpha_1^2+\alpha_3^2)\sin 2(\omega_0 t - \psi_p) ,$$

$$\hat{a}_{24} = (1 + K_1)\dot{\psi}_p ,$$

$$\hat{a}_{26} = 2K_1\dot{\psi}_p\phi_p + (1+K_1)\dot{\theta}_p ,$$

Reproduced with permission of the copyright owner. Further reproduction prohibited without permission.

$$\hat{a}_{41} = -(\alpha_2^2-\alpha_3^2)\sin 2(\omega_0 t-\psi_p) ,$$

$$\hat{a}_{42} = -(1 + K_2)\dot{\psi}_p ,$$

$$\hat{a}_{43} = \alpha_2^2[1 + \cos 2(\omega_0 t-\psi_p)] + K_2\dot{\psi}_p^2 ,$$

$$\hat{a}_{46} = -2 K_2 \theta_p\dot{\psi}_p - (1+K_2)\dot{\phi}_p ,$$

$$\hat{a}_{65} = 2\alpha_3^2 \cos 2\omega_0 t .$$

Reproduced with permission of the copyright owner. Further reproduction prohibited without permission.

SELECTED BIBLIOGRAPHY

Chapter II

2.1 Goldstein, H., "Classical Mechanics", Addison-Wesley Publ. Co., Reading, Mass., June, 1959.

2.2 Ravera, R. J., Unpublished notes, Bellcomm, Inc., Washington, D. C., November, 1968.

2.3 Smith, P. G., "On the Secular Term In Spacecraft Angular Momentum", B68 12076, Bellcomm, Inc., Washington, D. C., December, 1968.

2.4 Sabroff, A., et al, "Investigation of the Acquisition Problem in Satellite Attitude Control", USAF Report AFFDL-TR-65-115, December, 1965, pp. 44-69.

2.5 Roberson, R. E., "Gravitational Torque on a Satellite Vehicle", J. Franklin Inst. 265, 1958, pp. 13-22.

2.6 DeBra, D. B. and Delp, R. H., "Satellite Stability and Natural Frequencies in Circular Orbit", J. Astr. Sciences, vol. VIII, no. 1, 1961.

2.7 DeBra, D. B., "Attitude Stability and Motions of Passive, Gravity-Oriented Satellites", AAS Preprint 62-6, January, 1962.

2.8 _____, "The Effect of Aerodynamic Forces on Satellite Attitude", J. Astr. Sciences, vol. VI, no. 3, 1959, pp. 40-45.

2.9 Garber, T. B., "Influence of Constant Disturbance Torques on the Motion of Gravity-Gradient Stabilized Satellites", AIAA Journal, vol. I, no. 4, April, 1963, pp. 968-969.

Reproduced with permission of the copyright owner. Further reproduction prohibited without permission.

2.10 Meirovitch, L. and Wallace, F. B., "On the Effects of Aerodynamic and Gravitational Torques on the Attitude Stability of Satellites", AIAA Journal, vol. 4, no. 12, December, 1966, pp. 2196-2202.

2.11 Nurre, G. S., "Effects of Aerodynamic Torque on an Asymmetric, Gravity-Stabilized Satellite", J. Spacecraft and Rockets, vol. 5, no. 9, September, 1968, pp. 1046-1050.

2.12 Frik, Martin A., "Attitude Stability of Satellites Subjected to Gravity-Gradient and Aerodynamic Torques", AIAA Paper, no. 69-832, August, 1969.

2.13 Yu, E. Y., "Aerodynamic Torque on a Space Vehicle", TM-68-1022-10, Bellcomm, Inc., Washington, D. C., December, 1968.

2.14 Elrod, B. D., "Aerodynamic Torque (Vector Formulation)", Unpublished notes, Bellcomm, Inc., Washington, D. C., 1968.

2.15 U. S. Standard Atmcsphere Supplements, 1966. Prepared under the sponsorship of Environmental Science Services Administration, NASA and USAF.

2.16 Benson, R. H., Fleischman, E. F., Hill, R. J., "Earth-Orbital Lifetime and Satellite Decay", Astronautics and Aeronautics, January, 1968, pp. 38-45.

Chapter III

3.1 "Instrument Unit Applications for Saturn I Workshop", IBM no. 68-220-0002. Prepared for Marshall Space Flight Center (MSFC), Huntsville, Ala., MSFC no. III-6-602-91, July, 1968.

3.2 Fearnsides, J. J., "Attitude Control for AAP 1/2 and AAP 2/3A: A Progress Report", B69-03026, Bellcomm, Inc., Washington, D. C., March, 1969.

3.3 Regetz, John D., Jr. and Nelson, Thomas M., "Feasibility Study of Optimum On-Off Attitude Control System for Spacecraft", NASA TN D-4519, April, 1968.

3.4 Dunn, S. S. and Edelman, R., "Minimum Power Spacecraft Attitude Control Laws for Small Constant Disturbance Torques", IEEE Transactions on Automatic Control, vol. AC-13, no. 6, pp. December, 1968, pp. 691-694.

Reproduced with permission of the copyright owner. Further reproduction prohibited without permission.

3.5 Englehart, William C., "Performance Characteristics of a 'Damped' Mass Expulsion Attitude Control System", AIAA Journal of Spacecraft and Rockets, vol. 6, no. 2, January, 1969, pp. 148-155.

3.6 Mendel, Jerry M., "Performance Cost Functions for a Reaction-Jet-Controlled System During an On-Off Limit Cycle", IEEE Transactions on Automatic Control, vol. AC-13, no. 4, August, 1968, pp. 362-368.

3.7 Chu, S. C., "Periodic Solutions of the Orbital Assembly Equations of Motion", Case 620, B69 04021, Bellcomm, Inc., Washington, D. C., April, 1969.

3.8 Brockett, R. W., "Finite-Dimensional Linear Systems", John Wiley and Sons, Inc., New York, N. Y., 1970, pp. 50-53.

Chapter IV

4.1 Willems, J. L., "Stability Theory of Dynamical Systems", John Wiley and Sons, Inc., New York, N. Y., 1970, pp. 109-112.

4.2 Brockett, R. W., "Finite-Dimensional Linear Systems", John Wiley and Sons, Inc., New York, N. Y., 1970, pp. 46-48.

4.3 Gantmacher, F. R., The Theory of Matrices, Vols. I and II, New York, Chelsea Publishing Company, 1959.

4.4 Athans, M. and Falb, P. L., "Optimal Control", McGraw-Hill Book Company, New York, N. Y., 1966.

4.5 Kalman, R. E., "The Theory of Optimal Control and the Calculus of Variations", in "Mathematical Optimization Techniques", R. Bellman (ed.), University of California Press, Berkeley, Calif., 1963.

4.6 Arscott, F. M., "Periodic Differential Equations", The MacMillan Company, 1964.

4.7 Busch, R. E. and Flugge-Lotz, I., "Attitude Control of a Satellite in an Elliptic Orbit", AIAA Journal of Spacecraft and Rockets, Vol. 4, No. 4, April, 1967, pp. 436-442.

4.8 Flugge-Lotz, I. and Craig, A., "The Choice of Time for Zeroing a Disturbance in a Minimum-Fuel Consumption Control Problem", Trans. ASME, J. of Basic Engr., March, 1965, pp. 29-38.

Reproduced with permission of the copyright owner. Further reproduction prohibited without permission.

Chapter V

5.1 Kalman, R. E. and Bertram, J. E., "Control System Design via the 'Second Method' of Lyapunov--Pt. I: Continuous-Time Systems; Pt. II: Discrete-Time Systems", J. Basic Engr., Trans. ASME, Vol. 82, 1960, pp. 371-393, 394-400.

5.2 LaSalle, J. P. and Lefschetz, S., "Stability of Lyapunov's Direct Method", New York, Academic Press, 1961.

5.3 Lyapunov, A. M., "Probleme general de la stabilite du Mouvement", Ann. Fac. Scl. Toulouse, Vol. 9, 1907, pp. 203-474.

5.4 Yoshizawa, T., "Asymptotic Behavior of Solutions of Differential Equations", Contrib. Diff. Eqs., Vol. I, 1963, pp. 371-387.

5.5 LaSalle, J. P., "An Invariance Principle in the Theory of Stability", Differential Equations and Dynamical Systems, Proc. of the Intntl. Symp., Puerto Rico, Academic Press, New York, 1967, pp. 277-286.

5.6 _____, "Stability Theory for Ordinary Differential Equations", J. Diff. Eqns., Vol. IV, 1968, pp. 57-65.

5.7 Schultz, D. G. and Gibson, J. E., "The Variable Gradient Method for Generating Lyapunov Functions", Trans. AIEE, Vol. 81, 1962, pp. 203-210.

5.8 Margolis, S. G. and Vogt, W. G., "Control Engineering Applications of V. I. Zubov's Construction Procedure for Lyapunov Functions", IEEE Trans. Auto. Control AC-9, 1963, pp. 104-113.

5.9 Willems, J. C., "The Analysis of Feedback Systems", MIT Press, Cambridge, Mass., 1971.

5.10 Willems, J. L., "Stability Theory of Dynamical Systems", John Wiley and Sons, New York, 1970.

5.11 Variya, P. P. and Liu, R., "Bounded-Input Bounded Output Stability of Nonlinear Time-Varying Differential Systems", J. SIAM Control, Vol. 4, 1966, pp. 698-704.

5.12 Zames, G., "On the Input-Output Stability of Time-Varying Nonlinear Feedback Systems--I: Conditions Derived Using Concepts of Loop Gain, Conicity, and Positivity; II: Conditions Involving Circles in the Frequency Plane and Sector Nonlinearities", IEEE Trans. Auto. Control, AC-11, 1966, pp. 228-239, 465-476.

Reproduced with permission of the copyright owner. Further reproduction prohibited without permission.

5.13 Sandberg, I. W., "Some Results on the Theory of Physical Systems Governed by Nonlinear Functional Equations", Bell. Syst. Tech. J., Vol. 44, 1965, pp. 871-894.

5.14 Popov, V. M., "Absolute Stability of Nonlinear Systems of Automatic Control", Automation and Remote Control, Vol. 25, 1964, pp. 765-778.

5.15 Brockett, R. W., "The Status of Stability Theory for Deterministic Systems", IEEE Trans. Auto. Control, AC-11, 1966, pp. 596-606.

5.16 Partovi, S. and Nahi, N. E., "Absolute Stability of Dynamic Systems Containing Nonlinear Functions of Several State Variables", Automatica, Vol. 5, 1969, pp. 465-473.

5.17 Willems, J. C., "On the Asymptotic Stability of the Null Solution of Linear Differential Equations with Periodic Coefficients", IEEE Trans. Auto. Control, AC-13, 1968, pp. 65-72.

Reproduced with permission of the copyright owner. Further reproduction prohibited without permission.

VITA

Name: John Joseph Fearnsides

Permanent address: 8024 16th Street, N. W.
Washington, D. C. 20012

Degree and date to be conferred: Ph.D., 1971

Date of birth: May 28, 1934

Place of birth: Philadelphia, Pennsylvania

Secondary education: Northeast Catholic High School
Philadelphia, Pennsylvania, 1951

Collegiate institutions attended	Dates	Degree	Date of degree
Drexel University	1957-1962	BSEE	1962
Drexel University	1962-1964	MSEE	1964
University of Maryland	1964-1971	Ph.D.	1971

Major: Electrical Engineering

Minors: Physics, Mathematics

Reproduced with permission of the copyright owner. Further reproduction prohibited without permission.